THE EFFECT OF HYDROGEN SUBSTITUTION ON THE REAL-WORLD CO_2, NO_X, AND PM EMISSIONS OF A HEAVY-DUTY DIESEL TRUCK

by

Jeffrey Dean Meiklejohn

B.Eng., British Columbia Institute of Technology, 2017

A THESIS SUBMITTED IN PARTIAL FULFILMENT OF
THE REQUIREMENTS FOR THE DEGREE OF

MASTER OF APPLIED SCIENCE
in
THE FACULTY OF GRADUATE AND POSTDOCTORAL STUDIES
(Mechanical Engineering)

THE UNIVERSITY OF BRITISH COLUMBIA
(Vancouver)

August 2019

The following individuals certify that they have read, and recommend to the Faculty of Graduate and Postdoctoral Studies for acceptance, a thesis entitled:

The effect of hydrogen substitution on the real-world CO_2, NOx, and PM emissions of a heavy-duty diesel truck

submitted by Jeffrey Dean Meiklejohn in partial fulfillment of the requirements for

the degree of Master of Applied Science

in Mechanical Engineering

Examining Committee:

Dr Steven Rogak

Co-supervisor

Dr Patrick Kirchen

Co-supervisor

Jean-Louis Iaconis

Supervisory Committee Member

Abstract

Hydrogen substitution can reduce the diesel consumption and CO_2 output of diesel engines. This thesis investigates its effect on the real-world, on-road emissions of CO_2, NOx and particulate matter (PM) from a heavy-duty diesel truck. Testing was conducted on a Class 8 truck fitted with a 13 L common-rail direct-injection (CDI) engine and a supplemental intake manifold-injection hydrogen fuel system. The peak hydrogen energy substitution rate was 40%, while the observed average was 24%. The truck operated with Gross Combined Vehicle Weights (GCVWs) between 20,000 kg and 60,000 kg. A Portable Emissions Measurement System (PEMS) was built and was used to sample engine-out, pre-aftertreatment exhaust gases. Torque was measured on the driveshaft with a wireless transducer, CO_2 was measured via non-dispersive infrared sensor, NOx was measured with an electrochemical sensor, and PM was measured via light scattering and gravimetric methods. Data was logged at 10 Hz by a data acquisition system (DAQ) that was also connected to the truck's J1939 communication networks. From this data, detailed emission maps were generated which showed the varied emissions across the engine's speed/load operating range. For accurate comparison on-road testing was conducted in both hydrogen/diesel and plain diesel fueling modes, totaling over 2500 kilometers logged. Overall CO_2 emissions decreased by 25±1%, which was approximately equal to the hydrogen displacement. Engine-out NOx emissions increased by 10±1% and engine-out PM emissions increased by 2±3%. For PM measurement, high correlation ($R^2 = 0.9$) was found between integration of the instantaneous light scattering and the total gravimetric measurement methods. Overall thermal efficiency was virtually unchanged between the two fueling modes, with small decrease noted at low loads and small increase at high loads. Increased exhaust gas temperature (EGT) was measured while operating in hydrogen/diesel mode and increased in-cylinder temperature is suspected as the cause of the increased NOx emissions. Preliminary analysis of the post-aftertreatment NOx showed a decrease of 36±2% in hydrogen/diesel mode versus the diesel baseline, suggesting that the increased engine-out NOx does not increase tailpipe emissions. Furthermore, the consumption of diesel exhaust fluid (DEF) only increased by 3±3% in hydrogen/diesel mode, suggesting a higher conversion efficiency.

Lay Summary

Diesel engines power most of the world's heavy-duty vehicles and are a significant source of CO_2, oxides of nitrogen (NOx) and particulate matter (PM). Substituting hydrogen for diesel in these engines is a potential pathway to reduce CO_2 emissions and diesel fuel consumption but the effect on NOx and PM needs to be understood.

A custom portable emissions measurement system (PEMS) was designed and built to enable real-world, on-road testing. Over 2500 km of detailed data was collected under real driving conditions. To isolate the hydrogen's effect on engine operation, NOx and PM emissions were measured raw, before the emissions control systems.

Detailed data analysis found CO_2 decreased 25±1%, NOx increased 10±1% and PM increased 2±3% respectively. Preliminary analysis showed that the truck's emission control systems can handle the increased NOx emissions with no net increase in NOx output to the environment.

Preface

The research objectives of this thesis were outlined by Dr Steven Rogak and Dr Patrick Kirchen from the University of British Columbia, Vancouver as part of a collaborative research effort between the University of British Columbia and an industrial partner. Over the course of the project Steven Rogak and Patrick Kirchen provided guidance and feedback, as did Jean-Louis Iaconis and Patrick Steiche, engineers from the industrial partner.

The heavy-duty diesel truck on which the testing was conducted was provided by the industrial partner. The hydrogen fuel system was installed on the truck by the industrial partner and calibrated by a separate, specialty engineering firm.

The data acquisition system, including the wireless torque transducer, used for logging the emissions data was first developed by Patrick Steiche and Jeff Yeo, MASc students at the time, in a related project between the University of British Columbia and the industrial partner. It was however modified and added to by myself and Patrick during this project.

I designed and built the PEMS system myself, with the following exceptions: water-jet cutting on the mounting bracket, and the machining on the dilution nozzle restriction orifice were done by UBC student Brett Huemer. Brett also assisted in lab testing the dilution nozzle.

On-road testing was conducted while the truck was operated by a commercial fleet. They supplied the drivers while I rode along as a passenger to conduct the experiments. During these field measurement campaigns, I received extensive support from Patrick Steiche.

I wrote all the Python code used for processing the results with the following exception: the base code for plotting the emission maps comes from Calvin Lefebvre, a data scientist at the industrial partner, although I modified it substantially for my use.

A portion of the results from this research were presented at: The 2019 Spring Technical Meeting of the Canadian Section of the Combustion Institute on May 15, 2019 at the University of British Columbia, Kelowna.

Between October 2017 and February 2019, I participated in several Mitacs-Accelerate internships at the industrial partner. The overall title of the project was “Development and Demonstration Engine Technology for Class 8 Heavy Duty Trucks Fueled by Waste Hydrogen”.

Table of Contents

List of Tables

List of Figures

List of Acronyms

AFT – Adiabatic Flame Temperature

aTDC – After Top Dead Centre

BTE – Brake Thermal Efficiency

CGVW – Combined Gross Vehicle Weight

CI – Compression Ignition

DAQ – Data Acquisition System

DPF – Diesel Particulate Filter

ECU – Engine Control Unit

EGR – Exhaust Gas Recirculation

EGT – Exhaust Gas Temperature

FTP – Federal Test Procedure

HDDT – Heavy Duty Diesel Trucks

ICE – Internal Combustion Engine

ID – Inner Diameter

ISC – In Service Compliance

LHV – Lower Heating Value

MEL – Mobile Emissions Laboratory

NOx – Oxides of Nitrogen, includes both NO and NO_2

NTE – Not to Exceed

OD – Outer Diameter

PEMS – Portable Emissions Measurement System

PM – Particulate Matter

RH – Relative Humidity

RMS – Root Mean Square

RPM – Revolutions per Minute

SCR – Selective Catalytic Reduction

SCRE – Single Cylinder Research Engine

TWC – Three Way Catalyst

VSP – Vehicle Specific Power

WHTC – World Harmonized Test Cycle

List of Symbols

A/F – air to fuel ratio

φ – equivalence ratio

ω – engine rotation speed

ṁ – mass flow rate

v̇ – volumetric flow rate

E – Young's modulus

Chapter 1 - Introduction

Diesel engines are ubiquitous in heavy-duty transportation. Although proven and reliable, they are a major consumer of fossil fuels and a major source of greenhouse gas (CO_2), Oxides of Nitrogen (NOx), and Particulate Matter (PM) emissions. Hydrogen-diesel co-combustion is a technology which offers a potential pathway to reduce CO_2 output and diesel fuel consumption in these prevailing powertrains. The effects on NOx and PM emissions, however, needs to be understood.

Increasingly stringent diesel emission regulations have led to the development of dedicated emission control systems called exhaust aftertreatment systems. An aftertreatment system is a collection of devices which apply supplementary chemical and physical processes to the exhaust after it exits the engine but before it enters the atmosphere. Specifically, a diesel particulate filter (DPF) captures PM emissions and later reburns them, while selective catalytic reduction (SCR) injects urea to enable the conversion of NOx into nitrogen and water vapour [1]. Aftertreatment systems do not address vehicle CO_2 output; sequestration is not viable with current technology. Ultimately it is the post-aftertreatment tailpipe emissions which matter to human health and to the environment. Achieving that goal, however, requires a detailed understanding of the combined engine and aftertreatment system. To facilitate that, this study focuses on the raw emission values produced when hydrogen/diesel co-combustion is implemented on a heavy-duty diesel truck.

Emission measurement of internal combustion engines for both research and regulatory purposes is most often done in a laboratory setting. These conditions are valuable for detailed calibration and repeatability, but ultimately it is the emissions produced in real-world use that matter. On-road testing may subject the engine to operating conditions not represented in laboratory testing protocols, and this can reveal real emissions which greatly exceed what is predicted by lab testing. On-road emission testing is a growing field which can serve to make future iterations of standardized testing more representative of real driving conditions and thereby reduce real-world emissions.

This thesis brings together these key ideas: testing a novel combustion technology under on-road operating conditions to assess its real-world impact.

1.1 Thesis Objectives and Overview

The overall objective of this research work is to answer the question: *what is the effect of hydrogen substitution on the engine-out CO_2, NOx, and PM output of a heavy-duty diesel truck under real-world conditions?*

To achieve that objective the thesis is made up of the following sections:

Chapter 2: Background and Literature Review begins with a review of hydrogen/diesel co-combustion and its expected effects on CO_2 NOx, and PM emissions, an overview of diesel aftertreatment technologies, and finally a review of on-road emission testing and the portable emissions measurement systems (PEMS) used to achieve it. The major gaps in the literature are summarized and the thesis objectives are detailed.

Chapter 3: Experimental Setup details the development of the PEMS system which was designed and built for this project.

Chapter 4: Data Collection and Processing covers details of the field campaigns done to collect data and the steps taken to process it.

Chapter 5: Results and Analysis gives a detailed look at the emissions recorded, their sensitivity to changes in operating conditions and measurement error.

Chapter 6: Summary, Conclusions, and Future Work addresses the original objectives, presents additional discoveries, and recommends future research.

Chapter 2 - Background and Literature Review

This section presents the relevant background in two areas: *Section 2.1* reviews hydrogen/diesel co-combustion, *Section 2.2* reviews the relevant diesel emission control technologies, while *Section 2.3* reviews on-road emission measurement.

2.1 Hydrogen/diesel Co-Combustion

Fossil fuels including diesel are used extensively worldwide in the combustion engines that power land, sea, and air vehicles. Although convenient and reliable, the combustion of fossil fuels in these applications is a major source of air pollution and GHG emissions. Hydrogen is an appealing alternative fuel for combustion engines because pure combustion of hydrogen produces only water as a product, as shown in **Equation 2-1**.

$$2H_2 + O_2 \rightarrow 2H_2O \qquad (2\text{-}1)$$

Hydrogen can be produced from a variety of non-renewable and renewable sources, the later preferable from a GHG reduction perspective. Often hydrogen as a fuel is equated with reaction in a fuel cell which produces electricity and in turn drives an electric motor. While this has an efficiency advantage over a hydrogen internal combustion engine (ICE), using hydrogen in a combustion engine has other benefits: it utilizes proven and less expensive ICE powertrains with relatively small modifications, and it does not require the hydrogen purity needed by a fuel cell [2]. The last point has implications for potential sources of hydrogen. These sources include fossil fuels through steam methane reforming, renewable energy via electrolysis, or capturing hydrogen as a waste product from industrial chemical production. The latter two options are preferred from a lifecycle GHG reduction perspective. In particular, the truck which is the subject of this research project is intended to be fueled by waste hydrogen. The lower purity requirement of a hydrogen ICE gives an advantage over a hydrogen fuel cell in this application.

Hydrogen has been investigated for use as a fuel for both spark ignition and compression ignition internal combustion engines [2]. The following background will focus, however, on that which is most applicable to the subject of this thesis: a hydrogen/diesel compression ignition engine in a heavy-duty truck.

To understand the effects of burning hydrogen in a compression ignition engine, it is helpful to compare its properties to that of diesel fuel, as presented in **Table 2-1**. Many of the effects discussed in the proceeding sections will trace back to these properties.

Table 2-1: Fuel properties comparison [2]

Property	Diesel	Hydrogen
Lower Heating Value [MJ/kg]	43	120
Stoichiometric A/F ratio	14.5	34.2
Energy Density at STP [MJ/m^3]	35,800	10.3
Autoignition Temperature [K]	530	858
Cetane Number	48-50	0
Flame Speed [m/s]	0.3	2.65-3.25
Flammability Limits [% vol.]	0.7-5	4-75
Density at STP [kg/m^3]	848	0.0083
Diffusivity [cm^2/s]	0.038	0.63
Adiabatic Flame Temperature [K]	2100	2483
Specific CO_2 emissions [kg/kg_{fuel}]	3.16	0

Most notable for a compression ignition engine are two factors: autoignition temperature and laminar flame speed. In a spark ignition engine, high autoignition temperatures give beneficial knock resistance. In a compression ignition engine, however, this high autoignition temperature can inhibit ignition, which can lead to excessive ignition delay that can ultimately cause misfire [2]. Once combustion is initiated, hydrogen's high laminar flame speed leads to faster cylinder pressure rise and higher peak cylinder pressures. If peak cylinder pressure exceeds the mechanical strength of the engine components, damage will occur. Together these factors limit the operating range of a pure hydrogen compression ignition engine and make it very difficult to implement in a real-world application such as a heavy-duty truck. Instead the present approach is a dual-fuel engine, where diesel injection provides the timing control but the total quantity of diesel is scaled back and hydrogen is burned instead. The amount of energy supplied by the hydrogen, often called the substitution ratio, is calculated as shown in **Equation 2-2**.

$$Substiution\ ratio = H_2\ energy\ fraction = \frac{\dot{m}_{hydrogen} LHV_{hydrogen}}{\dot{m}_{hydrogen} LHV_{hydrogen} + \dot{m}_{diesel} LHV_{diesel}} \quad (2\text{-}2)$$

Where $\dot{m}_{hydrogen}$ and $\dot{m}_{diesel}$ are the respective fuel mass flows delivered to the engine and $LHV_{hydrogen}$ and LHV_{diesel} are the lower heating values of each fuel. This method of representing hydrogen displacement, on a per energy input basis, is common in the reviewed literature and is what will be used throughout this thesis.

The dual-fuel configuration reduces but does not eliminate the challenges of implementing hydrogen in a compression ignition engine. In a dual-fuel engine, Hailin et al [3] found that hydrogen caused an increased ignition delay at low loads and an increase in peak cylinder pressures at high loads. Sandalci and Karagoz [4] also found that peak cylinder pressure and peak heat release rates increase with increased hydrogen substitution. Zhou et al. [5] tested 10-40% energy H_2 displacement on a 4 cylinder naturally aspirated diesel and found increased heat release rate and peak cylinder pressure, along with increased ignition delay in most cases but reduced ignition delay in the highest load cases. Wu and Wu [6] found that substituting 10-20% hydrogen on a single cyclinder engine increased ignition delay and peak cylinder pressure. Tsujimura and Suzuki [7] observed abnormal combustion in a hydrogen/diesel engine as hydrogen displacement reached and exceeded 50%. Overall ignition delay and increased peak cylinder pressure limit the amount of hydrogen displacement possible on a retrofitted diesel compression ignition engine. In the case of the truck used in this project, the 40% peak displacement chosen by the third party calibrator matches closely with many of the previously mentioned experiments

Hydrogen may be injected directly into the cylinder or introduced indirectly via the incoming air charge by injection into the intake manifold or intake ports. The later setup is more common as it is simpler and cheaper to implement because it does not require a high-pressure hydrogen fuel injector and supporting system. Indirect injection is used on the truck in this study. An important consequence of indirect hydrogen injection is the displacement of intake air. This effect is typically presented as hydrogen volume fraction, as calculated in **Equation 2-3**.

$$H_2 volume\ fraction = \frac{\dot{v}_{hydrogen}}{\dot{v}_{hydrogen} + \dot{v}_{air}} = \frac{\dot{m}_{hydrogen}/\rho_{hydrogen}}{\dot{m}_{hydrogen}/\rho_{hydrogen} + \dot{m}_{air}/\rho_{air}} \quad (2\text{-}3)$$

Where $\dot{v}_{hydrogen}$ is the volumetric flow rate of the inducted hydrogen and $\dot{v}_{air}$ is the volumetric flow rate of the incoming air charge. Note that hydrogen's low density means that even a relatively

low mass flow rate of hydrogen can make up a large volume fraction of the total intake charge entering the engine. As some studies define experimental test points in terms of hydrogen volume fraction instead of the substitution ratio, it is useful to compare the two. To convert from substitution ratio to hydrogen volume fraction requires knowledge of the global equivalence ratio, as calculated in **Equation 2-4**. **Figure 2-1** illustrates the comparison for a range of typical equivalence ratios found in a CI engine.

$$\phi = \frac{\dot{m}_{hydrogen} \cdot A/F_{hydrogen} + \dot{m}_{diesel} \cdot A/F_{diesel}}{\dot{m}_{air}} \quad (2\text{-}4)$$

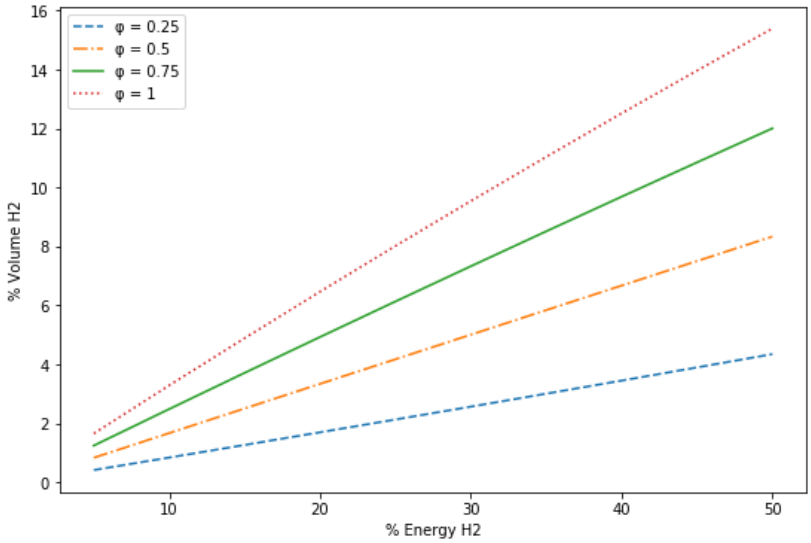

Figure 2-1: Hydrogen volume displacement vs energy displacement

As shown in **Figure 2-1**, the volume fraction of hydrogen becomes significant at higher engine loads and substitution ratios. This is important because the volume occupied by the hydrogen replaces that amount of incoming air. Oxygen in the incoming air is ultimately the limiting combustion reactant, so hydrogen displacement via port injection will limit peak power output. As is the case for the truck tested in this research project, hydrogen substitution may need to be varied across the operating range, scaled back when high engine power is required. In addition, displacement of intake air can also impact pollutant formation, which will be discussed further in *Sections 2.1.2 and 2.1.3*.

2.1.1 H_2 Effect on Efficiency and CO_2

Hydrogen is carbon-free fuel and will produce no CO_2 when burned, thus CO_2 output should decrease at the same rate as hydrogen substitution. If brake specific carbon dioxide output is the quantity of interest [CO_2 g/kW.h], however, some care must be exercised in this assumption. As shown in **Equation 2-5** and **Equation 2-6**, that is only true if the brake thermal efficiency (BTE) stays the same.

$$BSCO_2 = \frac{\dot{m}_{CO_2}}{T\omega} \quad (2\text{-}5)$$

$$BTE = \frac{T\omega}{\sum \dot{m}_{fuel} LHV_{fuel}} \quad (2\text{-}6)$$

Where $BSCO_2$ is the brake-specific CO_2 output in [g/kW.h], $\dot{m}_{CO2}$ is the mass flow of CO_2 in [kg/hr], T is the measured engine torque in [N-m] and ω is the engine rotation speed in rad/s.

On a single-cylinder research engine, Tsujimura and Suzuki [7] found that hydrogen decreased thermal efficiency at low loads but increased it at high loads. Based on analysis of measured heat release curves, they attributed the efficiency loss at low loads to hydrogen passing through the combustion chamber unburned, a phenomenon referred to as hydrogen slip, although they did not measure hydrogen concentration in the exhaust directly. At high loads, they attributed the increased thermal efficiency to advanced combustion phasing.

Liew et al [8] found that lab testing of hydrogen substitution on a 6 cylinder, 11L heavy-duty diesel engine reduced CO_2 output mostly in proportion to the displacement ratio but with some additional benefit coming from increased thermal efficiency. In their testing of 0-46% hydrogen substitution on a single-cylinder research engine, Sandalci and Karagoz [4] found that CO_2 output decreased beyond the hydrogen substitution rate, indicating an increase in thermal efficiency.

Besides CO_2, the alternative products for the carbon in the diesel fuel include carbon monoxide (CO), particulate matter (PM), and unburned hydro carbons (THC). All of these should be very small relative to CO_2 and, except for PM, are not measured in this study. Other researchers [8], [4], [9] have found that hydrogen substitution in a hydrogen/diesel dual fuel engine decreases emissions of CO and THC, suggesting that the addition of hydrogen may enhance the combustion of the diesel fuel.

2.1.2 H_2 Effect on NOx Production

An unintended and harmful byproduct of internal combustion engines is the production of Nitric Oxide (NO) and Nitrogen Dioxide (NO_2), herein referred to together as NOx. The dominant source for NO production in internal combustion engines is the extended Zeldovich mechanism [1] [10], as shown in **Equation 2-7, Equation 2-8, and Equation 2-9.**

$$O + N_2 \rightleftharpoons NO + N \quad (2\text{-}7)$$

$$N + O_2 \rightleftharpoons NO + O \quad (2\text{-}8)$$

$$N + OH \rightleftharpoons NO + H \quad (2\text{-}9)$$

The Zeldovich NOx mechanism is also often referred to as thermal NOx as it depends strongly on temperature, with significant NOx formation occurring above 1800 K [1]. For internal combustion engines most of the NOx will be NO, however, Heywood [10] cited experimental results where NO_2 formed 10-30% of the total NOx in a compression ignition engine operating at low load. Upon entering the atmosphere, NO will gradually turn into NO_2 through reaction with ozone.

In terms of thermal NOx formation, hydrogen has several, potentially competing, effects. Hydrogen's higher adiabatic flame temperature (AFT) can drive the peak cylinder temperature higher and therefore increase NOx emissions. Conversely, once combusted hydrogen's product (water vapour) offers a high heat capacity it may moderate temperature rise and, in the case of indirect hydrogen injection, the displacement of intake air means less surplus air to form NOx.

NOx emissions from hydrogen/diesel co-combustion has been studied by numerous researchers in a laboratory setting. In lab experiments with 0-6% volume addition of hydrogen to an 11L, 6 cylinder engine, Yang et al [11] found that NOx emissions increased notably with hydrogen substitution rate. In experiments of 0-20% hydrogen substitution on a single cylinder research engine, Wu and Wu [6] noted a sharp increase in NOx emissions but only at higher loads when the in-cylinder temperature exceeded a threshold of about 1600 K. In experiments on a supercharged single cylinder research engine, Talibi et al [12] found increased NOx but only when the hydrogen substitution ratio exceeded 10%. Testing a 6 cylinder 11L engine with up to 50% hydrogen substitution, Li et al [3] noted no NOx increase up to 16% hydrogen substitution vs plain diesel but greatly increased NOx emissions at higher substitution ratios.

Tsujimura and Suzuki [7] found that NOx increased but not significantly and suggested that decreased oxygen availability and increased in-cylinder heat capacity were moderating factors. Sharma and Dhar [13] found that at 20% hydrogen substitution and 75% load NOx output increased but at all other test points, which were lower hydrogen substitution and/or lower load, that NOx output decreased versus the diesel baseline. Zhou et al [5] found NOx decreased at low loads and increased at high loads. Wu and Wu [6] found decreased NOx with hydrogen addition at low loads but increased NOx at higher loads. Liew et al [8] found that for hydrogen volume displacements between 0-6% that at 10% load NOx output decreased as hydrogen substitution increased, at 15-30% loads NOx remained roughly the same, while at 50 and 70% loads NOx increased as hydrogen volume increased. Overall it seems that at lower loads and substitution ratios, a temperature increase is either not present or at least not sufficient to increase NOx formation. At higher loads and substitution ratios though, once a certain threshold is exceeded, NOx formation will increase. With that in mind, a critical question is formed: *is this threshold exceeded during real driving conditions?* The answer to that is probably not universal, however, the goal of this research is to determine if that is true for a particular implementation of the technology in a particular real-world application. Therein lies the motivation to measure engine-out NOx emissions with hydrogen substitution under real driving conditions, something which it appears has never been done before.

2.1.3 H_2 Effect on PM Production

Particulate Matter (PM) is another critical emission from diesel engines. PM refers to any fine (<10 μm) inhalable particles or droplets. PM from a combustion source is composed primarily, but not entirely, of black carbon (soot). Notably, PM from a diesel contains traces of engine wear metals and lubricating oil, in addition to black carbon. The source of black carbon is the diesel fuel which undergoes pyrolysis, rather than complete combustion, in the locally rich areas at the core of the diesel jet [10].

Hydrogen substitution can potentially reduce PM formation in several ways. As hydrogen displacement increases the amount of diesel injected decreases, less carbon is available to form PM. Hydrogen's high diffusivity may help to reduce the locally rich pockets by improving charge motion in the cylinder, and its higher adiabatic flame temperature may oxidize the PM before it can exit the cylinder, both of which can reduce PM. Conversely though, at higher displacement rates, indirect hydrogen injection displaces a noticeable amount of intake air, leading to a richer overall mixture and this could be compounded by the faster burning hydrogen out competing the diesel for available oxygen in locally rich areas of the cylinder, potentially increasing PM formation.

Experiments on an 11L 6 cylinder engine by Liew et al. [8] showed reduced PM emissions with the greatest improvement occurring at lower loads and lower substitution rates and tapering off towards no change at 100% load. They attributed the change primarily to the decreased diesel flow rate. It should be noted that in this experiment the engine control unit (ECU) responsible for controlling the diesel injection was not changed from its base calibration, and therefore the gains from hydrogen substitution were likely not optimized. Talibi et al. [12] found significantly reduced PM emissions with 15% hydrogen substitution, little change between 15-30% hydrogen substitution and increased PM above 30% substitution. Sharma and Dhar [13] found up to 20% PM reduction using hydrogen substitution between 5-20%. Yang et al. [11] conducted trials on a 6 cylinder engine and found a notable decrease in PM emissions as hydrogen substitution increased, which they attributed to ignition delay and enhanced diffusion combustion. Zhou et al. [5] found that increasing hydrogen substitution reduced PM in all cases. Wu and Wu [6] also found that PM decreased across the range with hydrogen addition. Sandalcı and Karagöz [4] saw noticeable decrease in smoke (PM) emissions with increasing hydrogen substitution ratio. Talibi et al. [9] saw a decrease in PM at low loads, little change at medium loads, and a slight

increase in PM emissions at high engine loads with the addition of hydrogen. They attributed this to the competing effects of soot formation caused by oxygen deficiency, and oxidation caused by elevated temperature, having different relative strengths at different load points. As with NOx formation, the effect of hydrogen on PM formation seems to have some dependence on load and hydrogen substitution rate. Generally, lab experiment has shown that hydrogen substitution reduces engine out PM emissions with some exceptions occurring at high loads and high hydrogen substitution rates. As with NOx emissions, the motivation to measure on-road PM emissions is now clear: *under real driving conditions does hydrogen substitution decrease or increase engine-out PM emissions?* This research attempts to answer that question for one specific deployment of hydrogen/diesel co-combustion technology in a heavy-duty truck application.

2.1.4 Summary of Hydrogen Substitution Effects

According to the literature reviewed in the previous sections, substituting hydrogen for diesel in a compression ignition engine can have the following effects, as summarized in **Table 2-2**.

Table 2-2: Summary of hydrogen substitution effects

Emission	H_2 effects that increase emission	H_2 effects that decrease emission	Overall effect
CO_2	-	H_2 is carbon-free fuel	Decrease
NOx	Higher adiabatic flame temperature Higher flame speed	Displacement of oxygen Higher heat capacity of products High diffusivity	Usually increase
PM	Displacement of oxygen Higher flame speed	Less carbon available Higher adiabatic flame temperature	Usually decrease

2.2 Diesel Emissions Control Systems

In order to meet regulatory emission limits for on-road use, modern diesel engines are equipped with dedicated emission control systems, often called diesel aftertreatment systems. A block diagram of a typical aftertreatment system with key emissions reduced at each step is presented in **Figure 2-2**.

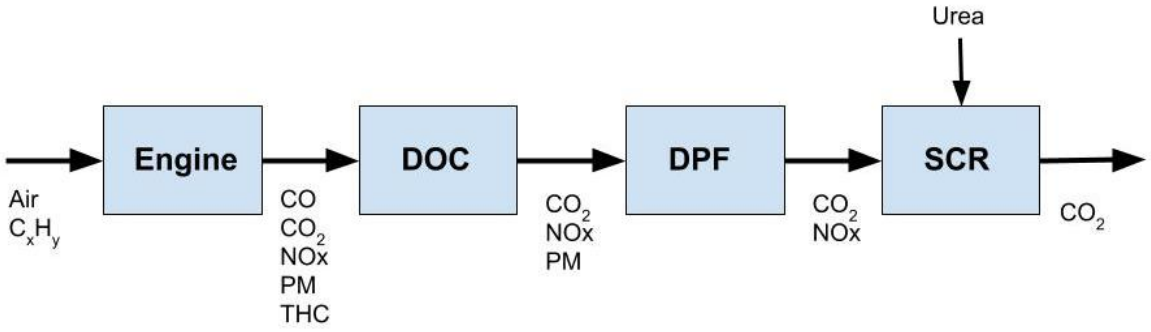

Figure 2-2: Diesel aftertreatment system schematic

Virtually all diesel vehicles manufactured for North American and European markets now use this configuration to meet the increasingly strict criteria emission limits for diesel engines (as shown in **Figure 2-3**, but note that such an aftertreatment system will not reduce CO_2 output. The following sections will briefly discuss the DOC, DPF and SCR in order to provide context for subsequent discussions on raw NOx and PM values.

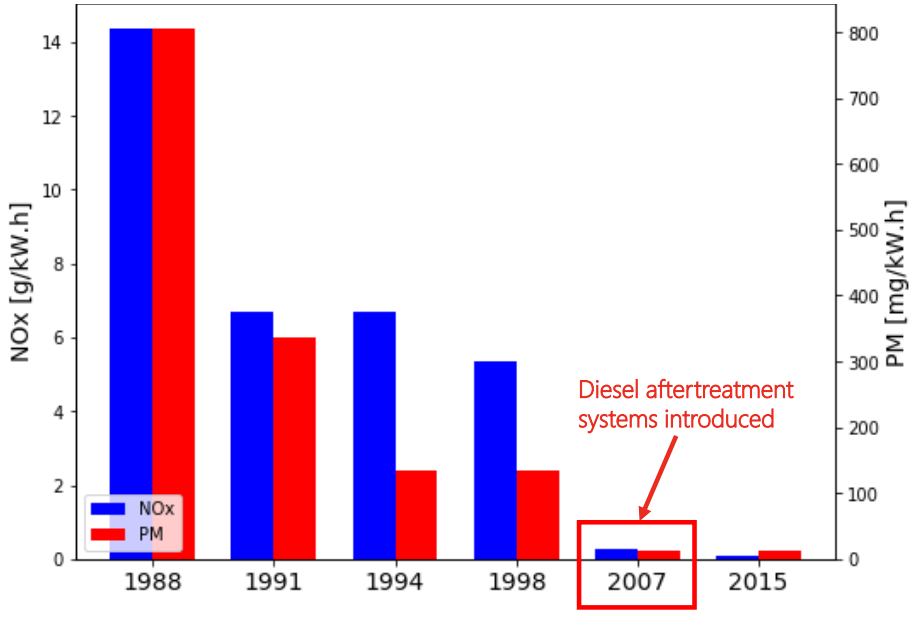

Figure 2-3: EPA heavy-duty emissions by year

2.2.1 Diesel Oxidation Catalyst

After fuel and air is burned in the engine, the first treatment occurs in the Diesel Oxidation Catalyst (DOC). In the DOC, unburned fuel (THC) and carbon monoxide is converted to CO_2. In addition, NO will tend to be converted to NO_2, which has implications to the downstream aftertreatment components but causes no net reduction in NOx emissions [14]. This inability to reduce NOx is the key difference between a DOC and the three-way catalyst (TWC) used on gasoline engines operated at stoichiometric conditions. The lean fuel-air mixture in diesel engines prevents a DOC from reducing NOx to O_2 and N_2 the way a TWC can. Therefore, a dedicated NOx control technology is needed.

2.2.2 Diesel Particulate Filter

After exiting the DOC, exhaust enters the Diesel Particulate Filter (DPF). The DPF is typically a wall flow design, where exhaust passes through the filter which is parallel to the direction of flow. A typical pore size on a DPF is several microns, much larger than the diameter of typical diesel PM. The DPF therefore does not operate as a sieve, instead Brownian diffusion is the dominant deposition mechanism for most of the particles [1]. Both these attributes help to give the DPF high loading capacity, but nevertheless it will still rapidly fill up with PM. As the filter load increases so does the pressure drop across it. This increases exhaust backpressure which decreases engine power and efficiency. Eventually the restriction becomes too great and the accumulated PM must be burned off the filter in a process called regeneration, or more specifically active regeneration. Active regeneration is accomplished by injecting extra unburned diesel fuel either with late injection timing to the engine, or a with dedicated separate injection nozzle in the exhaust system. This fuel will then burn in the DOC and cause a sufficiently high temperature in the DPF to oxidize the PM. With either arrangement, engine power is reduced and fuel consumption is increased while an active regeneration is happening. In the most severe cases an active regeneration must take place while the vehicle is parked [15].

In addition to this active regeneration, passive regeneration occurs when conditions are present to oxidize the PM accumulated on the DPF without actively injecting more diesel fuel. Namely higher exhaust gas temperatures and higher levels of NO_2 tend to bolster passive DPF regeneration, and thereby provide the benefit of less active regenerations [1] [14].

2.2.3 Selective Catalytic Reduction

In the final stage of the aftertreatment system, exhaust gas enters the Selective Catalytic Reduction (SCR). Diesel Exhaust Fluid (DEF) is aqueous urea, which readily decomposes when injected into hot exhaust to supply ammonia [16]. The NH_3 may then react with NOx as shown in **Equation 2-10, Equation 2-11 and Equation 2-12** to produce nitrogen and water vapour.

$$4NO + 4NH_3 + O_2 \rightarrow 4N_2 + 6H_2O \quad (2\text{-}10)$$

$$2NO_2 + 4NH_3 + O_2 \rightarrow 3N_2 + 6H_2O \quad (2\text{-}11)$$

$$NO + NO_2 + 2NH_3 + O_2 \rightarrow 3N_2 + 3H_2O \quad (2\text{-}12)$$

Equation 2-10 tends to dominate because the majority of NOx molecules are NO. However, **Equation 2-12** is a faster reaction, so a higher NO_2/NO ratio may assist overall NOx conversion at lower temperatures when all reaction rates are lower [17].

2.2.4 Exhaust Gas Recirculation

In addition to the diesel aftertreatment system, Exhaust Gas Recirculation (EGR) is a technique for controlling engine-out NOx emissions. Exhaust gas is redirected back to the intake side of the engine and displaces a portion of the incoming intake air as shown in **Equation 2-13**.

$$EGR = \frac{\dot{m}_{egr}}{\dot{m}_{egr} + \dot{m}_{air}} \quad (2\text{-}13)$$

Where EGR is the exhaust gas recirculation rate as a fraction of the total intake charge entering the cylinder, $\dot{m}_{egr}$ is the mass flow of the recirculated exhaust and $\dot{m}_{air}$ is the mass flow of the incoming fresh air. EGR provides NOx control by limiting peak temperatures and oxygen availability in the cylinder, although the second factor can increase PM production [10] [1]. In studies of hydrogen/diesel co-combustion, researchers Talibi et al [9] found that careful control of the EGR rate could be used to moderate or eliminate NOx increase and also reduce PM at hydrogen substitution rates of up to 10%. Shin et al. [18] found that, under low load and high EGR conditions, hydrogen substitution reduced NOx production compared to the diesel baseline. In their testing of a 6-cylinder Mack heavy-duty engine however, Liew et al. [8] found that changes in EGR commanded by the base diesel ECU could trigger unexpected NOx spikes until the supplemental hydrogen controller could react to the change.

2.3 On-Road Emission Measurement

This section provides the context and motivation for on-road emission measurement and for the specific approach taken in this research project. *Section 2.3.1* explains the current in-lab engine dyno certification procedure for heavy-duty engines, *Section 2.3.2* outlines the limitations to this approach and the motivation for on-road testing, while *Section 2.3.3* provides the necessary background in portable emissions measurement systems (PEMSs) to justify the custom PEMS that was developed for this work.

2.3.1 Heavy-Duty Engine FTP Certification

In Canada, heavy-duty trucks with a CGVW greater than 6350 kg are emission certified in accordance with the American Federal Test Procedure (FTP) for heavy-duty engines. Unlike light-duty vehicles, this certification is performed on an engine dynamometer and the emission limits are defined in terms of power output [g/kW.hr] or [g/BHP.hr]. The cycle, as shown below in **Figure 2-4**, takes the engine through a variety of speed and load points intended to represent real-world use.

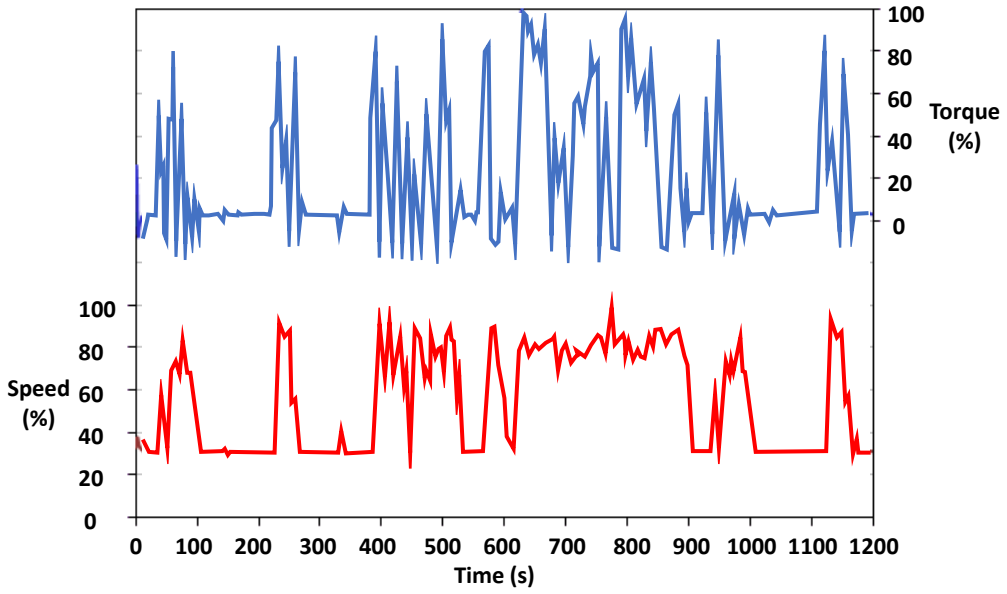

Figure 2-4: FTP for heavy-duty engines (adapted from [19])

The test is performed once from cold start and then at least 3 times from hot start. The cold start and average hot start results are then multiplied by 1/7 and 6/7 respectively and added together

to give emission number for that engine [20]. For consistency between tests, lab conditions are maintained at sea level, 77 ^{o}F, and controlled humidity [21]. The World Harmonized Test Cycle (WHTC) is a similar transient cycle for engine dynamometer testing utilized for Euro VI heavy duty engine certification. FTP and WHTC both regulate CO, THC, NOx, and PM emissions. The central question behind the FTP, WHTC, or any standardized laboratory emission test, is: *how well do the emissions measured in lab represent the emissions produced in the real world?*

2.3.2 On-Road Testing: Motivation and Procedures

A limitation of the standardized test cycle is that it may not accurately model real driving conditions. Changes in the drive cycle can notably change the emissions output to the environment. For example, in their on-road emissions measurement of 7 China III and China IV emissions diesel trucks analysis, Wang et al. [22] found that both gaseous emissions and PM increase with Vehicle Specific Power (VSP) [kW/kg], with faster speeds and harder accelerations being responsible for higher VSP and, in the worst cases, doubling some emissions. In a study of 8 heavy-duty diesel trucks using various emission control technologies, Dixit et al. [23], found that NOx emissions were below certification levels during highway cruising conditions but may substantially exceed them during cold starts and low speed operation. In a study of 5 Euro VI heavy-duty trucks using a Semtech-DS PEMS and a modified TSI NPET, Grigoratos et al. [24] intentionally took trucks outside the specified In Service Compliance (ISC) range and found that although all emissions were generally still within regulatory requirements, specific emissions, including NOx and PM, were all noticeably higher when the vehicles were operating at low speeds. In-use monitoring can also detect potentially unexpected consequences of alternative technologies or control strategies. For instance, a study by Cao et al. [25] found that, although CO_2 output and diesel consumption was cut 13-26%, a diesel-electric hybrid excavator had 26-27% higher in-use PM emissions versus the equivalent diesel excavator from the same manufacturer despite the two machines both being rated to the same power and certified to the same Tier 3 emissions level. Changes in the in-use operating range of the diesel engine, including a lowered idle speed, were the suspected culprit and these changes were not predicted by the test cycle. In-use testing can also detect changes to vehicles emission output over time. For example, during a detailed multi-year road side emissions study conducted at multiple locations in Southern California, Oreble et al [26] found that the on-road PM emissions of first generation DPF equipped trucks increased as the trucks aged, suggesting degradation of DPF performance over time.

One measure to limit real world emissions not captured by the FTP test cycle was the introduction of the supplemental in-use not-to-exceed (NTE) emission limit, as shown in **Figure 2-5**.

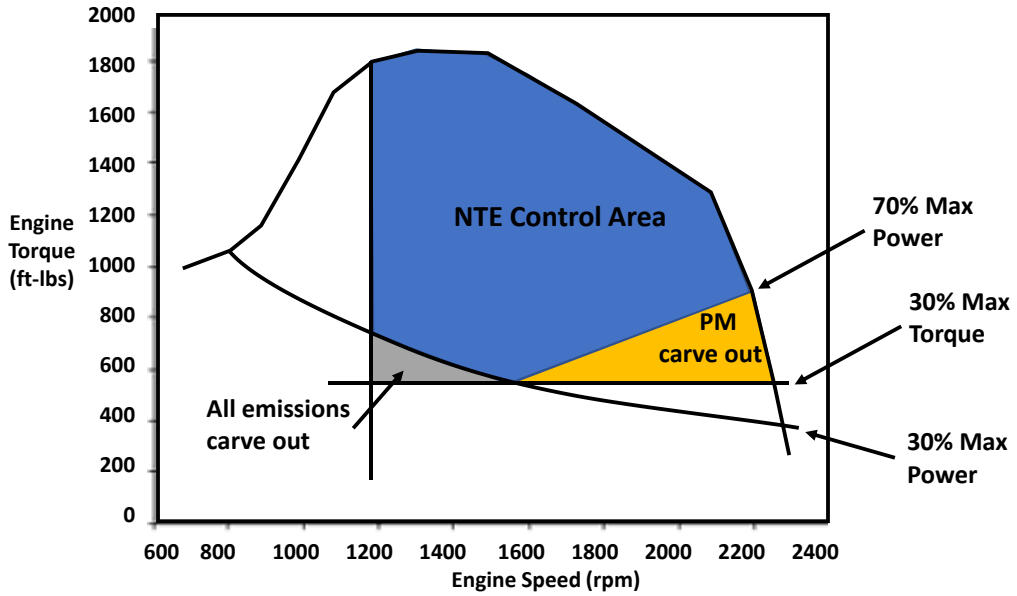

Figure 2-5: Not-To-Exceed emissions control area map (adapted from [27])

The NTE control area is an area within the engine's operating map, defined by speed and torque limitations, where the measured emissions are not allowed to exceed 1.5 times their FTP limit value. Several additional limitations exist on the NTE control area too, minimum temperatures for coolant and intake manifold, and a requirement of averaging over at least 30 seconds in the NTE control area for a valid measurement. The last is perhaps the most significant for an on-road diesel truck application as many driving conditions could preclude the truck from going more than 30 seconds without shifting gear, an event which will go outside the NTE area and exclude the measurement. The aforementioned study of 8 HDDTs using various emission control technologies Dixit et al. [23], found that 90%+ of the urban driving observed did not meet NTE criteria, with the 30 second window requirement providing the greatest impediment. In some cases, for example drayage trucks at the port, none of the observed drive cycle was considered valid by NTE criteria. Euro VI regulations have a similar In Service Compliance (ISC) map with a conformity factor, currently also set at 1.5, above the WHTC value. In both cases, the purpose of this multiplier is to account for the fact that in-use measurements have more inherent error than in lab measurements.

2.3.3 Portable Emissions Measurement Systems

The drive to measure in-use emissions has prompted the development of the portable emissions measurement system (PEMS). There are a variety of commercially manufactured PEMS now on the market which fit into two general categories. The first are units which meet the requirements for compliance testing: as specified in the American Code of Federal Regulations (CFR) Title 40 Part 1065 for North American NTE testing [20] or the European Union Regulation (EC) 595/2009 for the ISC component of Euro VI regulations. These are larger, more complex, and more expensive systems where certification level measurement accuracy is required.

In addition to certification level PEMS, however, several manufacturers have developed non-complaint systems aimed at being smaller, cheaper, and easier to use [28] [29]. While not suitable for certification, these devices are more accessible and allow data to be collected from a greater number of vehicles operating in more varied conditions, to analyze emission trends from different drive cycles or changes in engine calibration and potentially to identify notably high emitters and prompt further testing. The PEMS needed for this research project falls into the second category, with the goal specifically being to identify changes in engine-out, pre-aftertreatment emissions based on hydrogen substitution.

While it appears that no other researchers have taken on-road emission measurements of a hydrogen/diesel heavy-duty truck, several studies have been done with research type PEMS on diesel vehicles. In particular, this review focusses on PEMS which use: non-dispersive infrared (NDIR) CO_2 measurement, electrochemical NOx measurement, and light scattering PM measurement. Johnson et al. [30] compared a Semtech DS PEMS unit to two CFR40 1065 complaint MELs during on-road testing of a 2004 Caterpillar Class 8 truck. They found that the Semtech's NDIR CO_2 measurement consistently overpredicted CO_2 by 4±2%. Yang et al. [31] tested a NTK NCEM mini-PEMS vs a 1065 compliant AVL M.O.V.E. system on a 2012 Duramax light duty diesel pickup and found NOx via the NTK's electrochemical NOx sensor (based on an OEM design) and the NDUV reference to agree within 10%. This suggests that, while not a replacement for reference instruments, electrochemical NOx sensors can be a useful research tool. In a study of both a Class 8 diesel truck on under 6 different drive cycles on a chassis dynamometer and a 350 kW diesel generator [32] tested 4 commercially produced PEMS systems and 4 other PM measurement devices against Federal Reference Methods (FRM) for

CO_2, NOx, and PM. All 4 PEMS tested in this study used NDIR for CO_2 detection. Absolute accuracy fell in the range of -35% to +12%, although all showed good R^2 values of >0.93. In the case of the PEMS which used an electrochemical NOx sensor they found very good correlation (R^2 = 0.998) but that NOx was overpredicted by 12-30%, they attributed 10% of that as a constant offset due to omitted humidity correction. Two light scattering PM measurement methods were compared. The first, which was part of a commercially produced PEMS, read significantly lower PM (-60-80%) than the FRM. The other light scattering instrument, a TSI DustTrak, showed good correlation (R^2 = 0.9) but gave consistently higher results than the FRM (+24-43%). Khan et al. [33] tested a variety of PM-PEMS devices versus UC Riverside's mobile emission reference laboratory (MEL) on a 2008 Cummins Class 8 truck with adjustable DPF bypass, enabling PM between 1-45 [mg/kW.h]. They found that the TSI Dustrak 8530 light scattering instrument gave concentrations about 26% lower compared to the MEL baseline. Correlation was fairly good with an R^2 of 0.74 but the researchers noted relatively poor performance at the lowest concentrations and cited the instruments detection limit as a possible cause. The best performer in the test, a photo-acoustic, unit showed concentrations about 10% below the reference with an R^2 of 0.88. Cheung et al. [34] specifically tested a TSI DustTrak 8250 light scattering photometer against a gravimetric filter sampling on a light duty diesel truck and found that while the DRX provided high sensitivity and fast time response, the correlation between average PM measurement from the photometer and filter collections was found to vary depending on engine operating conditions. From this they concluded that the DustTrak is sensitive to changes in particle properties.

Light scattering methods like the DRX can provide instantaneous readouts making them suitable for time resolved measurements. They have a fairly low detection limit, which propagates to about 0.5 mg/kW.h under typical on-road test conditions [35]. Unfortunately, they are sensitive to particle size and composition and while they can be calibrated to improve accuracy [36], the problem is that if the particle size and composition changes, the calibration will no longer be accurate. Furthermore, the smallest particle they can detect is 50-100 nm [35] [36] and therefore will miss many of the smallest particles. Given these limitations of the DustTrak as a PM sensor, a gravimetric measurement of PM was also included as a backup. Gravimetric measurements cannot provide any time or size resolution but can serve to confirm the total integration of the DustTrak's instantaneous concentration reading. Teflon filters were chosen for this task, as glass fiber filters can introduce a noticeable adsorption artifact when used to measure PM in diesel exhaust, as noted by Mamakos et al. [37] in their evaluation of 3

commercially produced partial flow PEMS-PM systems versus 2 full flow reference systems on 5 heavy-duty diesel trucks.

In summary, of the three measurements, CO_2 via NDIR seems the most robust, followed by electrochemical NOx detection, and finally light scattering PM detection. To address the uncertainty around light scattering PM measurement, a secondary PM measurement like gravimetric filter sampling, can be applied.

2.4 Summary, Literature Gap, and Motivation

The effects of hydrogen substitution CO_2, NOx, and PM emissions of a diesel engine have been studied in laboratory settings but never in a real-world application. The effect of hydrogen on NOx and PM emissions seems to have dependency on the engine's operating conditions. The goal therefore is to see the effects of hydrogen substitution under real world operating conditions.

Diesel aftertreatment systems can greatly reduce NOx and PM emissions, but they have no effect on CO_2. Engine out changes in CO_2 will be directly realized in the tailpipe emissions, while changes in tailpipe NOx and PM depend on how the aftertreatment system responds to the engine out emissions. Aftertreatment systems are complicated and may introduce their own emission artifacts. Because of this an important step towards a detailed understanding in tailpipe emissions is to conduct measurement of raw, engine-out emissions.

On-road testing requires a PEMS and has never been done on a hydrogen/diesel heavy-duty truck before. On-road measurement is a growing field though and a variety of PEMS units have been tested on heavy-duty diesel trucks, and these studies provide guidance for designing a suitable unit. Past evaluations have shown that NDIR CO_2 measurement, electrochemical NOx detection, and light scattering PM detection (when backed up by gravimetric measurement) can provide results which are suitable for research purposes.

Chapter 3 - Experimental Setup

This chapter begins with an overview of the test truck and the Portable Emissions Measurement System (PEMS) that was built for the project. Next, details are provided on the measurement instruments and the exhaust sampling system. Finally, the torque measurement and the connections to the truck's on-board computer networks are discussed.

3.1 Experiment Overview

All measurements presented in this work have been collected from the same truck, a 2018 Peterbilt 579 chassis equipped with a Paccar MX13 common-rail diesel engine and an Eaton-Fuller automated 18-speed transmission. The truck is one unit of a larger fleet and runs in regular service in that fleet, where it pulls bulk cargo B-train trailers, as shown in **Figure 3-1**. Operating combined gross vehicle weight (GCVW) during testing was 20,000 kg with empty trailers, and 60,000 kg with the trailers fully loaded.

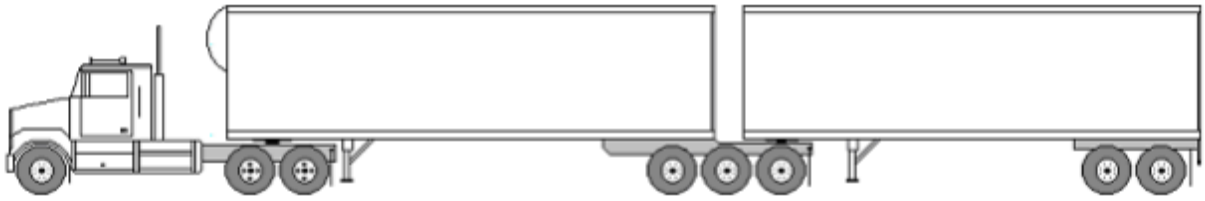

Figure 3-1: B-train truck example (adapted from [38])

Compared to the standard unit in the fleet, this truck features some specific additions. First is the hydrogen fuel system as added by the industrial partner and calibrated by a third-party engineering company. The key parts include hydrogen storage tanks, intake manifold fuel injectors, and hydrogen injection controller. Details on this system are limited on request of the industrial partner, but the key attributes are that the system delivers hydrogen to the engine via injection to the intake manifold (as shown in **Figure 3-2**) and that the peak hydrogen substitution rate is 40%.

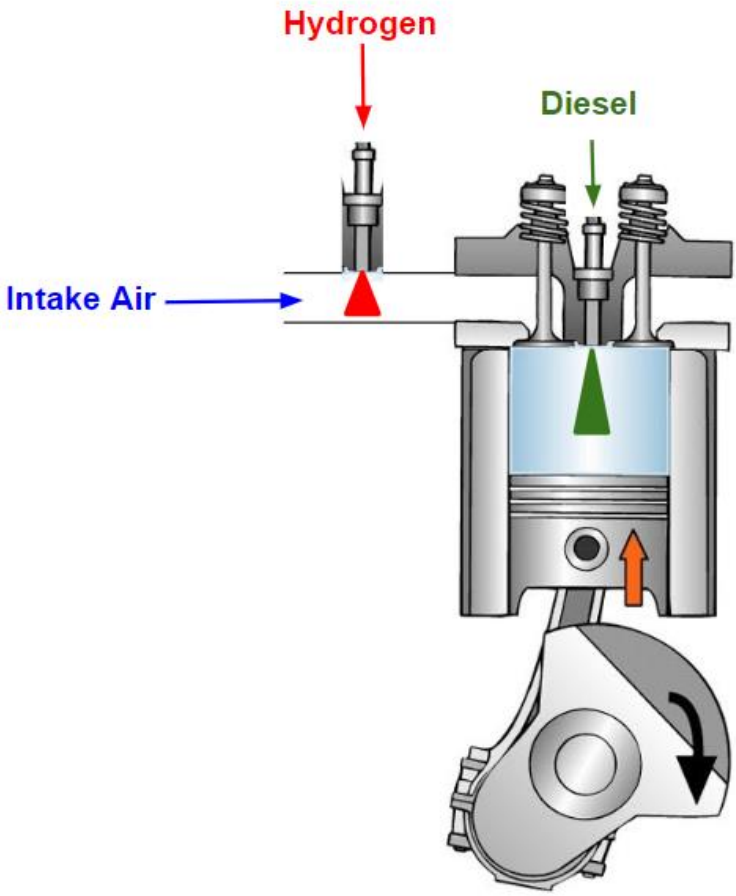

Figure 3-2: Hydrogen/diesel fuel injection arrangement

To enable on-road emission measurement, a custom-built portable emission measurement system (PEMS) is mounted on the truck chassis on a custom, vibration isolated, mounting bracket. Torque is measured on the driveshaft by strain gauges and broadcast via wireless transmitter. A data acquisition system (DAQ) is located in the truck's cab. A test operator rides in the truck along with the driver and runs the DAQ via laptop. The system logs information from the hydrogen fuel system, PEMS, torque transmitter, and the truck's on-board CANbus networks. A GPS is also connected to the system and provides location information at 1 Hz, while all other data is logged at 10 Hz. A custom bracket, including vibration absorbing mounts was designed and built to secure the PEMS on the truck chassis while custom wiring allowed control of key functions from inside the cab. Selected pictures of the truck and PEMS system are shown in **Figure 3-3**, **Figure 3-4**, and **Figure 3-5**.

Figure 3-3: PEMS bracket

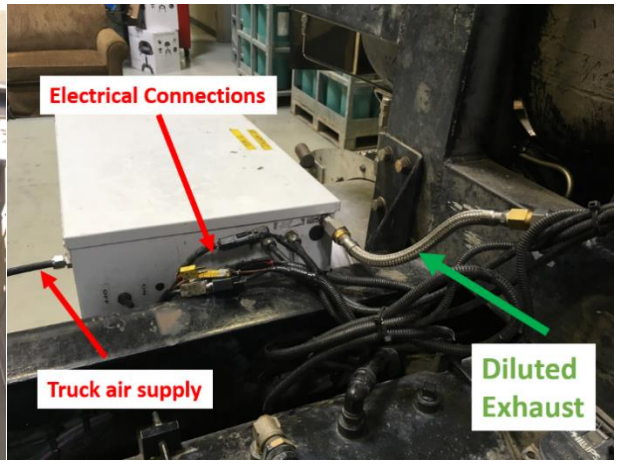

Figure 3-4: PEMS connections

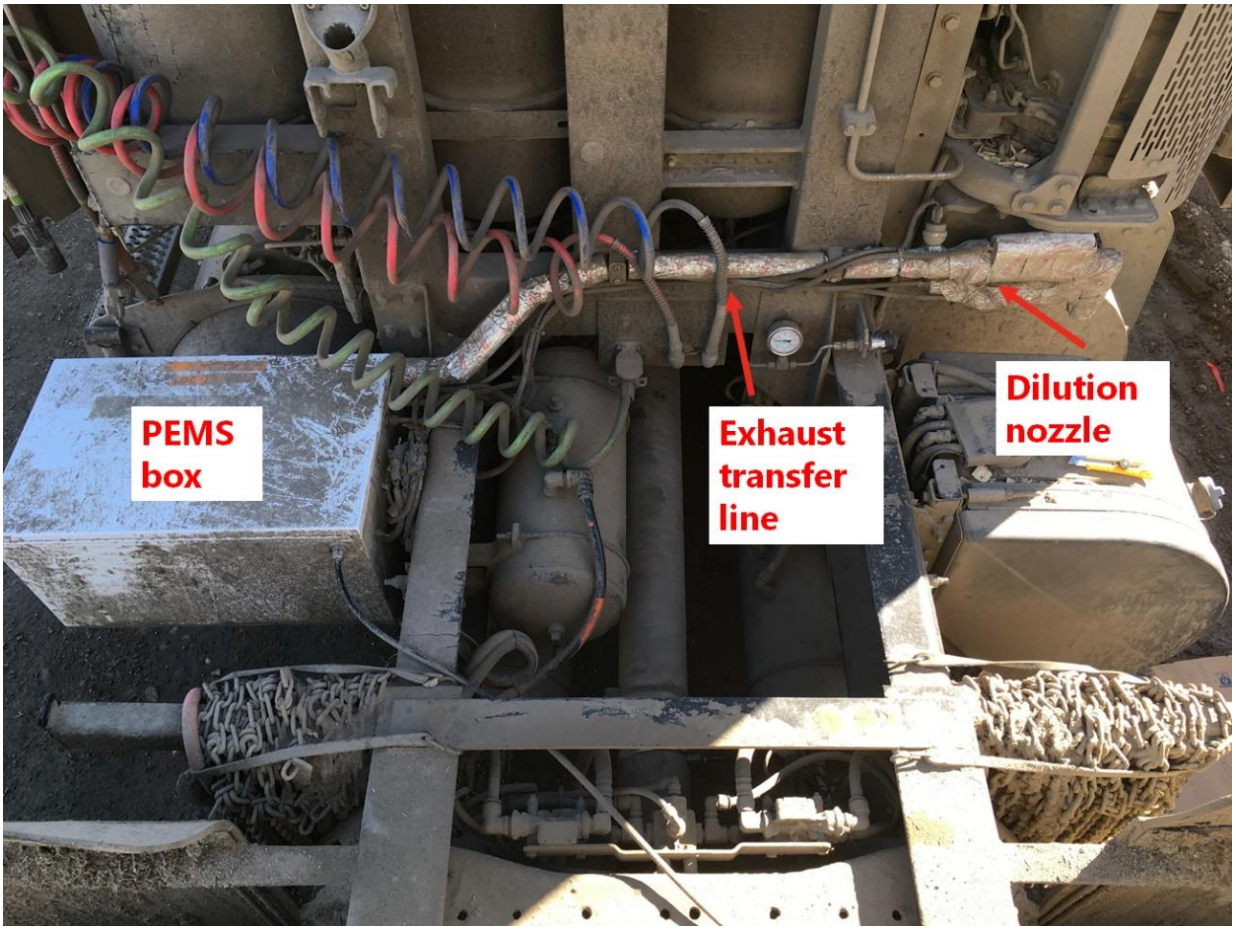

Figure 3-5: PEMS on truck chassis

3.2 Portable Emissions Measurement System

The Portable Emissions Measurement System (PEMS) was designed and built specifically for this project and is made up of the exhaust handling and dilution system, and the measurement instruments. The overall layout is shown in **Figure 3-6**. Note that all emission measurements are made after exhaust exits the truck's engine but before it enters the aftertreatment system. This was done to specifically investigate hydrogen's effect on engine-out emissions. Emissions released to the environment depend on the function of the aftertreatment system and, in the case of NOx and PM, should be substantially lowered for aftertreatment systems equipped with SCR and DPF, as found on the test truck.

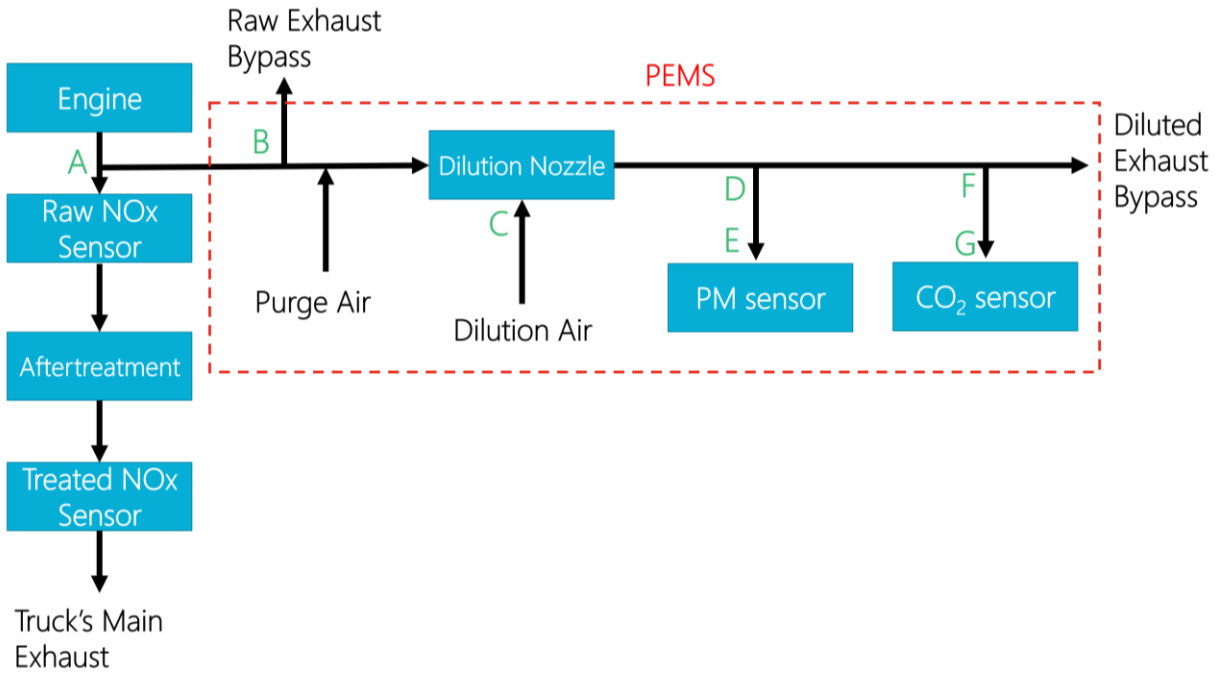

Figure 3-6: PEMS layout

The exhaust gas handling and dilution system includes dilution air preparation, dilution nozzle, system purge valve, and accompanying pressure and temperature sensors. Further details on this system is provided in *Section 3.2.1* through *Section-3.2.4*. The measurement instruments are the truck's OEM electrochemical NOx sensor, the light scattering TSI DustTrak DRX PM monitor, and the LI-COR LI-820 non-dispersive infrared absorption CO_2 sensor. To provide a backup integral PM measurement, Measurement Technologies Laboratories Teflon filters were also used inside the DRXs internal filter cassette. Further details of these instruments are presented in *Section 3.2.5*.

3.2.1 Exhaust Measurement Instruments

3.2.1.1 LI-COR LI-820 CO_2 Analyzer

Carbon dioxide in the exhaust stream was measured by an LI-820 CO_2 meter (LI-COR Biosciences) which operates on the principle of non-dispersive infrared absorption. The LI-820 was chosen for its wide measurement range of 0-20,000 PPM, automatic pressure compensation, and ability to accurately measure CO_2 in the presence of water vapour. This last point is important because the combustion products mean noticeable water vapour in the exhaust, even after dilution with dry air. The LI-820 does not have its own internal pump so a 12V DC diaphragm pump was selected with a flow rate of 1 LPM, this corresponds to the highest flow rate recommended by LI-COR in the interest of reducing exhaust transport time. Lab calibration was performed on the LI-820 against reference CO_2 concentrations, calibration record included in ***Appendix 2***.

3.2.1.2 Electrochemical NOx Sensor

For NOx measurement the truck's OEM electrochemical NOx sensors were used. An electrochemical NOx sensor is made up of two electrochemical pumping cells in series, as shown in **Figure 3-7**. The first cell pumps out O_2 and reduces NO_2 to NO, leaving only NO to converted to N_2 in the second cell. Based on the principle of operation it is clear this sensor will not distinguish between NO and NO_2, instead reporting a combined NOx value. For this experiment engine-out and post-aftertreatment NOx concentrations were recorded from the truck's J1939 messages on the truck's CANbus network.

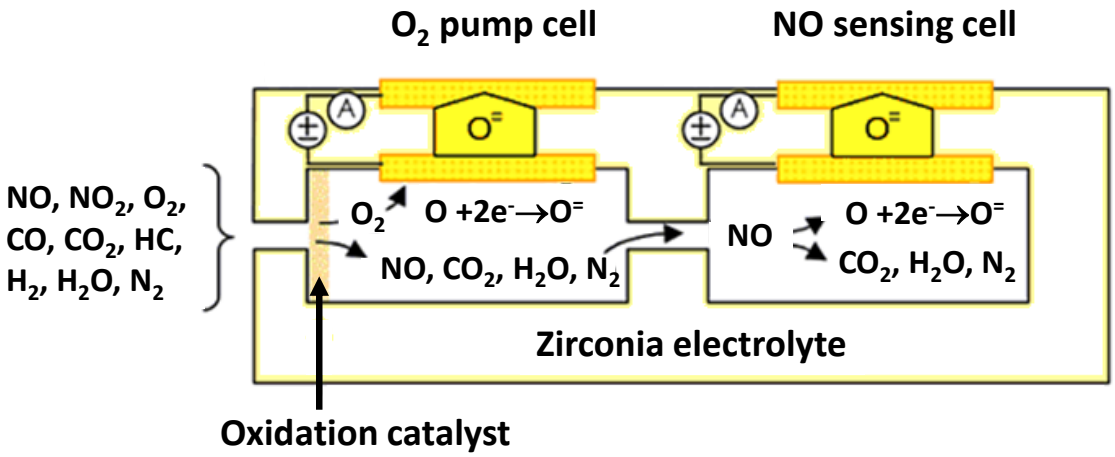

Figure 3-7: Electrochemical NOx sensor schematic (adapted from [39])

Unfortunately, electrochemical NOx sensors are cross sensitive to NH_3 [40], [41], [42]. Cross sensitivity of the outlet NOx sensor to ammonia slip was investigated by [41] and they found that NOx concentration reported by the electrochemical NOx sensor downstream of the SCR was cross sensitive to unreacted ammonia by the relation given in **Equation 3-1**.

$$[NOx]_{sensor} = [NOx]_{real} + K(T)[NH_3] \qquad (3\text{-}1)$$

Where K(T) is a positive scaling factor that increases as temperature increases. Under typical engine operating conditions, the value of K(T) is about 1 [41]. Therefore, care must be taken when the value of an electrochemical NOx sensor is used downstream of the SCR; the measured NOx will be higher than the real NOx if ammonia slip is present.

3.2.1.3 TSI DustTrak DRX

Particulate matter was measured by a DustTrak DRX 8533 (Testing Systems International, St Paul). The DRX measures particulate concentration based on light scattering and provides real time output which makes it well suited for on-road measurements at 10 Hz. DRX instrument output was recorded in two ways: on the National Instruments DAQ via the 0-5 Volt analog output channel, and on the device's internal memory. The first was done to allow easy synchronization with the other measured parameters. The second was done to overcome some shortcoming in the analog output, namely the limited range possible, and thereby to allow direct comparison between integrated DRX values and gravimetric values. The last point is important because while the DRX provides good time resolution, it should not be expected to provide an exact mass concentration measurement. Specifically, the DRXs output is calibrated against the Arizona Road Dust standard [36] and not diesel exhaust PM. Flowrate through the DRX is 3 lpm as provided by the internal pump. The exact flow rate is not important for light scattering measurement, but it is critical for the gravimetric sample. The DRXs flowrate was set before the field campaign with a GilAir Gillibrator precision flow meter and verified after returning to be within 2%. During the campaign flow was checked daily against a rotameter. This did not provide the same accuracy but gave qualitative assurance that the DRXs internal pump was operating correctly during the testing. The DRX repeatability was also verified in lab against a duplicate DRX, presented in **Appendix 2**.

3.2.1.4 MTL Teflon Filters

As a backup to the light scattering based PM measurement provided by DRX, Measurement Technology Laboratories (MTL) gravimetric filters were used to compare run-total PM. The filters used were 37mm MTL Teflon filters, which fit in the DRX internal filters cassette. These filters have low adsorption characteristics [37] [43] and their rigidity makes them relatively easy to use in the field. Pre and post weighing of the filters was done on a 40 CFR 1065 compliant MTL AH500 automated balance with claimed repeatability of =/- 0.5 µg [44] . Several unused travel samples were also weighed before and after to isolate any erroneous environmental effects. Gravimetric filters don't provide the same time resolved PM information as the DRX, however, they can be compared to the integrated value of the DRX over an entire run. This comparison is discussed in *Section 5.8*.

3.2.2 Exhaust Sampling System Design

The gas sampling system is responsible for extracting exhaust from the truck, suitably diluting it, and delivering it to the gas analysis instruments. Suitable dilution of exhaust means to ensure that the following conditions are met: Pollutant concentrations must be at a suitable level for the range of the measurement instruments, sensor saturation must be avoided while also making good use of the available measurement range. Temperature and pressure must be within the limits of the instrument, this is to avoid erroneous reading or damage to the instrument. Humidity must be in a suitable range for the instrument, specifically condensation must be avoided. Raw exhaust gas is too hot for the CO_2 or PM instruments to sample directly and cooling it will cause condensation because of the high water content, especially when hydrogen displacement is high. Therefore, to achieve these requirements, the exhaust must be diluted with clean, dry air. **Table 3-1** presents the relevant constraints and the dilution ratio that was required to achieve them.

Table 3-1: Dilution requirements

Parameter	Highest Predicted Raw Value	Instrument Limit	Dilution required
CO_2	13.1 %	2 %	7:1
H_2O	0.166 g H_20 /g dry exhaust	95% RH @ 20℃	11.5:1
Temperature	400℃	50℃	14:1

Dilution requirements are based on dry dilution air at ambient temperatures up to 40℃. Full calculations are presented in ***Appendix 1***. The highest dilution requirement, based on temperature, is conservative as heat losses in the sampling system are not considered. PM dilution requirements were not calculated as raw PM concentration was unknown. In practice the chosen dilution ratio of about 16:1 seemed to work well for the TSI DustTrak DRX.

3.2.3 Dilution Air Supply and Preparation

Dilution air was provided by the truck's onboard compressed air system. The truck's on-board air preparation system did an acceptable job of removing water and oil from the air, but particle filtration was inadequate. To achieve particle-free dilution air, a two-step filtration system was added: a 5 micron primary filter follow by a 0.01 micron coalescing filter.

Pressure in the truck's on-board compressed air system is nominally 125 psi. In practice though this pressure varies depending on compressor status and other loads on the system. For this reason, a mass flow controller was used to ensure a stable flow of dilution air to the dilution nozzle. The dilution air supply system also incorporates a pressure protection valve to ensure that, in the event of malfunction or failure of the dilution system, the integrity of the truck's overall compressed air system will not be compromised.

To verify that the dilution air stays PM free, as well as to check the background CO_2 concentration at various points during the run, a purge valve was implemented. When the system purges the CO_2 and PM instruments measure the dilution air only, there is no exhaust gas present in the sample. As part of the test protocol system, purges were done multiple times during each test run. Key components of the dilution air prep system can be seen in **Figure 3-8**.

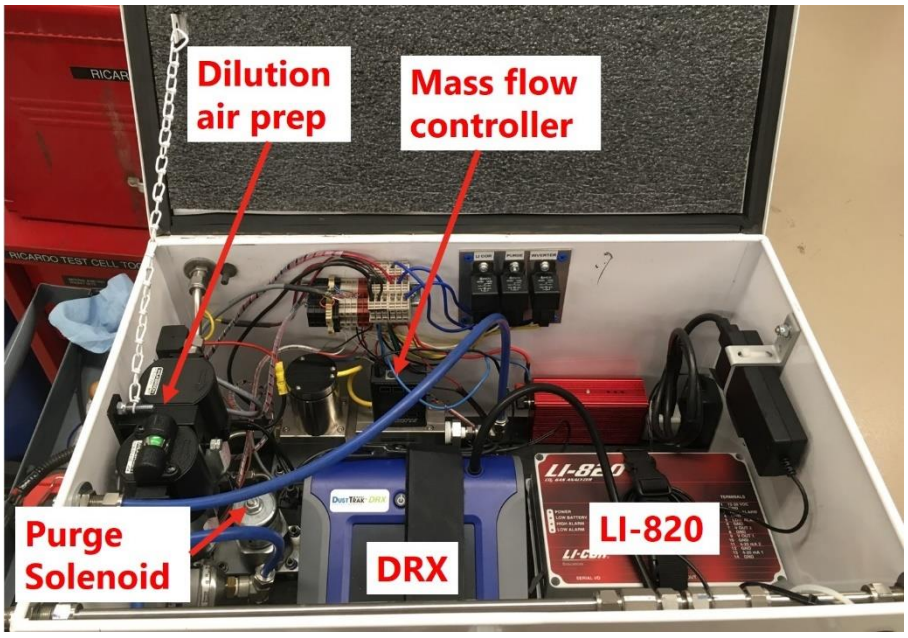

Figure 3-8: PEMS internal components

3.2.4 Dilution System

The key requirement of the dilution system is maintaining a stable dilution ratio over the varying range of engine operation, most notably over a range of exhaust backpressure. Preliminary data logs from the truck indicated back pressure at the inlet to the aftertreatment system, which was the closest point to the PEMS sampling location, was in the range of 0.4-21 kPa. Managing a stable dilution ratio over this wide range was a key design challenge. The diameter and length of the undiluted sample piping A-B (**Figure 3-6**) was selected to control sample flow over the range of expected pressures. The design intent is to keep the pressure at the eductor inlet as close to ambient as possible, while at the same time ensuring there was always enough flow to stop the eductor nozzle drawing in air through the bypass at node B. In addition, this piping was kept as short as possible to keep the system latency as constant as possible and to minimize particle losses (see *Section 3.2.5* and *Section 3.2.6* for further discussion). A small amount of exit tubing was needed to direct bypass gas away from the truck, and a larger diameter was used to minimize pressure fluctuations at the nozzle. Logging pressure upstream of the restrictor plate during testing showed that pressure there only fluctuated about 1 kPa during testing. **Figure 3-9** shows the sampling system on the truck.

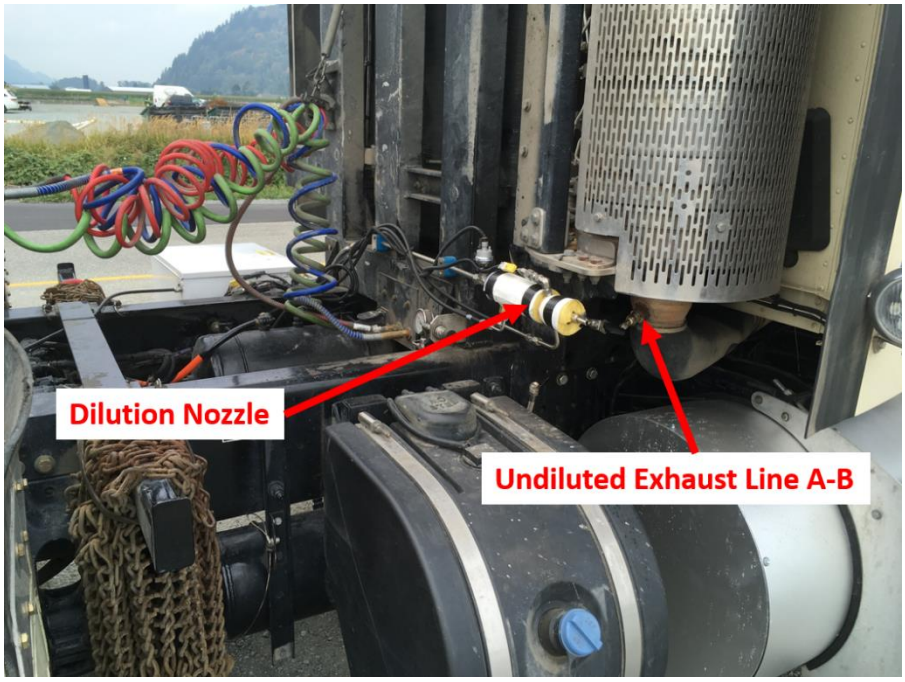

Figure 3-9: Exhaust sampling on truck

For the dilution nozzle itself, several designs were tested. The final design combines an eductor-type nozzle with a restriction orifice on the sampled gas. This was selected because while the intent of the undiluted bypass is to provide sampled gas to the nozzle at ambient pressure, this was not completely possible. Versus an earlier tested version with no restriction orifice, this design is less sensitive to fluctuations in the pressure of the sampled gas. The restriction orifice used has a single hole drilled with a #57 drill bit, giving a nominal diameter of 1.1mm. This size gave good pressure control but was also large enough not to clog with PM during the testing. **Figure 3-10** cutaway view of the nozzle, it was designed to fit inside a standard ½" Swagelock T.

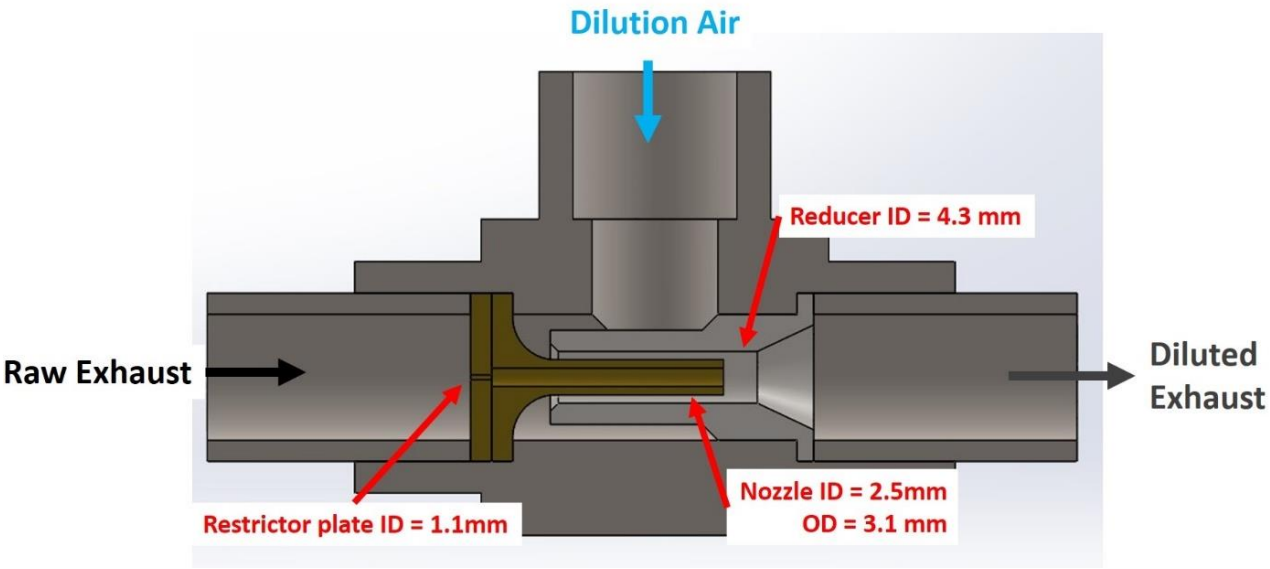

Figure 3-10: Dilution nozzle detail

The actual dilution ratio was provided by the nozzle was verified by running the PEMS system against the AVL Emission Test Systems CEB2 laboratory emissions bench on UBC's single-cylinder research engine (SCRE). SCRE control parameters were adjusted to vary the pressure seen at the nozzle. The results are shown in **Appendix 2**. The function of the dilution system can also be evaluated on truck by running a comparison of the measured CO_2 to expected CO_2. Expected CO_2 is modelled the carbon balance using the measured air and fuel flow data, calculation shown in **Appendix 1,** and the results are presented in **Figure 3-11**.

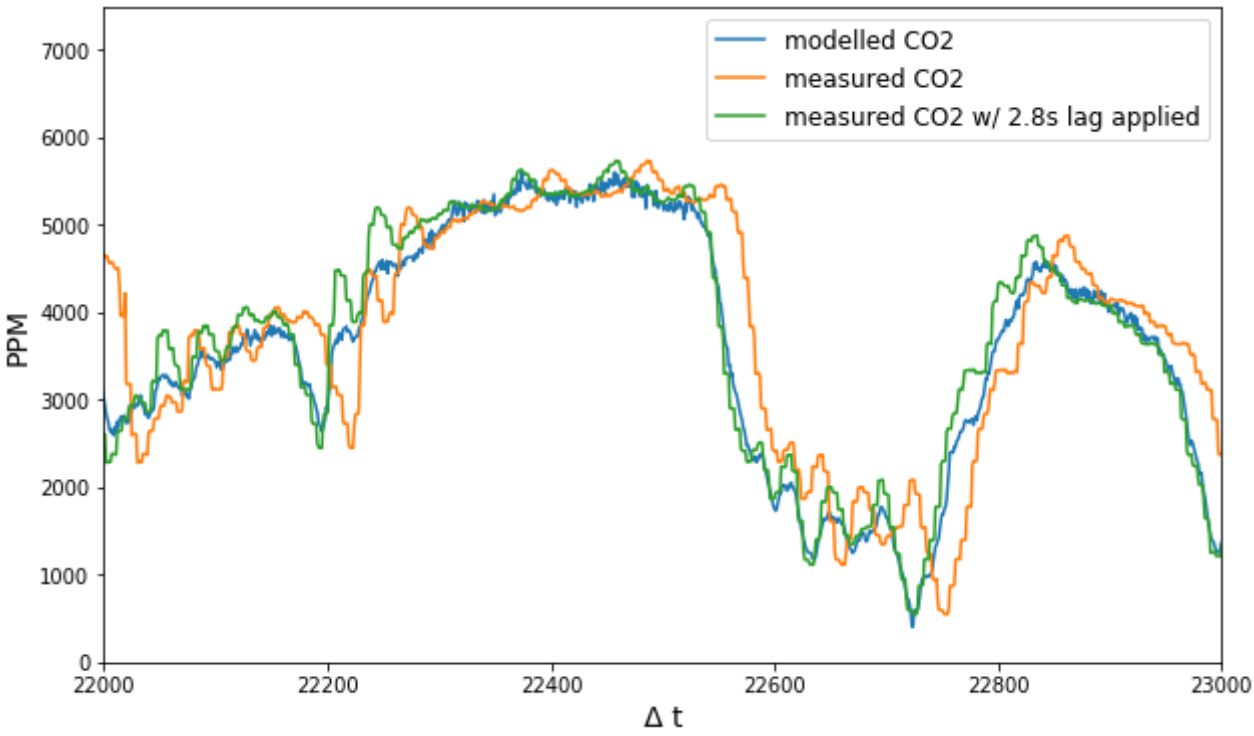

Figure 3-11: Modelled vs measured CO_2

The results show a good agreement between modelled and measured CO_2. A perfect match is not expected given the errors in the measured parameters and some error in the modelling approach itself.

3.2.5 System Latency Design and Testing

The transient nature of on-road testing and the desire to characterize engine emissions in terms of engine speed and load necessitated controlling and measuring system latency. In addition to the response time of each instrument, the PEMS introduces latency based on the gas residence time in the sampling lines.

Between the extraction point and the measurement instruments the exhaust passes through several sections of tubing, as shown in **Figure 3-6**. First undiluted exhaust travels from the extraction point to the dilution nozzle threshold, as shown in Figure 3-6 this is section A-B and section B-C. In section A-B the flow rate is variable dependent on the truck's exhaust back pressure. Variable flow rate means variable latency but by keeping this section short and small diameter the variation in latency is very small, as shown in **Table 3-2**. Although variable, the residence time in line A-B is much shorter than 0.1s across the operating range and therefore system latency can be considered constant at the 10 Hz sampling frequency.

In section B-C the flow rate is controlled by the suction provided by the dilution nozzle. The intent was to make this flow rate constant and, based on verification of the dilution ratio presented in *Section 3.2.4*, this was largely achieved. For the purpose of latency calculations flow rate in section B-C is assumed constant. Sections C-D and C-F are the diluted transfer lines which connect the outlet of the dilution nozzle to the PEMS box. The initial design placed the PEMS box on the truck's right hand frame rail, right next to the exhaust connection point in order to keep this distance short. However, interference with other components on the truck necessitated moving the box to the other side of the truck and therefore required extending the line, as shown in **Figure 3-5**. Backpressure at the dilution nozzle outlet needs to be low for the nozzle to work which required a large diameter tube. The flow rate in these sections is much higher because the 40 lpm dilution air is now added and this helps counteract the larger diameter and extended length. Sections D-E and F-G are the flexible rubber lines which connect the DRX and LI-COR respectively. In these sections flow rate is determined by the instrument's sample pump.

Table 3-2: Calculated system latency

Section ID	Inner Diameter [mm]	Length [cm]	Flow Rate [lpm]	Residence Time [s]
A-B	3.86	15	5-45	0.02 - 0.002
B-C	7.04	15	2.5	0.14
C-D	10.2	180	42.5	0.21
D-E	3	20	3	0.05
C-F	10.2	185	42.5	0.21
F-G	2	26	1	0.13
			DRX Total	0.42
			LI-COR Total	0.69

The residence time calculations presented in **Table 3-2** are based on a plug flow model and neglect all the small geometric details of the system's reducers and T-fittings, and the flow passages within the instrument itself. Such calculations helped to guide the system design but the only way to truly know the system latency was to measure it. To accomplish this latency was tested in two ways. The first was by looking at the signal response created during system purge events. Actuating the purge solenoid causes an instantaneous pressure spike upstream of the dilution nozzle and simultaneously prevents exhaust being drawn into the dilution nozzle. Therefore, looking at the time lag between this pressure spike when the measured PM and CO_2 fall to background levels gives a way to measure latency. Based on purge events the real latency was found to be much longer than the calculations estimated, 2.6s for the DRX and 2.8s for the LI-COR. One explanation is that the simplified plug flow model does not consider any mixing, recirculation, or other flow effects as the exhaust travels through the piping system. Likely more significant, however, is the response time of the instrument itself, something which the residence time calculation doesn't include. The real latency of the system is the summation of the residence time and the instrument response time.

For CO_2 concentration an additional method of verifying the lag is to compare modeled CO_2 output with the measured value, as discussed in *Section 3.2.4* and shown in ***Figure 3-11***.

3.2.6 Particle Loss Estimation

Particle losses are a byproduct of any sampling system. To minimize losses, however, several principles were adhered to when designing and building the sampling system: the number of bends were minimized and bend radii were kept as large as practical, exhaust velocity was maintained via flow rates and tube diameters, and the lines were insulated to try to minimize thermal gradient. Particle loss was estimated using the FlareNet-Particle-Penetration-Calculator [45] and presented below in **Figure 3-12**.

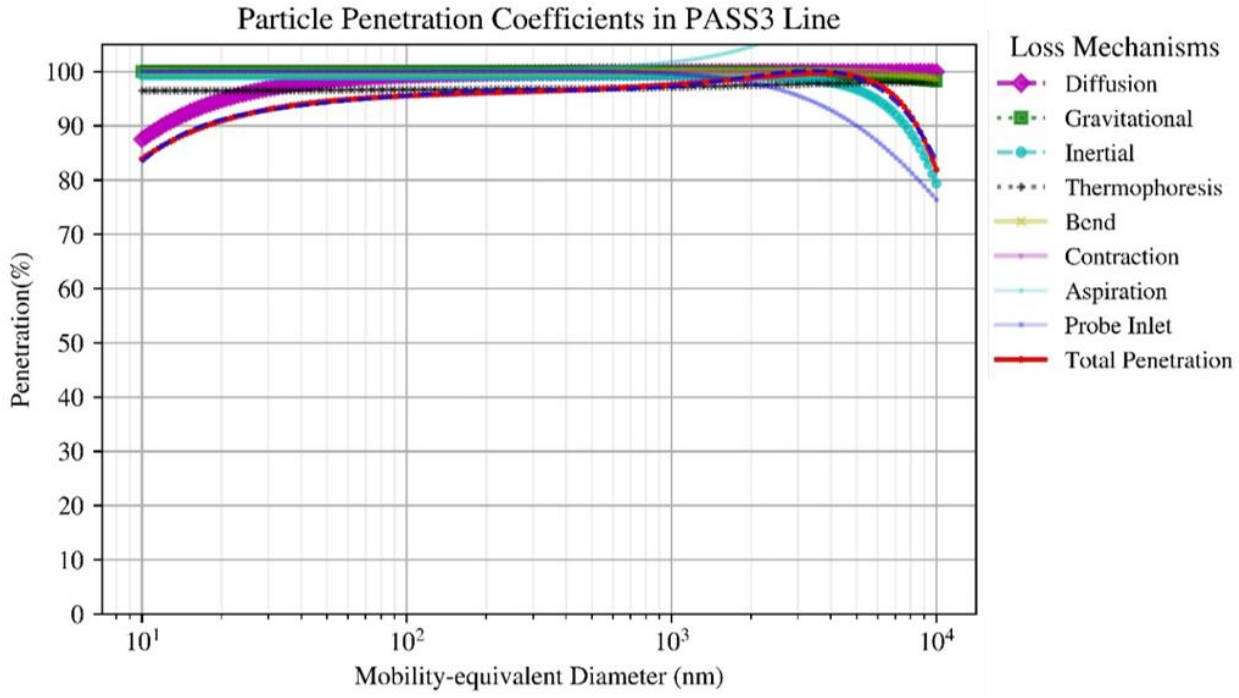

Figure 3-12: Particle transport efficiency estimation

The resultant loss estimate curve is favourable given the particle size range of interest. The particle sizes most affected by diffusion losses, below 50 nm, are below the detection range of the DustTrak DRX [36] [37]. The particles most affected by loss at the bends and sampling inlets, above 1000 nm, are generally not expected in diesel exhaust [46]. Moreover, the goal of this research is to evaluate the change in PM emissions from hydrogen substitution rather than an absolute number. Therefore, the key thing is that sampling losses stay constant between fueling modes. To this point the sampling system was not altered at all during the test week geometry and flow rates were always the same. In addition, the penetration efficiency hardly changes between 100 nm and 1000 nm, the sensitivity of loss to particle size will be minor provided particles stay within this expected range.

3.3 Torque Measurement

To produce a specific emission in [g/kW.h], engine speed and torque need to be measured. Engine speed is easily recorded from connection to the truck's CANbus. Torque measurement, however, is more complicated. While a variety of torque messages are available on the truck's CANbus, none are accurate when the truck is operating in hydrogen mode. Furthermore, even in diesel mode the engine torque is only an estimate based on various other operating parameters. For these reasons, direct torque measurement was used in both diesel and hydrogen/diesel dual-fuel operating modes.

To measure torque directly a Binsfield TorqueTrak 10k wireless torque measurement system was used. This system is comprised of a strain gauge mounted directly on the truck's driveshaft, along with a wireless transmitter. A receiver inside the cab then connects to the data acquisition system. Torque is calculated by the **Equation 3-2**, with the parameters for torque calculation are shown in **Table 3-3**.

$$T_{FS} = \frac{V_{FS}\pi E4({D_o}^4 - {D_i}^4)}{V_{EXC}GN16000(1+\upsilon)G_{XMT}D_o} \qquad (3\text{-}2)$$

Table 3-3: Torque parameters legend

Symbol	Parameter
VFS	Full scale output voltage
E	Modulus of elasticity
Do	Shaft outer diameter
Di	Shaft inner diameter
VEXC	Bridge excitation voltage
G	Gauge factor
N	Number of gauges
v	Poisson's ratio
GXMT	Transmitter gain

Measuring torque on the driveshaft requires that engine torque must be calculated based on current gear ratio selected in the transmission. To enable this a connection to the Truck's V-CAN network was necessary, as this is where messages relating to the Eaton-Fuller automated 18-speed transmission reside. The engine torque is calculated based on the gear reduction of the current gear selected and is only calculated when the driveline is fully engaged. Time steps where the automated clutch is disengaged or partially engaged are excluded in the all specific emission [g/kW.h] calculations. Further discussion of torque measurement is included in the following chapter on data processing methodology, specifically in *Section 4.3.1.*

3.4 ECU/CANbus

The truck has several on-board Controller Area Networks to run the multitude of onboard systems. To allow access to these the National Instruments cDAQ was equipped with two National Instruments 9862 C series CAN interface modules. Most basic engine operation messages are found on the O-CAN network, transmission and driveline messages are present on the V-CAN network, while aftertreatment messages are found on the A-CAN network. The separate ECU which controlled the hydrogen fuel system also used the O-CAN. **Table 3-4** summarizes the key parameters and which network they were found on. In order to access all 3 relevant networks with only two 9862 modules, a workaround was needed. The solution was to connect the two modules to A-CAN and V-CAN and then have another device broadcast the needed O-CAN messages to the A-CAN network. The setup will not be covered in detail but bears mentioning because getting all the required messages was not a trivial task.

Table 3-4: J1939 parameters

J1939 parameter	Network
Air Flow	V-CAN
Diesel Flow	V-CAN
Hydrogen Flow	O-CAN[1]
Engine RPM	V-CAN
Exhaust Flow	A-CAN
NOx [PPM]	A-CAN
EGT	A-CAN
DEF	A-CAN
Gear Ratio	V-CAN
Driveline Engagement	V-CAN

[1]broadcast to A-CAN network for logging

Chapter 4 - Data Collection and Processing

This section details the on-road emission data that was collected over 2500+ kilometers of real-world testing. Test conditions are explained, and an example of raw time series data is presented followed by processing steps to achieve the results.

4.1 Experiment Campaign Details

After initial testing in the BC Lower Mainland, experimental data was collected while the truck was in regular service with a fleet located in northern British Columbia, Canada. The truck's regular use is to drive from its starting point with unloaded trailers, to a second location where those trailers are loaded, and then to return along the same route to the starting location with the loaded trailers. The distance between the two locations is approximately 120 kilometers, and mostly highway driving at a speed of approximately 95 km/hr (**Table 4-1**). An example of a vehicle speed history is shown in **Figure 4-1**. The truck does this trip twice each shift. This was beneficial because the truck could be run back-to-back diesel versus hydrogen/diesel mode on the same day with the same driver. Drive-cycle consistency will be discussed further in *Section 5.2.*

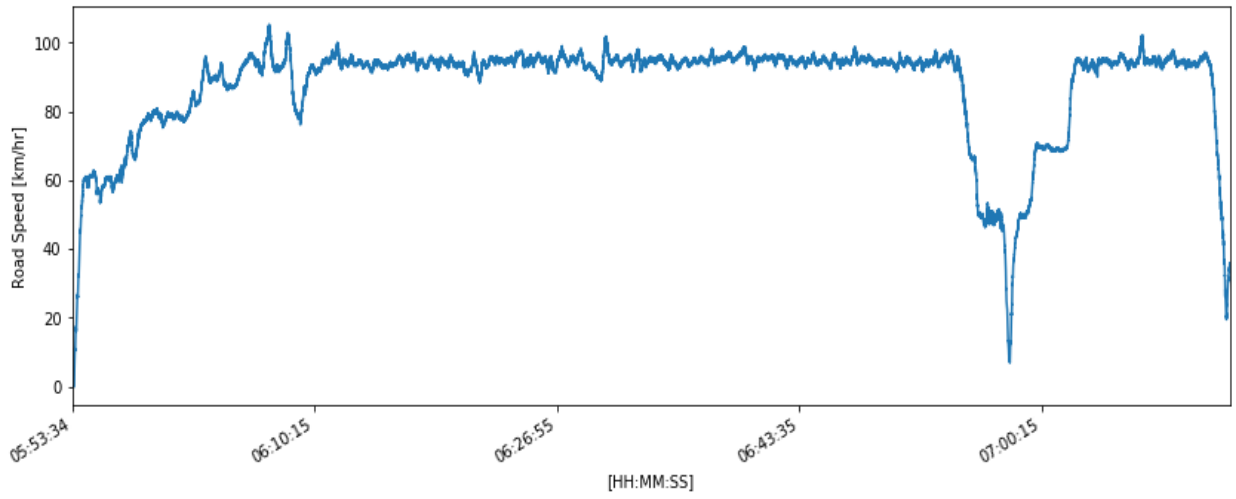

Figure 4-1: Vehicle speed trace example – diesel, unloaded

Table 4-1: Test route information

	Direction 1	Direction 2
Distance travelled	116 km	117 km
Starting elevation	575 m	688 m
Gross elevation gain	754 m	641 m
Net elevation gain	113 m	-113 m
Load condition	Empty B-train "unloaded"	Loaded B-train "loaded"
Gross Combined Vehicle Weight	20,000 kg	60,000 kg

The complexity of the measurement and data logging system, and the limited ability to correct things once a shift had started, necessitated the development of a detailed pre-trip inspection routine, shown in **Appendix 7**.

On-road testing, especially on a working truck, is difficult to do. As shown in **Table 4-2**, it took several tries to get a sufficient amount of good data. The notes on **Table 4-3** show some of the potential problems that can occur with the truck, the PEMS, or the logging system. Note that a complete dataset has 4 components: diesel and diesel/hydrogen runs, each in both unloaded and loaded condition.

Table 4-2: Measurement campaigns

Date	Location	Days of testing	Complete datasets	Incomplete datasets
August 2018	Lower Mainland BC	2	0	1
October 2018	Northern BC	3	1	2
March 2019	Northern BC	4	4	1

4.1.1 March 2019 Campaign Details

The final measurement campaign took place in the spring of 2019. Experimental data was collected during the period from Tuesday March 26, to Friday March 29, 2019, summarized in **Table 4-3**. The results presented in ***Section 5*** are based on this campaign only.

Table 4-3: March 2019 campaign details

Date + Weather	Driver	Runs	Fuel Mode	Notes
March 26, 2019	Driver #1	Unloaded	H_2/Diesel	DPF regeneration
Low: 0 C		Loaded	H_2/Diesel	
High: 2 C		Unloaded	H_2/Diesel	
Cloudy + periods of light snow		Loaded	H_2/Diesel	
March 27, 2019	Driver #1	Unloaded	H_2/Diesel	Torque transducer - signal loss
Low: -2 C				
High: 8 C		Loaded	H_2/Diesel	CO_2 signal - loose ground wire
Sunny				MIL light
		Unloaded	H_2/Diesel	
		Loaded	H_2/Diesel	
March 28, 2019	Driver #1	Unloaded	Diesel	
Low: -6 C		Loaded	Diesel	
High: 9 C		Unloaded	Diesel	
Sunny		Loaded	Diesel	
March 29, 2019	Driver #1	Unloaded	Diesel	No torque transducer
Low: -7		Loaded	Diesel	No torque transducer
High: 10 C		Unloaded	H_2/Diesel	No torque transducer
Sunny		Loaded	H_2/Diesel	No torque transducer
	Driver #2	Unloaded	H_2/Diesel	No CO_2 signal
		Loaded	Diesel	
		Unloaded	H_2/Diesel	
		Loaded	H_2/Diesel	

4.2 Raw Time Series Data

The DAQ collects data from each of the analog and CANbus inputs at 10 Hz. This generates a detailed time series for each of the parameters of interest, an example of which is presented in **Figure 4-2**, **Figure 4-3,** and **Figure 4-4**. Shown is 10 minutes of an hour-long run on March 29, 2019 in which the unloaded truck was running in the hydrogen/diesel mode.

Viewing the data in its raw form like this reveals a fundamental issue: there are times during the run where a particular signal displays an erroneous reading. This is most obvious in the NOx [ppm] signal. First at 21:42:30 and then 3 more times during the run the value jumps instantly to exactly 3063.5 and then, after one of more time steps, drops back to a much lower value. This needs to be addressed before calculations are run on the data set and will be addressed in *Section 4.3*.

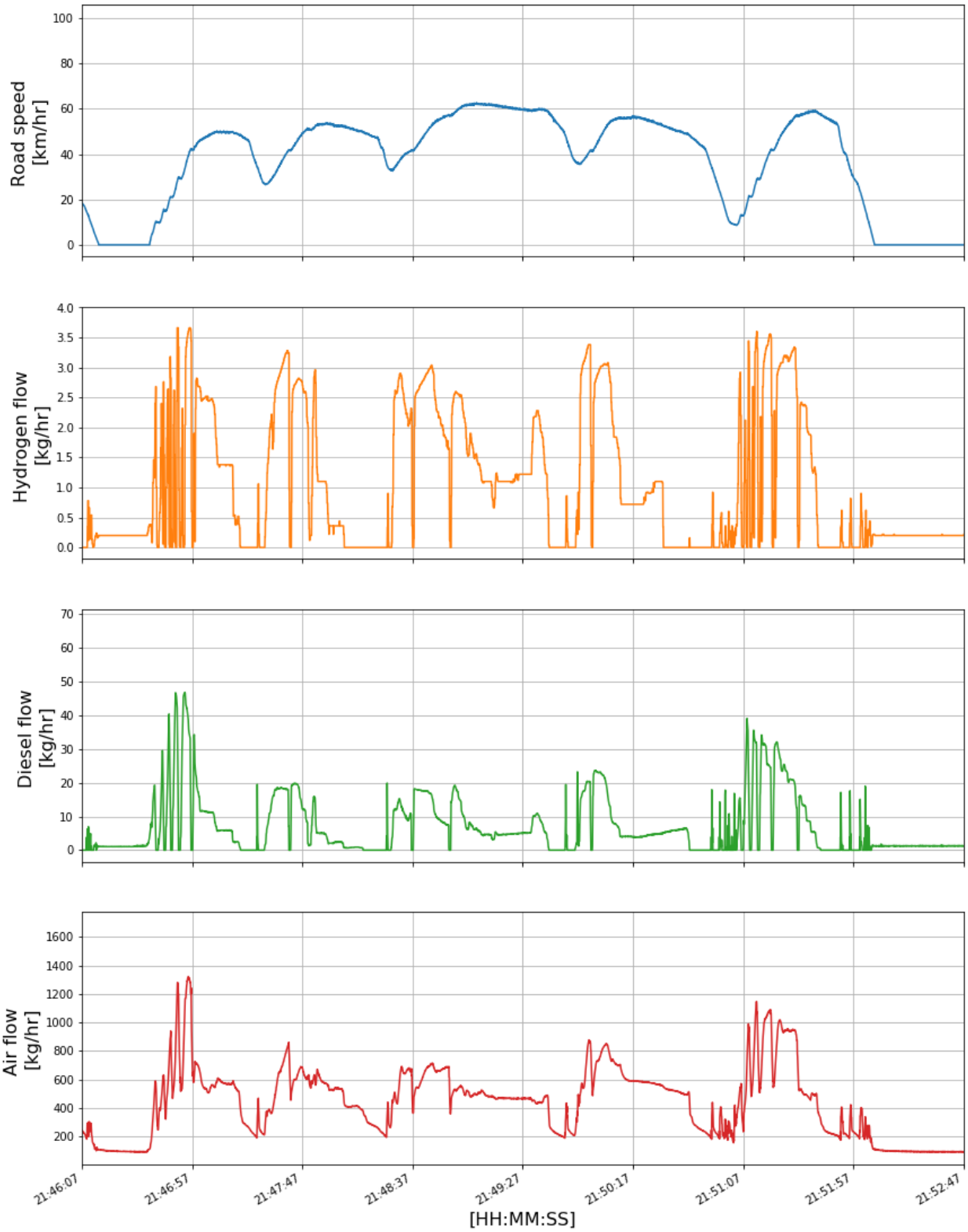

Figure 4-2: Raw time series (1 of 3)

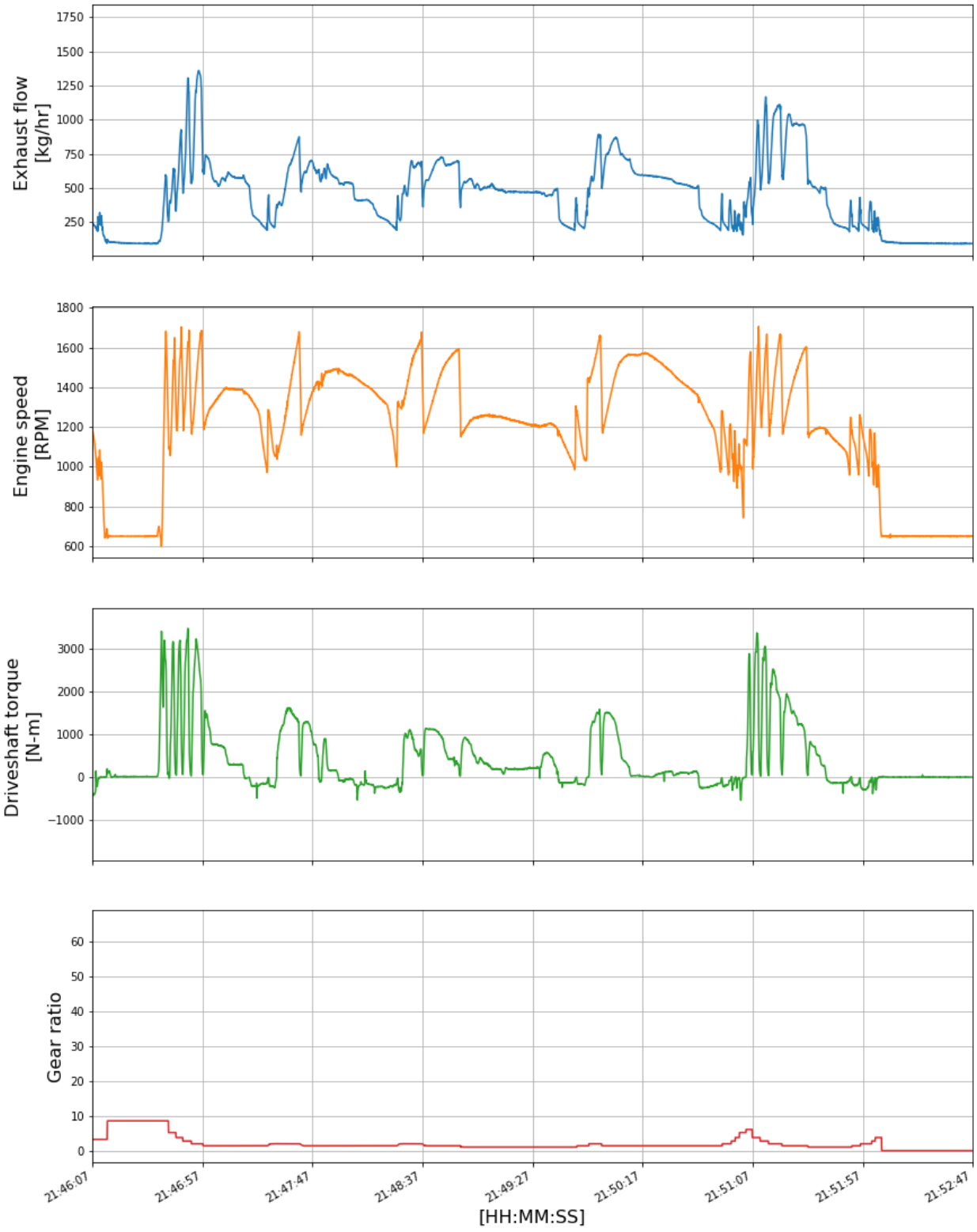

Figure 4-3: Raw time series (2 of 3)

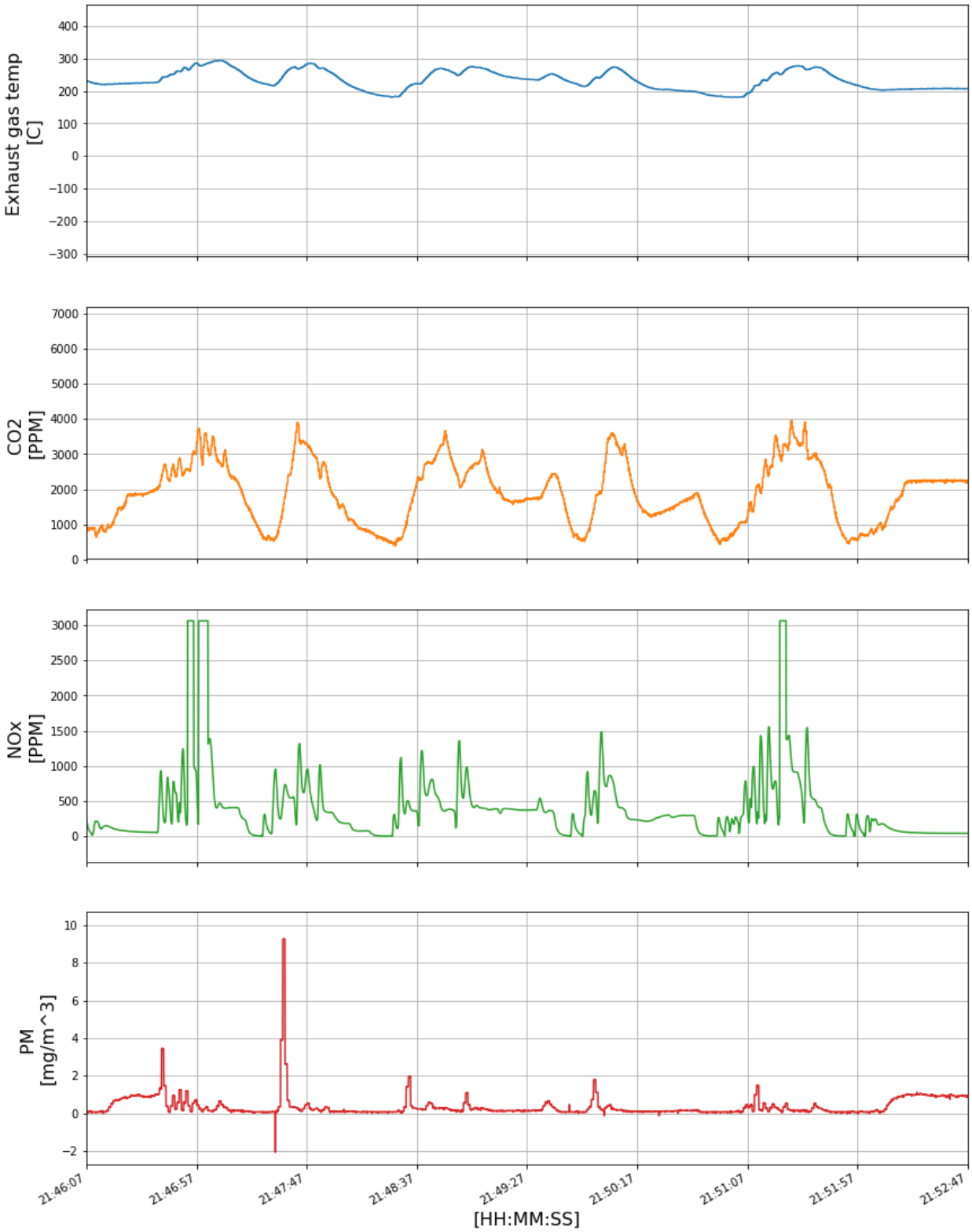

Figure 4-4: Raw time series (3 of 3)

4.3 Data Exclusion Criteria

In the order to generate high-quality results, it is necessary to examine the raw data and, in some cases, exclude certain data points that do not pass fidelity criteria. The following sections present these criteria for torque, CO_2, NOx, and PM signals.

4.3.1 Torque Exclusion Criteria

Torque is measured directly on the driveshaft with a strain gauge and wireless transmitter (*Section 3.3*). The parameter of interest however is engine torque. This requires dividing the measured torque by the transmission gear ratio, as shown in ***Equation 4-1***.

$$T = T_{engine} = \frac{T_{driveshaft}}{GR} \qquad (4\text{-}1)$$

It is important to note that this equation considers gearbox efficiency to be 100%, a necessary simplification based on the data available. Furthermore, for the relation to be true the driveline must be fully engaged: when clutch slip in the automated manual transmission is zero. This information is available via J1939 messages on the truck's V-CAN network as 'TransDrivelineEngaged' an example is presented in **Figure 4-5**.

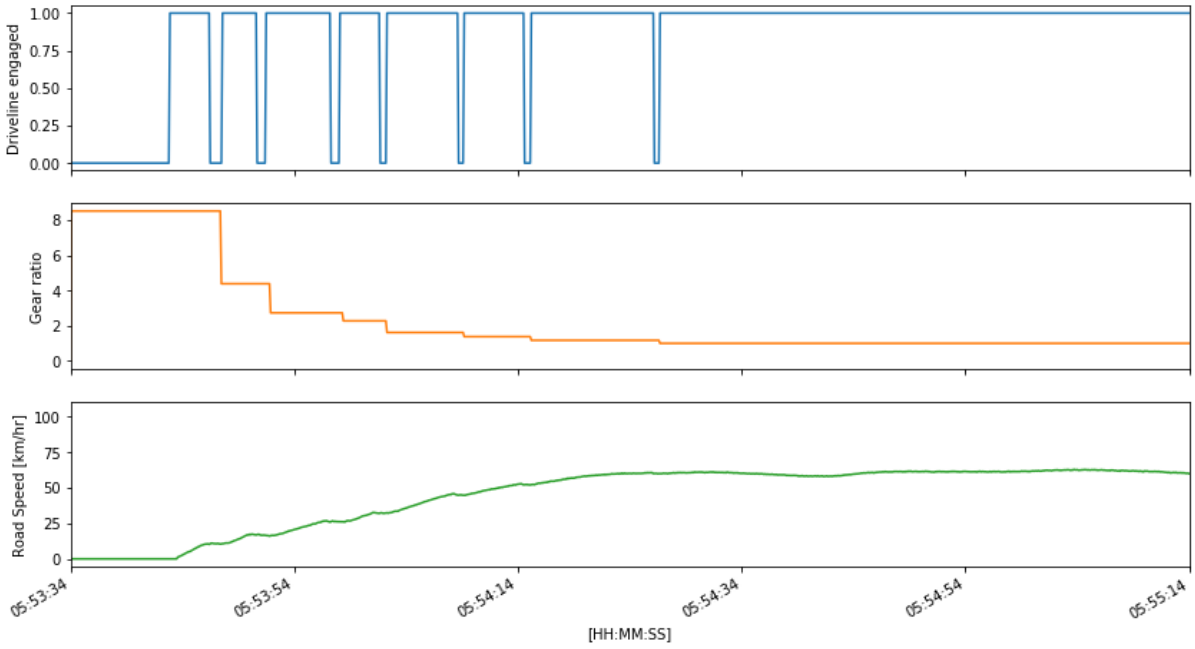

Figure 4-5: Torque exclusion example

As this example shows, there are two cases where the driveline is disengaged: first, if the truck isn't moving and second, if the truck is shifting. As shown in **Figure 4-5**, this is a binary message. One means that the driveline is engaged, while zero means that it is not. In either case a valid torque measurement isn't possible and the time step is excluded. In addition to this message two additional J1939 driveline status parameters were considered as exclusion criteria: 'TransShiftInProcess', and 'TransCurrentGear'. The first message shows true while the driveline is disengaged as well as immediately before and after. ('TransCurrentGear' <=18) is expected while the driveline is engaged. Sometimes, however, 'TransCurrentGear' displays erroneous value of 130. The question is, while ('TransCurrentGear' == 130), can the 'TransActualGearRatio' message be trusted and therefore can a valid torque measurement be taken.

With these additional exclusion parameters comes a tradeoff between the amount of data available and the confidence in the torque measurement. To facilitate this decision a comparison was done between the torque measured by the torque transducer against the broadcast J1939 torque value. While running in diesel mode, correlation between the two was calculated. A change in the fit (R^2 value) and or slope (bias) was then considered against the loss of data, see **Appendix 3** for details. A valid torque measurement should stay proportional to the broadcast reference torque, the slope should not change if valid points are added or taken away from other valid points. In addition, the regression to this fit indicates the noise in the torque measurement. An increase in R^2 value following the implementation of a drop criteria would indicate a higher quality subset of torque points following that drop.

From that analysis the ('TransShiftInProcess' !=1) exclusion was implemented as the number of data points lost is minimal and many of them are obvious outliers. The ('TransCurrentGear' <=18) exclusion, however, was not implemented because the slope and R^2 value hardly changed and over half the data points were lost. While most of the analysis presented herein includes the full data set, *Section 5.1.1* explores the effect of applying ('TransCurrentGear' <=18) and potential changes to the calculated emissions from the reduced data set.

4.3.2 CO_2 Exclusion Criteria

The LI-COR LI-820 CO_2 sensor uses a heated sample cell which must be maintained at 50℃ for accurate readings [47]. Practical constraints during the field campaign meant that the cell could not always be fully warmed up before the start of a shift. Therefore, cell temperature was also logged via an analog input to the DAQ to verify when the sensor was at temperature, an example is shown in **Figure 4-6**.

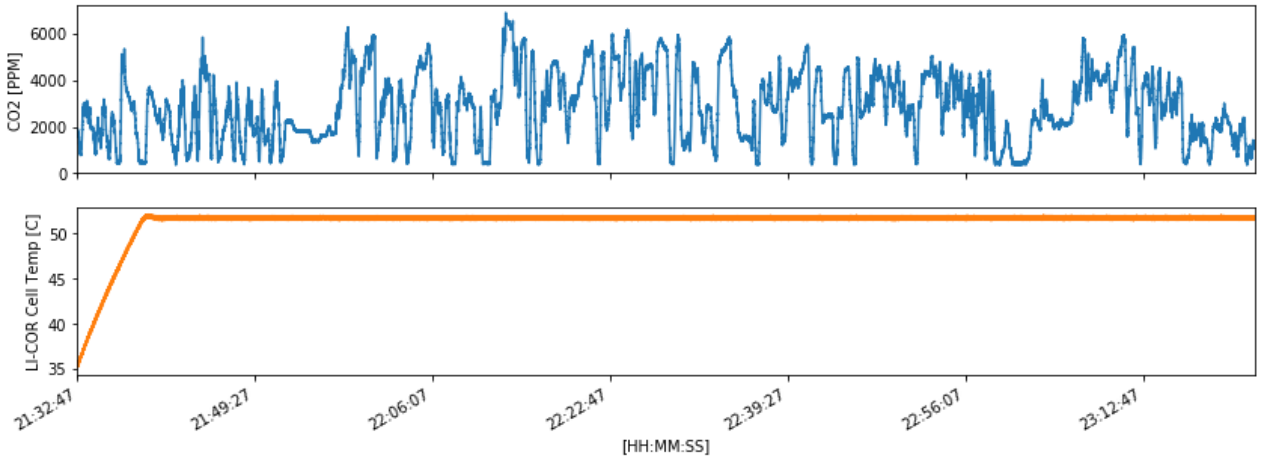

Figure 4-6: CO_2 exclusion example

Time steps in the file before the cell temperature reaches 50℃, in this case before about 21:40:00 were excluded from CO_2 calculations. It should be noted that in many cases the cell was already warmed up before the start of the run, so these exclusions were not necessary.

4.3.3 NOx Exclusion Criteria

The NOx signal, which comes from J1939 messages on the CANbus, sometimes displays an erroneous, non-physical value. In these cases, the reported value will jump, in a single time step, to exactly 3063 [PPM], the maximum J1939 value, and hold there for some amount of time, only to jump down to a real physical value, again in one time step. **Figure 4-7** shows an example of this.

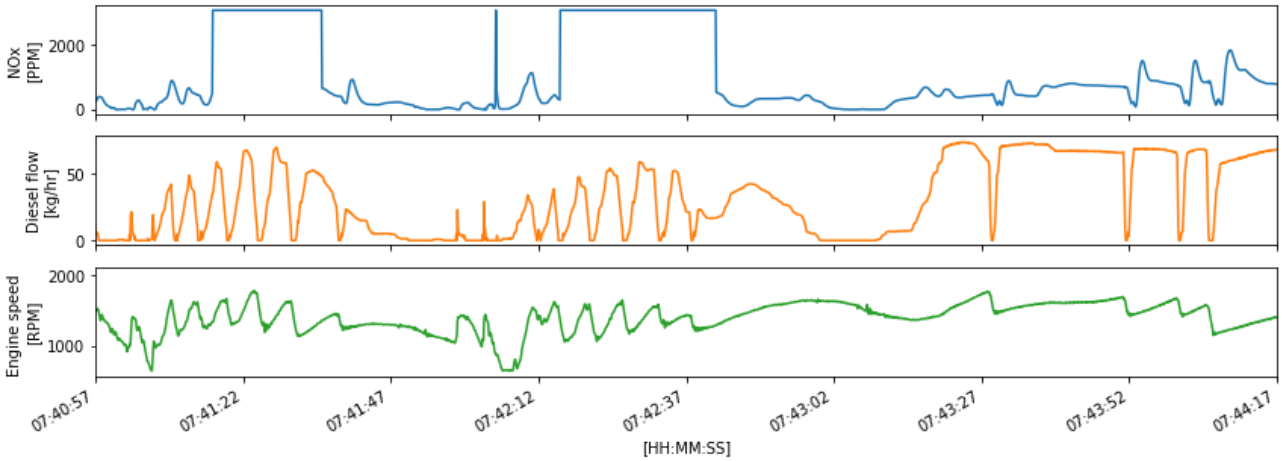

Figure 4-7: NOx exclusion example

The engine speed and fueling information presented alongside show that a physical explanation, namely sensor saturation, isn't likely here. Instead, 3063 [PPM] seems to be what is reported on the CANbus when stability criteria for sensor output is not met. When the reported NOx concentration is equal to 3063 [PPM] the point is excluded from NOx calculations. The NOx values recorded during the campaign were the uncorrected values. Later analysis revealed that, for engine-out NOx values, the corrected values were within 1% of the uncorrected values and not a significant error source. For post-aftertreatment NOx, the reported corrected values were essentially the uncorrected values with any negative readings truncated. This same truncation of negative values was done in the processing of the uncorrected post-aftertreatment NOx values recorded in this study. Measuring NOx values close to zero and truncating the negative values means that a small offset error could make a noticeable difference in the calculated result. This needs to be kept in mind when considering the absolute accuracy of the post-aftertreatment measurement.

4.3.4 PM Exclusion Criteria

The DustTrak DRX reports the particulate matter concentration to the DAQ as an analog input voltage. Isolating this signal from various sources of electrical interference proved to be quite challenging because of the way the DustTrak is grounded. Notably when running off the internal battery it worked properly, however, the non-isolated power adapter introduced noise through connection to an inverter. This was cured by grounding both the DustTrak body and the low side of the analog output to the same ground as the DAQ. There were still occasional non-physical blips in the DustTrak signal as shown in **Figure 4-8**.

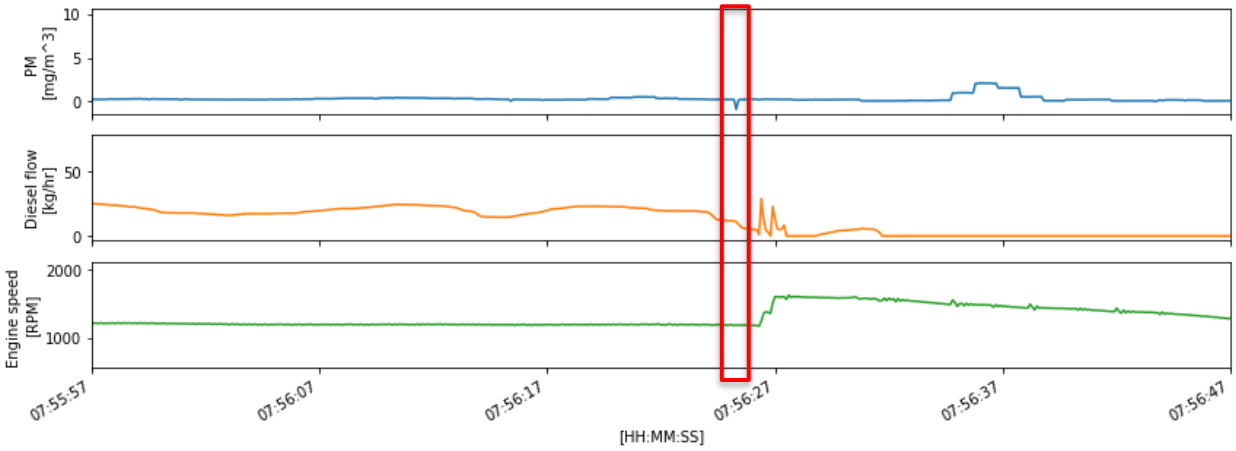

Figure 4-8: PM exclusion example

The figure shows, at approximately 07:56:25, a negative reported value for PM concentration. Time steps such as this were very infrequent and were excluded from calculation. For further assurance the PM concentration logged on the DAQ was compared to the DustTrak's internal memory and, outside of the small interference blips, the signals matched.

4.4 Emission Calculations

This section shows the underlying calculations that will be performed to generate the results in Section 5.

4.4.1 Run Total Calculations

Run total CO_2, NOx and PM emissions were done as follows:

$$CO_2 = \int_o^T CO_2 . \frac{M_{CO_2}}{M_{exhaust}} \cdot DR \cdot \dot{m}_{exhaust}\, dt \qquad (4\text{-}2)$$

CO_2 [ppm] is measured by the LI-COR. DR is the dilution ratio. Exhaust mass flow $\dot{m}_{exhaust}$ is a message logged from the truck's A-CAN network. M_{CO2} is 44 g/mol and $M_{exhaust}$ was approximated as a fixed value of 29 g/mol[1].

$$NOx = \int_o^T NOx \cdot \frac{M_{NOx}}{M_{exhaust}} \cdot \dot{m}_{exhaust}\, dt \qquad (4\text{-}3)$$

NOx [ppm] is measured by the truck's on-board electrochemical sensor and reported on the truck's A-CAN network, as is exhaust mass flow $\dot{m}$. M_{NOx} is 46 g/mol, which is the molar mass for NO_2. As per Title 40 part 1065 [20], NO and NO_2 concentrations are both converted to mass flow based on the molar mass of NO_2.

$$PM = \int_o^T PM \cdot \left(\frac{1}{\rho_{air}}\right) \cdot DR \cdot \dot{m}_{exhaust}\, dt \qquad (4\text{-}4)$$

PM [mg/m^3] is measured by the DustTrak. DR is the dilution ratio. Density of the diluted sample was calculated using fixed value for air at 25℃ of 1.18 kg/m^3.

Power delivered was calculated as:

$$P = \int_o^T T \cdot \omega\, dt \qquad (4\text{-}5)$$

Where T is engine torque as in **Equation 4-1**, and ω is engine speed as reported on the truck's V-CAN network.

[1]Stoichometric calculations showed that this value could vary by about 2% over the typical operating range and were about 2% lower at common operating points while in hydrogen/diesel mode. This could introduce a slight downward bias in the CO_2 and NOx emissions while in hydrogen/diesel mode.

4.4.2 Specific Emission Calculations

Calculation of power specific CO_2, NOx and PM emissions were done as follows in **Equation 4-6**, **Equation 4-7**, and **Equation 4-8**:

$$BSCO_2 = \frac{CO_2 \cdot \frac{M_{CO_2}}{M_{exhaust}} \cdot DR \cdot \dot{m}_{exhaust}}{T \cdot \omega} \quad (4\text{-}6)$$

CO_2 [ppm] is measured by the LI-COR. DR is the dilution ratio. Exhaust mass flow $\dot{m}$ and engine speed ω are messages logged from the truck's A-CAN network. M_{CO2} is 44 g/mol and $M_{exhaust}$ was approximated as a fixed value of 29 g/mol.

$$BSNOx = \frac{NOx \cdot \frac{M_{NOx}}{M_{exhaust}} \cdot \dot{m}_{exhaust}}{T \cdot \omega} \quad (4\text{-}7)$$

NOx [ppm] is measured by the truck's on-board electrochemical sensor and reported on the truck's A-CAN network, as is exhaust mass flow and engine speed ω. M_{NOx} was considered 46 g/mol.

$$BSPM = \frac{PM \cdot \left(\frac{1}{\rho_{air}}\right) \cdot DR \cdot \dot{m}_{exhaust}}{T \cdot \omega} \quad (4\text{-}8)$$

PM [mg/m^3] is measured by the DustTrak. DR is the dilution ratio. Density of the diluted sample was calculated using fixed value for air at 25℃ = 1.18 kg/m^3.

4.4.3 Percent Total Emission Calculation

In addition to the power specific emission rates, the contribution from each cell on the operating map to the run total is calculated for each emission as shown in **Equation 4-9**.

$$\%total\ emission = \frac{\int_0^{t_{operating\ point}} \dot{m}_{emission} dt}{\int_0^{t_{total}} \dot{m}_{emission} dt} * 100 \quad (4\text{-}9)$$

Chapter 5 – Results and Analysis

This chapter presents the processed results of the on-road emissions testing. Overall results based on individual run averages are presented first. Next the effect of excluding a large portion of data is evaluated. Variability in the drive cycle is investigated and later used to isolate true variability in the emissions. Detailed emission maps are presented for CO_2, NOx, and PM as a function of engine speed and torque. Finally, measurement error is discussed and quantified.

5.1 Overall Emissions by Operating Mode

Table 5-1 presents the average specific emissions for each operating mode, the average total PM via gravimetric sample, and average fuels and DEF consumption. In both the unloaded and loaded cases, the specific CO_2 output is significantly reduced, as is the consumption of diesel fuel. In both cases, engine out specific NOx increased to some extent. In the case of PM, specific output decreased with the addition of hydrogen when the truck was unloaded but increased when the truck was loaded. The amount of hydrogen consumed was similar in both cases despite higher diesel consumption in the loaded cases indicating a lower amount of hydrogen substitution when the truck was loaded. DEF consumption increased slightly in hydrogen/diesel in both unloaded and loaded cases.

Table 5-1: Average emissions and fuel consumption by load and fuel

load condition	Mode	CO_2 [g/kW.h]	NOx [g/kW.h]	PM [mg/kW.h]	PM[a] [mg]	Diesel [l]	H_2 [kg]	Diesel Exhaust Fluid [kg]
unloaded	H2/Diesel	583	6.6	40.5	0.11	30	3.0	2.0
	Diesel	825	5.8	42.3	0.12	39	-	1.8
loaded	H2/Diesel	618	7.2	35.4	0.16	49	2.7	3.3
	Diesel	818	6.7	34.2	0.12	62	-	3.2

[a] Accumulated gravimetric sample on Teflon filter.

The run total quantities for diesel, hydrogen, and diesel exhaust fluid values are determined by integrating the mass flow of each parameter, and each mass flow is determined via a logged J1939 parameter.

Table 5-1 is the simple average of the individual runs presented in **Table 5-2**. Care should be exercised when comparing the run to run power specific CO_2, NOx, and PM emission numbers. These numbers are the average emission of all the points during that run where a valid power measurement was possible (see Section 4.3.1). The total number of valid points, and their distribution on the engine's operating map is not equal between runs.

Table 5-2: Individual run key statistics

Fuel + Load	Date	CO_2 [g/kW.h]	NOx [g/kW.h]	PM [mg/kW.h]	Diesel [L]	H_2 [kg]	CO_2 [kg]	NOx [kg]	PM [kg]	Power delivered [kJ]	DEF [kg]
Unloaded Diesel	03/28/19	825	5.9	40.5	39.6	0	129	0.91	5.9	158	1.82
	03/28/19	822	5.8	43.4	38.7	0	125	0.85	6.2	153	1.69
Unloaded H2	03/26/19	541	7.0	31.9	31.0	3.11	77	1.02	4.8	117	2.08
	03/27/19	414[A]	6.4	39.5	30.2	2.29	0.2	0.94	5.2	148	1.94
	03/29/19	-[B]	6.4	50.1	28.3	3.09	0.0	0.91	7.0	146	1.78
	03/29/19	624	6.6	37.4	31.8	3.50	103	1.07	5.6	165	2.11
Loaded Diesel	03/28/19	821	6.5	29.8	58.5	0	181	1.49	5.6	234	3.04
	03/28/19	852	6.8	36.3	59.2	0	201	1.57	6.3	232	3.15
	03/29/19	767	6.7	31.6	68.5	0	207	1.7	6.5	263	3.52
Loaded H2	03/26/19	636	7.3	42.3	48.4	2.69	134	1.56	7.8	223	3.18
	03/26/19	549	7.7	34.1	46.0	2.36	112	1.52	4.9	206	3.15
	03/27/19	602	7.0	29.4	50.1	2.70	42	1.65	5.9	240	3.33
	03/27/19	667	7.2	37.4	47.8	2.51	149	1.59	6.3	223	3.19
	03/29/19	616	6.9	29.4	54.8	3.37	168	1.79	5.8	262	3.60

[A] Failing ground on LI-COR, excluded from CO_2 average

[B] No LI-COR signal, excluded from CO_2 average

5.2 Emission Variability Based on Data Exclusion Criteria

As was discussed in in *Section 4.3.1*, a decision had to be made on which data points gave a valid power measurement. Ultimately, the choice was made to go with the option which included more data points. The question that needs to be addressed though is: *would choosing the other criteria change the results?* To investigate this **Table 5-3** shows the effect of applying each drop criteria to the data. Each A column shows the base exclusion criteria ('DriveLineEngaged' == 1 & 'ShiftInProcess' != 1), while the each column B adds to this the additional drop criteria ('GearPosition' <= 18). To isolate the effect of an incorrect power calculation both specific emissions and concentrations are shown for each CO_2, NOx, and PM.

Comparing the data before and after the additional driveline exclusion reveals two major things. The first is that the change in specific emission is, in general, very similar to the change in magnitude of the concentration. This gives confidence that our power measurements are valid based on exclusion criteria A. The second thing is that change in CO_2 or NOx values based on the different exclusion criteria is small across the data set. Changes in PM, however, are more noticeable, suggesting greater sensitivity of PM to these points.

Table 5-3: Data exclusion based on driveline status comparison

A = less drop criteria, B = more drop criteria							
Fuel + Load	Date	CO_2 [g/kW.h] [ppm]		NOx [g/kW.h] [ppm]		PM [mg/kW.h] [mg/m^3]	
		A	B	A	B	A	B
Unloaded Diesel	03/28/19	826	830	5.9	5.8	40.8	40.2
		78538	81593	522	529	0.40	0.41
	03/28/19	823	823	5.8	5.8	43.7	41.4
		79864	81088	522	534	0.45	0.43
Unloaded H2	03/26/19	542	540	7.0	7.1	32.7	31.8
		48009	47550	626	629	0.32	0.32
	03/27/19	413	419	6.4	6.5	39.8	41.4
		43598	42537	617	632	0.42	0.44
	03/29/19	-	-	6.4	6.5	51.6	56.1
		-	-	621	613	0.56	0.62
	03/29/19	625	621	6.6	6.2	37.7	40.4
		60489	66098	598	610	0.37	0.42
Loaded Diesel	03/28/19	825	822	6.5	6.2	30.5	40.2
		92995	90833	684	636	0.34	0.37
	03/28/19	857	862	6.8	6.4	37.7	46.5
		97951	97537	729	679	0.40	0.49
	03/29/19	772	767	6.7	6.5	34.5	30.9
		84177	84727	687	669	0.34	0.32
Loaded H2	03/26/19	640	670	7.3	7.2	43.8	50.5
		76841	78690	792	771	0.47	0.53
	03/26/19	551	551	7.7	7.5	34.7	25.7
		65523	68180	841	771	0.38	0.53
	03/27/19	607	595	7.0	7.3	30.0	33.4
		73237	68382	825	818	0.36	0.40
	03/27/19	670	671	7.3	7.5	38.0	35.9
		83834	83622	842	873	0.47	0.45
	03/29/19	620	618	6.9	6.9	30.2	25.0
		73346	75086	746	766	0.33	0.29

5.3 Drive Cycle Consistency

In order to accurately compare emissions between hydrogen/diesel co-combustion mode and the diesel baseline, it is important to account for potential differences in the drive cycle between runs. To address this, the first step is to assess differences in road speed, which is done for the unloaded condition in **Figure 5-1** and then for the loaded condition in **Figure 5-2**.

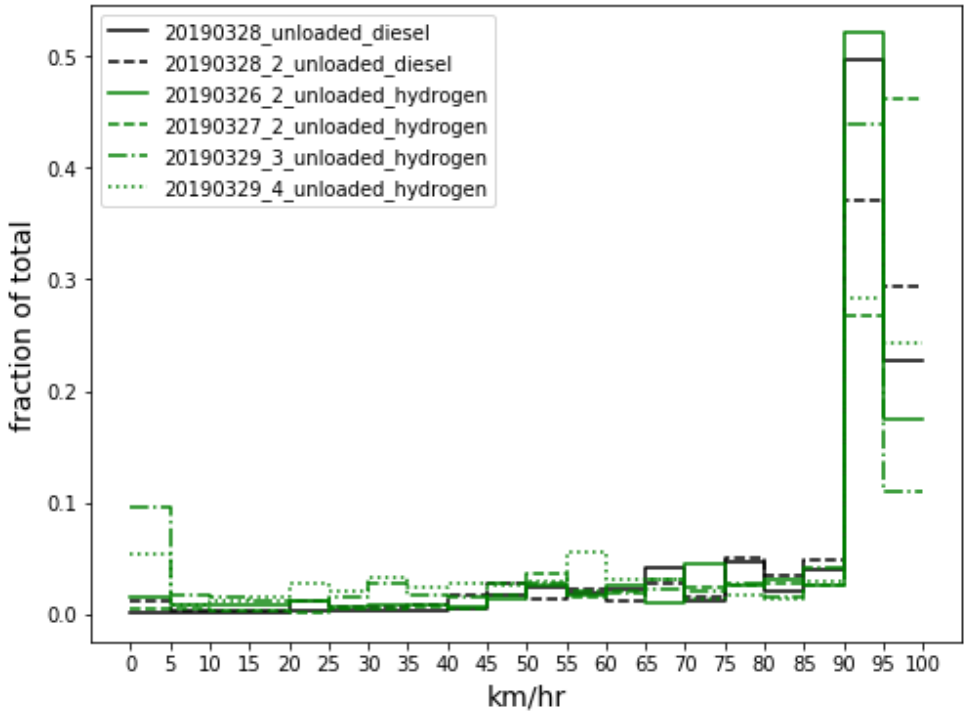

Figure 5-1: Vehicle speed – unloaded

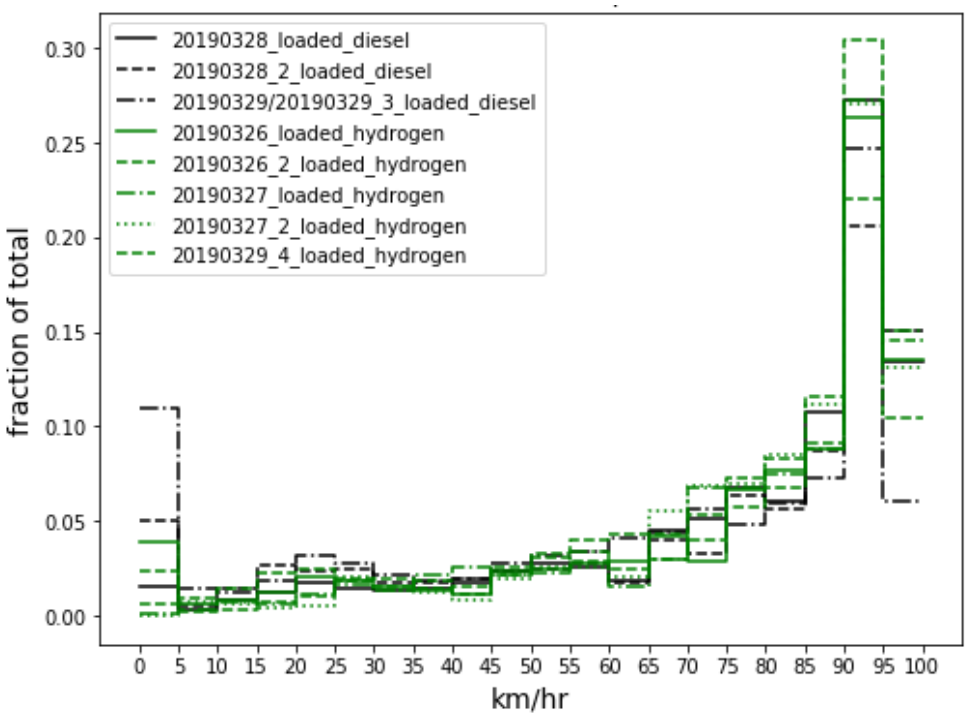

Figure 5-2: Vehicle speed – loaded

Measured road speed is overall quite consistent between fueling modes. While loaded, however, there is a slight trend of more time spent in the lower speed bins while operating in the baseline diesel configuration.

The next step is to look at measured power, which is calculated as shown in ***Equation 5-1***:

$$P = T\omega \qquad (5\text{-}1)$$

Where T is the measured engine torque in [N-m], and ω is the engine speed in [rad/s]. Measured power by run is presented in **Figure 5-3** and **Figure 5-4**.

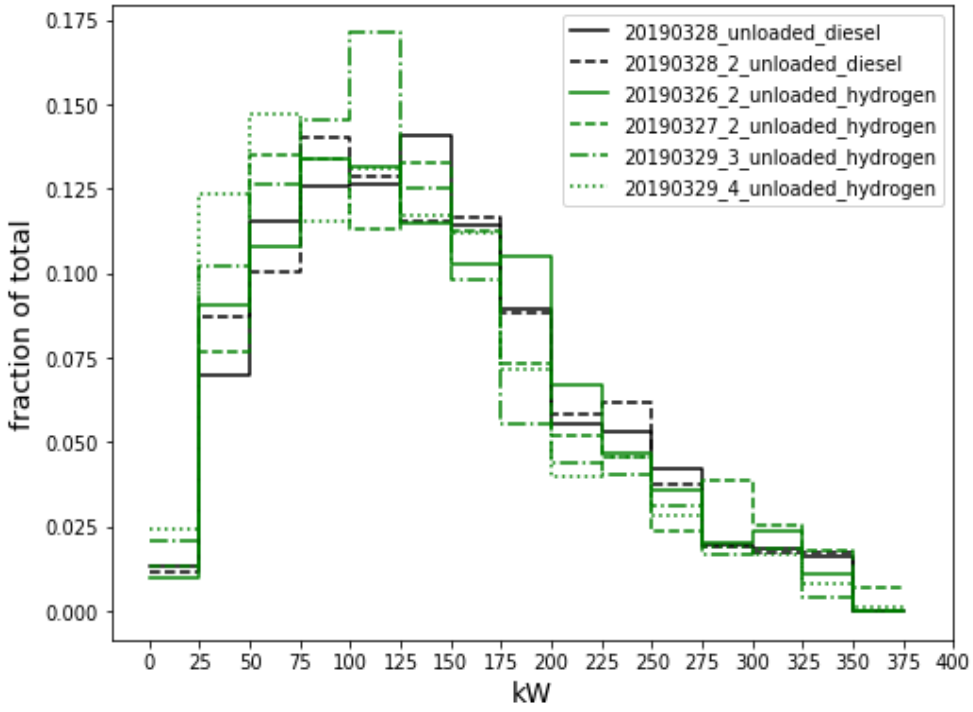

Figure 5-3: Measured power – unloaded

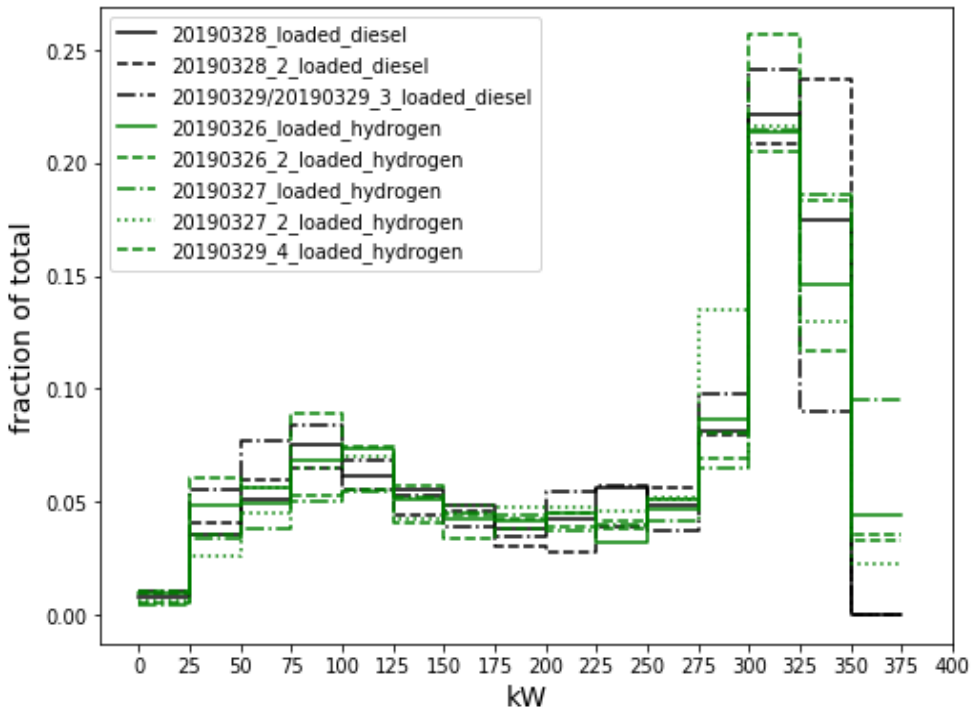

Figure 5-4: Measured power – loaded

Overall, the observed power profiles are quite different between unloaded and loaded runs but quite similar between the fueling modes. A slight difference between fueling modes appears in loaded configuration though, while operating in hydrogen/diesel mode there are noticeably more samples in the highest power bin, 350-375 kW. This indicates that the peak power output in hydrogen/diesel mode was slightly higher than the diesel baseline. This also serves as potential explanation for the difference in **Figure 5-2**, as higher peak power output can reduce the time spent accelerating through the lower speed bins and give a higher average speed up hills.

The potential effect of the differences in drive cycle on the overall emissions will be investigated later in *Section 5.6*, once the requisite emission maps have been introduced.

5.4 Emissions Maps

This section presents specific CO_2, NOx, and PM emissions across the engine speed and torque range. In addition to the specific emissions, other parameters of interest such as hydrogen displacement ratio, thermal efficiency, exhaust gas temperature, global equivalence ratio, and DEF consumption rate are also presented. For each parameter a baseline diesel map is shown, followed by the corresponding hydrogen/diesel co-combustion map. This allows an easy side by side comparison of the two to see the difference that hydrogen substitution makes. An example of one of these maps is shown below in **Figure 5-5**. Note that on maps where the map average is shown, that number is the weighted average.

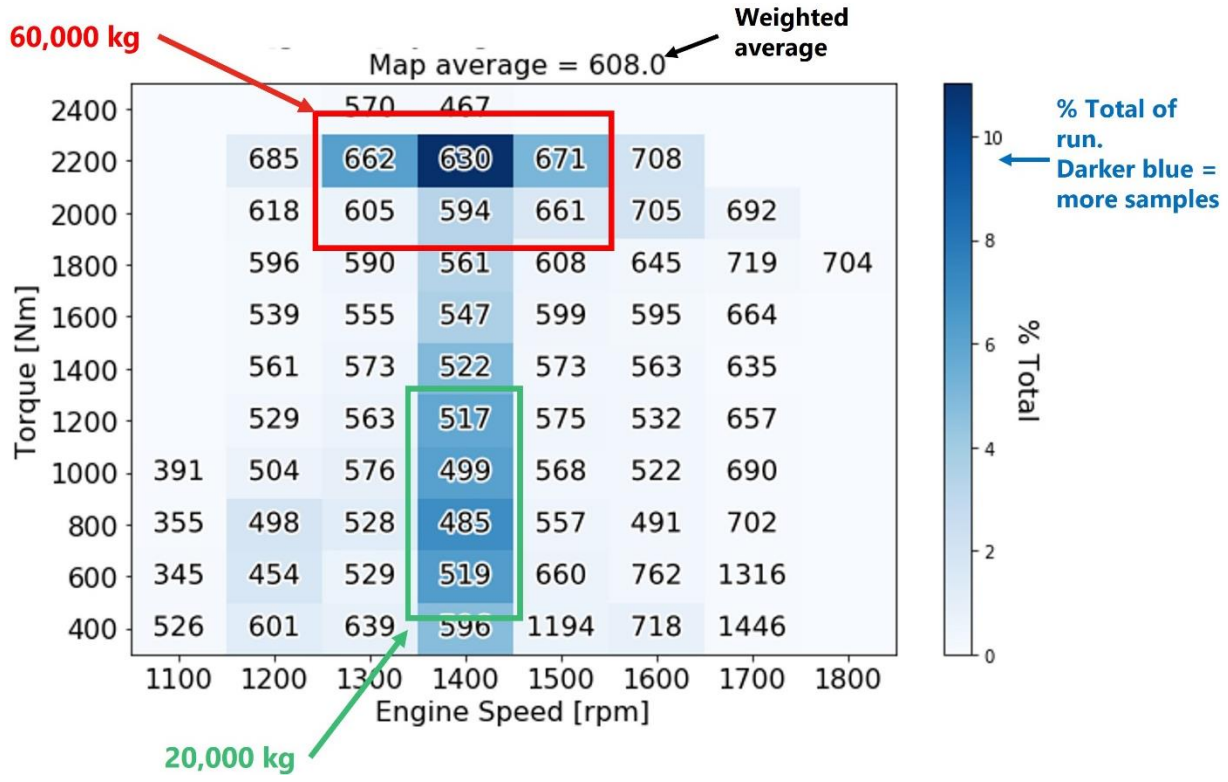

Figure 5-5: Engine operating map example

Points from both unloaded (20,000 kg) and loaded (60,000 kg) cases are combined on the same map. Cells on the lower end of the torque range are mostly from the unloaded runs while the higher torque cells generally come from the loaded runs. Note that the colour of the cell corresponds to the number of samples in that cell; darker cells represent more samples. Only load cells with (n>50) measurements, after erroneous data is dropped (*Section 4.3*), are shown on these maps. Example separate unloaded + loaded maps are found in **Appendix 4.1**.

5.4.1 Hydrogen Displacement Maps

To provide context for the upcoming specific emissions results it is important to look at hydrogen displacement across the operating range. Hydrogen displacement is calculated based on **Equation 2-2** and presented in **Figure 5-6**.

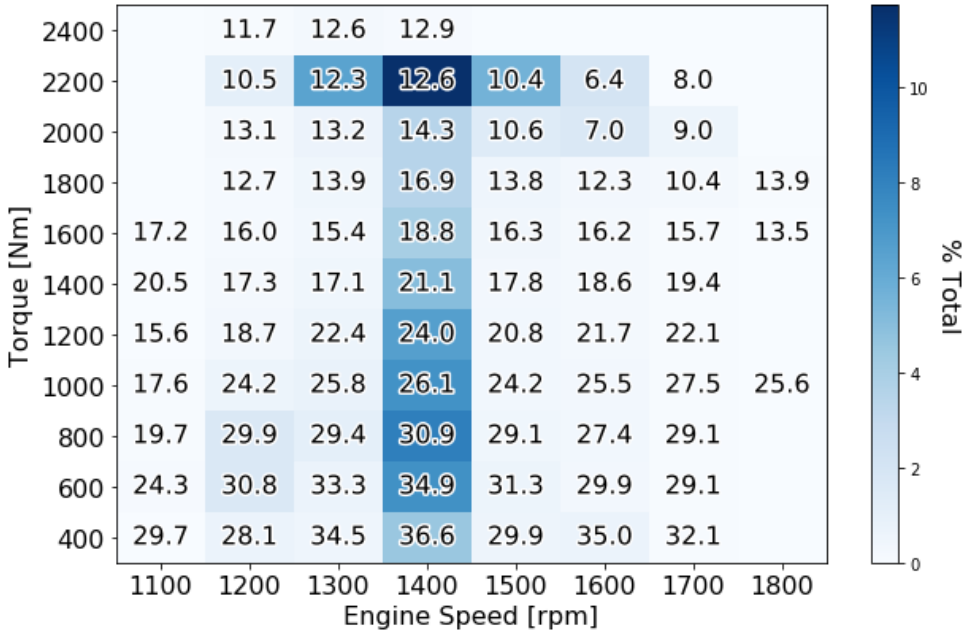

Figure 5-6: Hydrogen energy displacement

The important observation to make is that, while the system can displace up to 40% hydrogen, the average displacement in each load cell is always less. Focusing on the 1400 rpm engine speed column it is shown that in the case of the lower torque values, such as 600 and 800 N-m, displacement is quite high. Conversely, at higher torque values, such as 2200 N-m, hydrogen displacement is much lower.

Hydrogen is introduced to the truck's engine via injection into the intake manifold. This arrangement, as opposed to direct injection into the cylinder, displaces incoming intake air. Hydrogen volume displacement is calculated by **Equation 2-3** and presented in **Figure 5-7**.

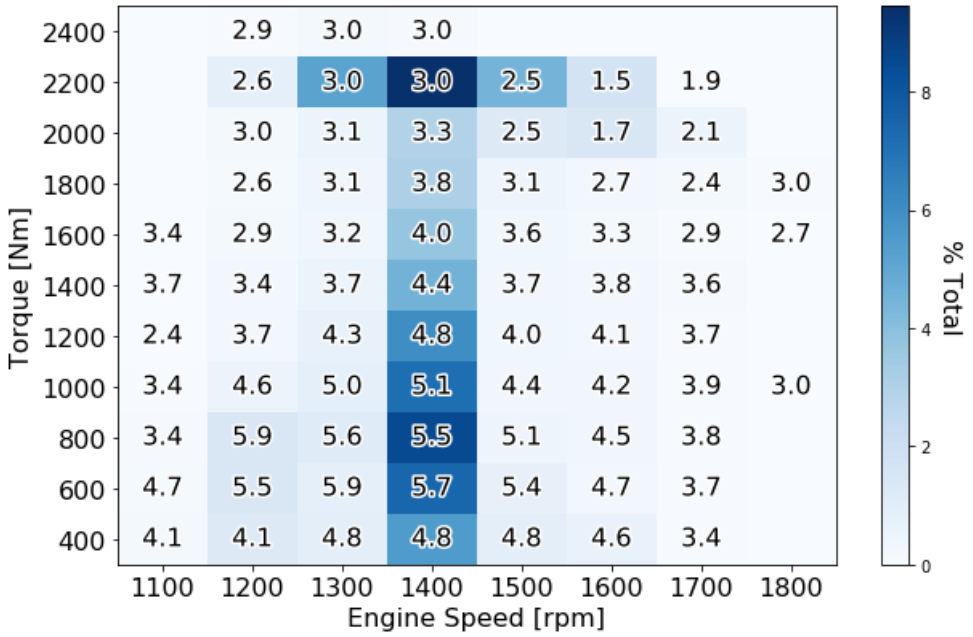

Figure 5-7: Hydrogen volume displacement

The volume displaced by the hydrogen is highest at the lower torque values where hydrogen energy displacement is also highest. The magnitude of the change, however, is not equal. Percent volume of hydrogen roughly doubles between 2200 and 600 N-m, however, the percent energy roughly triples between the same two cells. The difference occurs because of a concurrent change in the global equivalence ratio.

5.4.2 Thermal Efficiency Maps

The other important factor to look at before considering specific emission figures is any change to the thermal efficiency as a result of hydrogen substitution. Specific emissions are indexed against power and therefore a change in thermal efficiency will have confounding effect. **Figure 5-8** and **Figure 5-9** present the thermal efficiency for each fueling mode as calculated in **Equation 2-6**.

Overall, thermal efficiency does not change very much with the addition of hydrogen. Interestingly, however, the effect of the hydrogen addition seems different in different areas of the engine operating map. At higher torque values the thermal efficiency increases slightly, perhaps due to more complete combustion of the fuel charge. Conversely at lower torque values the thermal efficiency decreases slightly and this could be due to hydrogen slip; at lower loads a portion of the hydrogen might pass through the cylinder unburned. The rate of hydrogen slip is currently unknown and could be a topic for further investigation. From a total fuel consumption perspective, the thermal efficiency at the high torque points is more important simply because more fuel is burned here. Therefore, the 1% improvement in thermal efficiency at the common high torque point, 2200 N-m at 1400 rpm is notable.

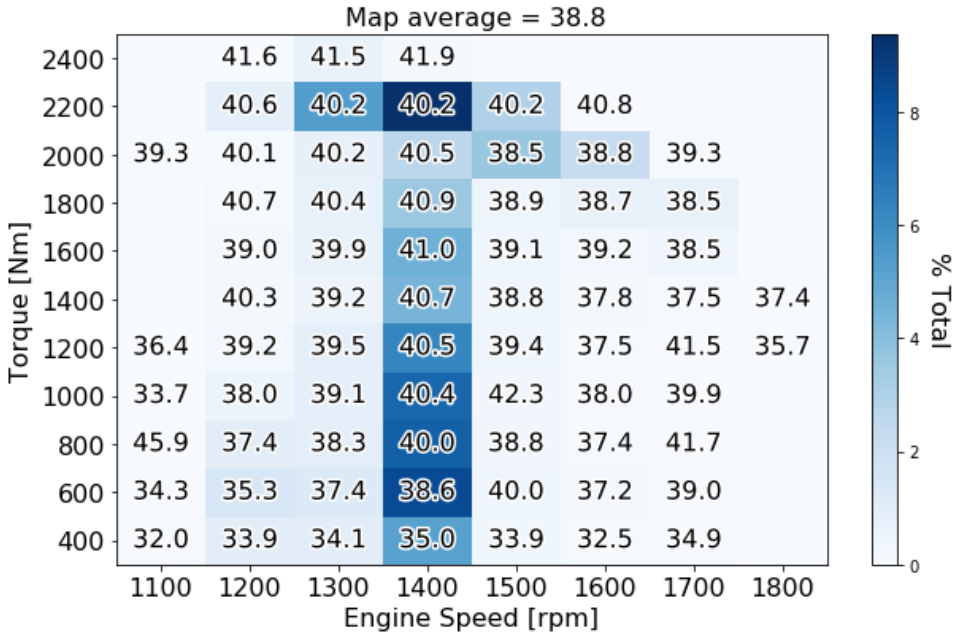

Figure 5-8: Thermal efficiency – diesel baseline

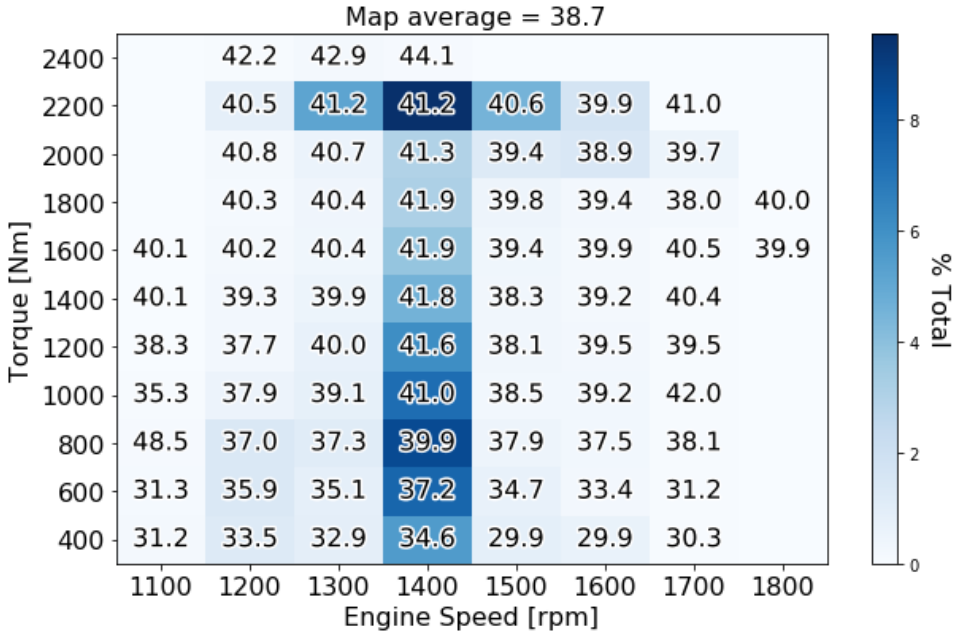

Figure 5-9: Thermal efficiency – hydrogen/diesel

5.4.3 CO_2 Maps

Figure 5-10 and **Figure 5-11** show the specific CO_2 emissions for each operating mode.

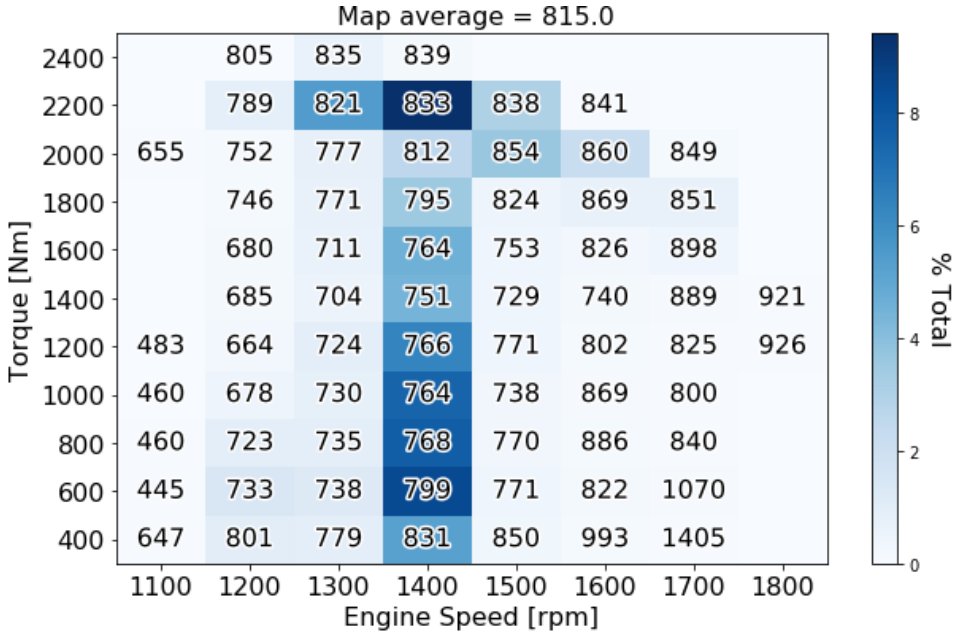

Figure 5-10: CO_2 [g/kW.h] – diesel baseline

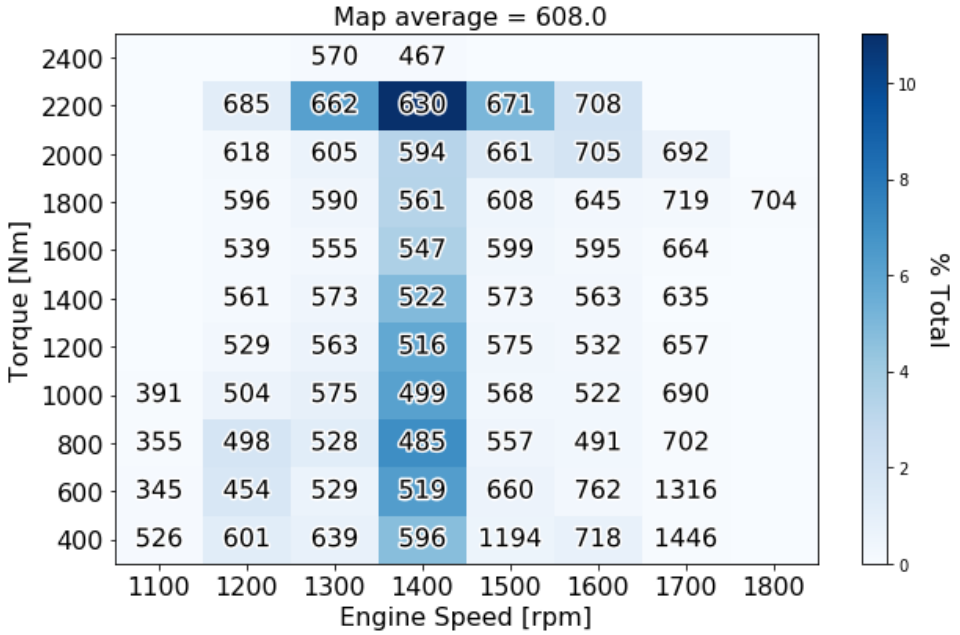

Figure 5-11: CO_2 [g/kW.h] – hydrogen/diesel

Hydrogen substitution results in a decrease in CO_2 output across the operating map. A greater decrease is seen at the low torque end of the map, corresponding with the area of higher hydrogen displacement.

In addition to the specific output it is useful to look at the total contribution to the run from a specific point on the operating map. Unlike the previous map, the results here will be separated into the unloaded and loaded cases for clarity.

CO_2 percent contributions for each fueling mode in the unloaded case is presented in **Figure 5-12** and **Figure 5-13.** In the unloaded case for both fueling modes, the highest contribution to CO_2 output comes from the lower torque region between 800 and 1200 N-m, which makes sense as this is where the engine spends most of its time while unloaded. An interesting difference to note, however, is that while operating in diesel-hydrogen mode a noticeably greater contribution comes from the high torque points at 2000 and 2200 N-m. This may be explained by the noticeably lower hydrogen displacement that occurs at these operating points, see *Section 5.2.1*.

For the loaded case the percent contribution of total CO_2 output is shown in **Figure 5-14** and **Figure 5-15**.

For both fueling modes the loaded case had the largest CO_2 contribution from the high torque points: 2200 N-m at 1200 and 1400 rpm. These are the most common operating points while the truck is loaded, so combined with the high power output their dominance is logical.

Overall, the run contribution plots show that CO_2 reduction efforts, such as increasing hydrogen displacement, should be focused on the most common operating points.

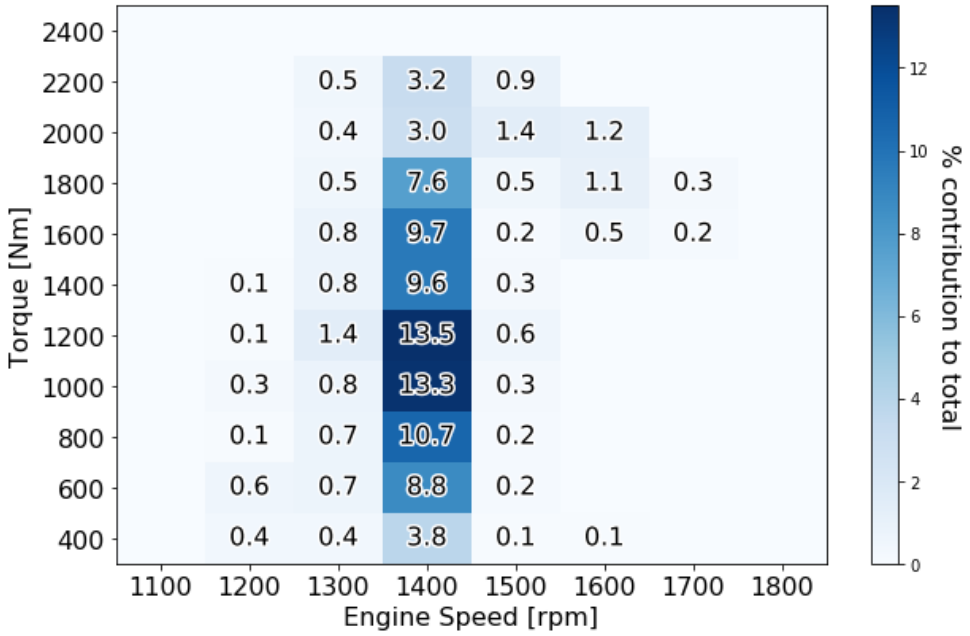

Figure 5-12: CO_2 % contribution – diesel unloaded

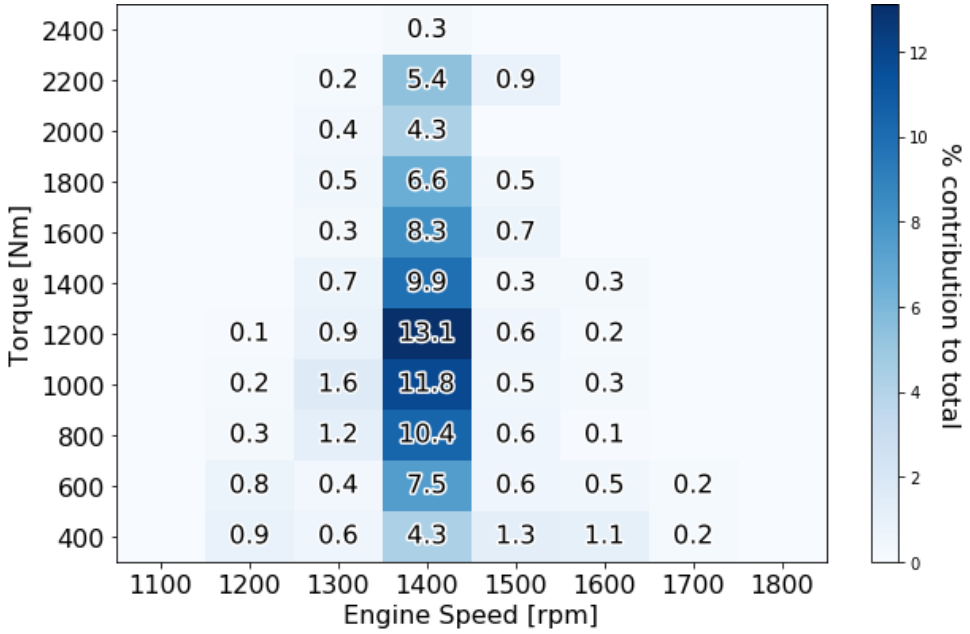

Figure 5-13: CO_2 % contribution – hydrogen/diesel unloaded

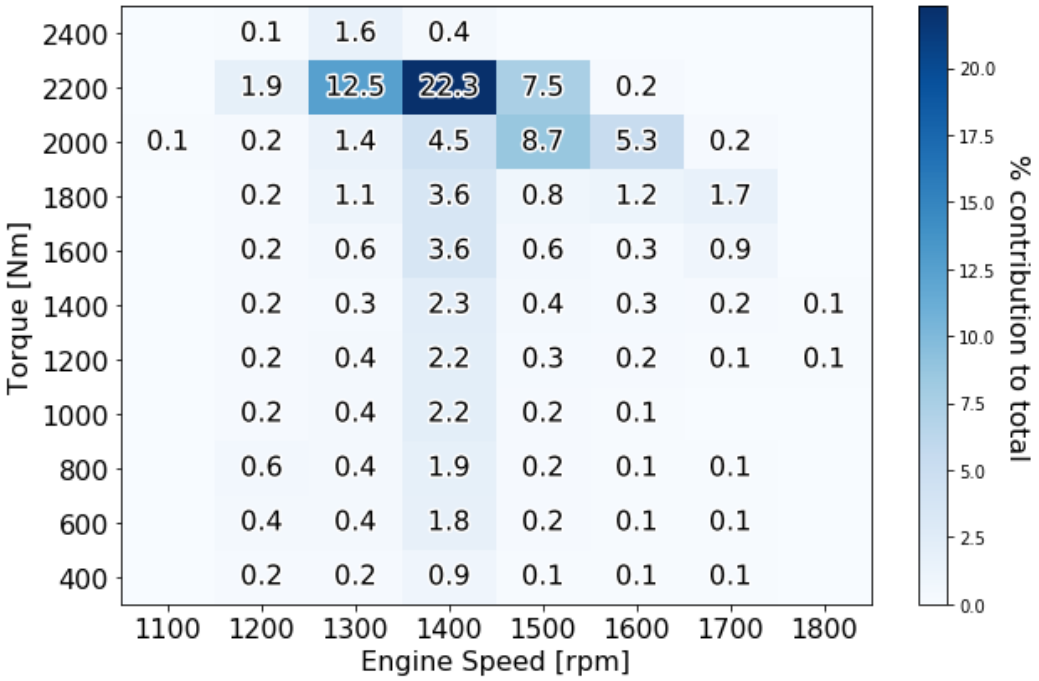

Figure 5-14: CO_2 % contribution – diesel loaded

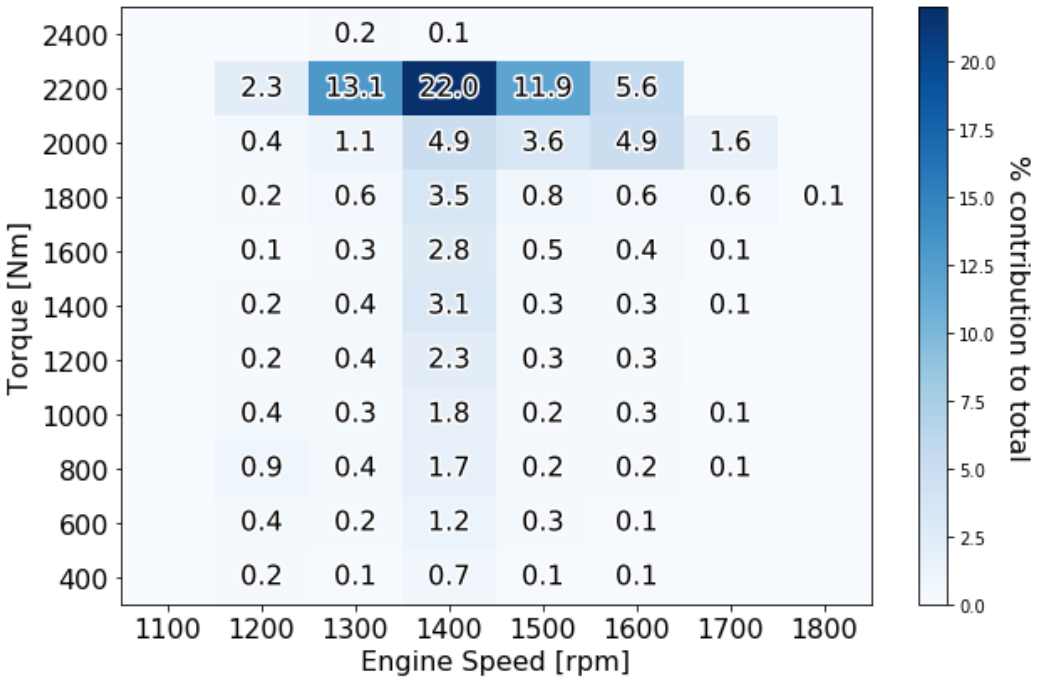

Figure 5-15: CO_2 % contribution – hydrogen/diesel loaded

5.4.4 NOx Maps

Specific NOx emissions are presented in **Figure 5-16** and **Figure 5-17**.

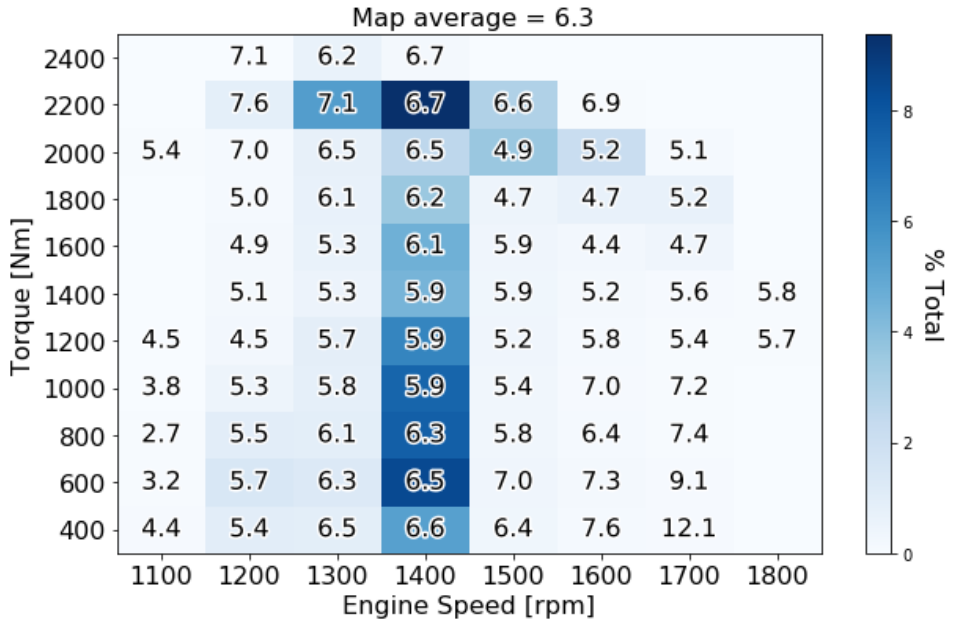

Figure 5-16: NOx [g/kW.h] – diesel baseline

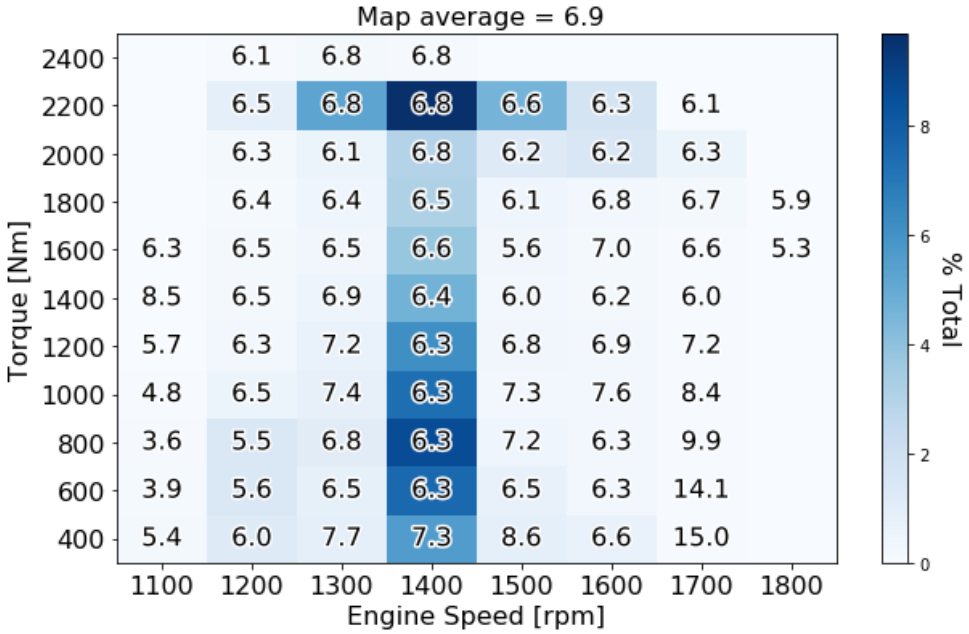

Figure 5-17: NOx [g/kW.h] – hydrogen/diesel

NOx emissions are slightly higher across the operating map in hydrogen/diesel mode. Higher in-cylinder temperatures are suspected as the cause of elevated NOx levels, see *Section 5.2.3* for EGT maps and *Section 5.3.4.1* for further discussion. An exception to this is the 600 N-m @ 1400 rpm point, where hydrogen displacement is quite high at 34.9% yet the NOx seems to decrease. This could be an example where, as seen in some previous studies, hydrogen substitution at low loads may not increase NOx production and can even reduce it. As discussed in the literature review this may be because at low loads the in-cylinder temperature increase caused by hydrogen substitution is still below a critical threshold. NOx formation may be inhibited by reduced oxygen concentration due to hydrogen displacement. As noted in the literature review, hydrogen substitution also tends to move more of the combustion into the pre-mixed phase which can also reduce NOx formation.

Observations like this on an individual cell need to be approach with caution though. The difference between the corresponding cells is only about 3% so error in the measurements must be considered, and so should the trend in the neighbouring cells. Measurement error will be discussed in ***Section 5.4***.

Contribution to the total NOx output is broken down into the unloaded and loaded cases. **Figure 5-18** and **Figure 5-19** present the unloaded cases for each fueling mode. In both fueling modes the largest NOx contribution while unloaded comes from the most common operating points 800 to 1200 N-m at 1400 rpm. The high torque point at 2200 N-m is somewhat overrepresented compared to the time spent there in each fueling mode, something which can be explained by high temperatures and a high exhaust flow rate at that point.

Figure 5-20 and **Figure 5-21** present the NOx contribution in the loaded case for each fueling mode, the highest contributions for both modes come from the high torque points at 2200 N-m.

The NOx contribution maps show a similar trend to the CO2 contribution maps in *Section 5.2.3*: across a run, either unloaded or loaded, the largest amount of NOx is produced at the most common operating points.

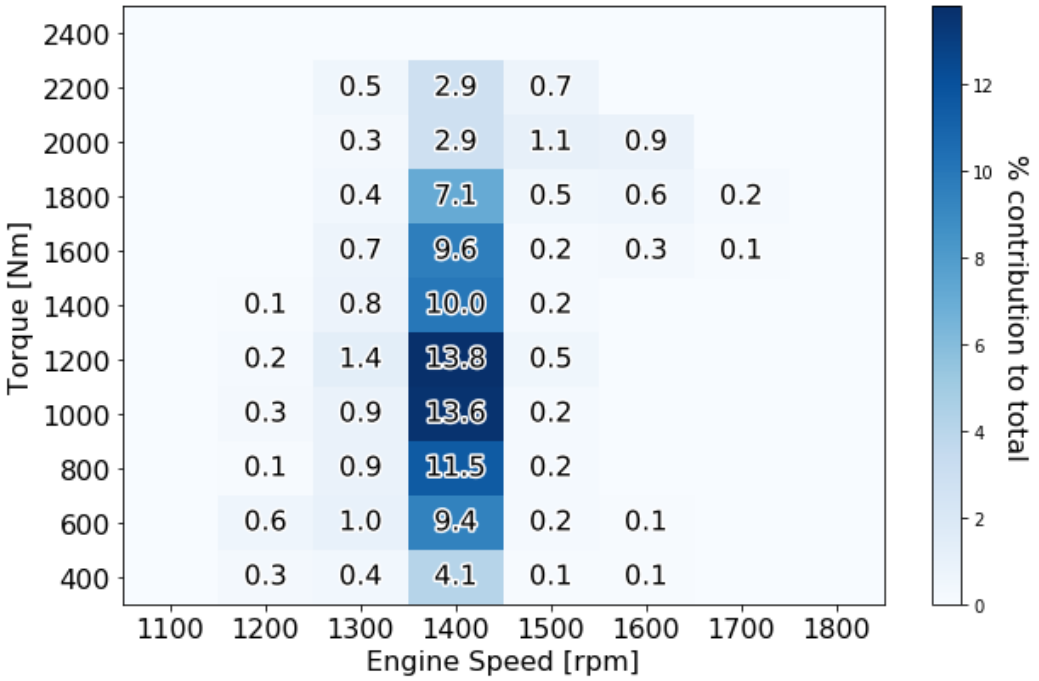

Figure 5-18: NOx % contribution – diesel unloaded

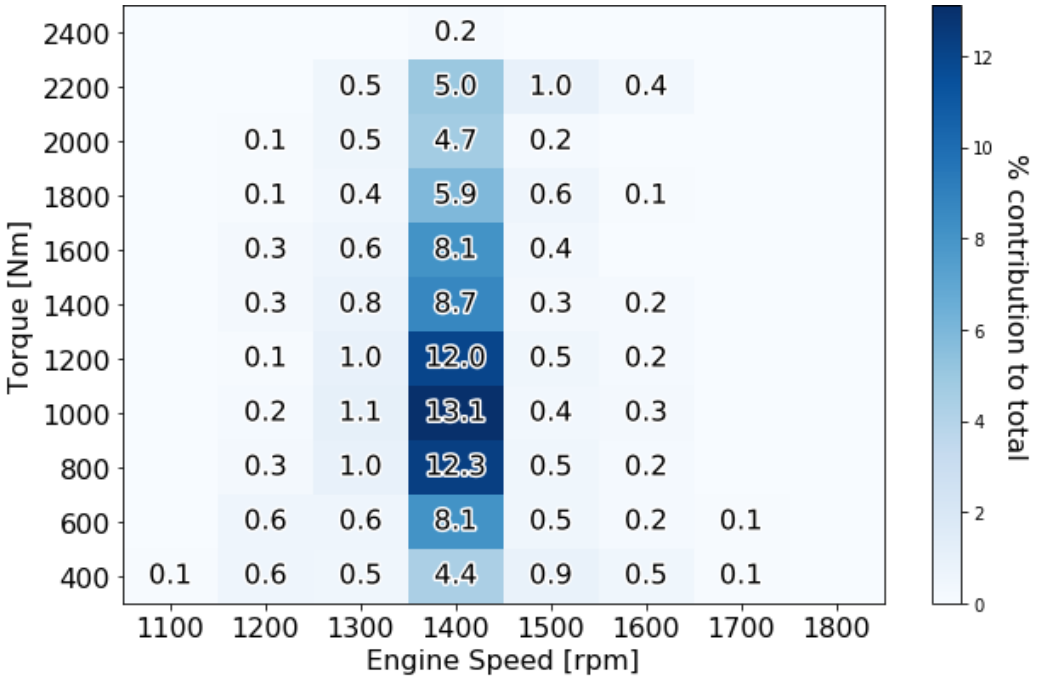

Figure 5-19: NOx % contribution – hydrogen/diesel unloaded

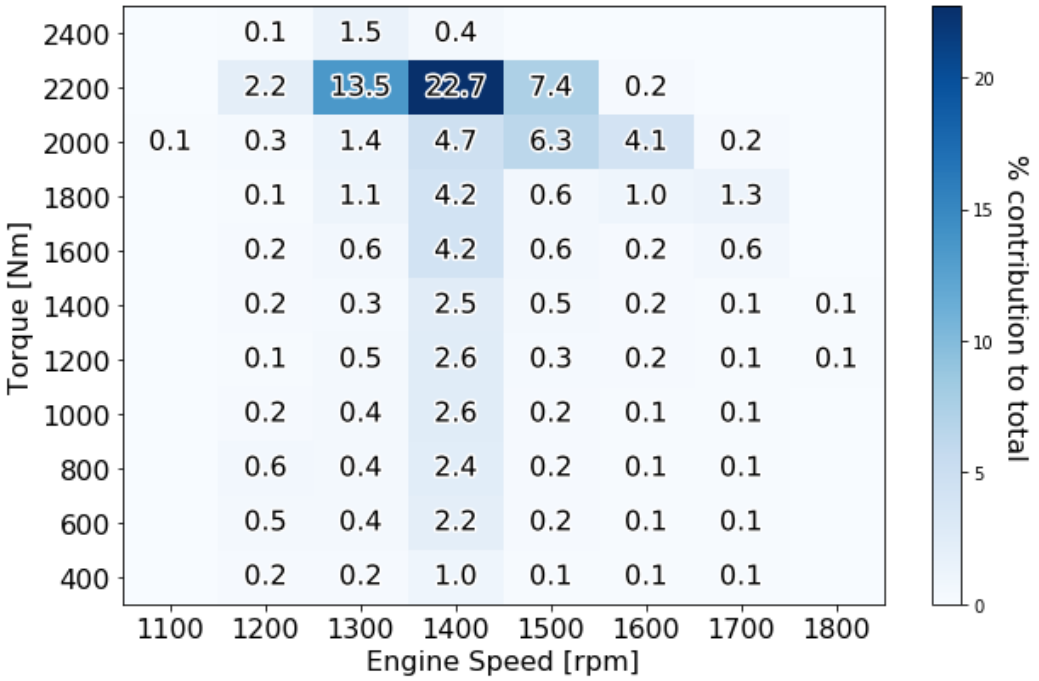

Figure 5-20: NOx % contribution – diesel loaded

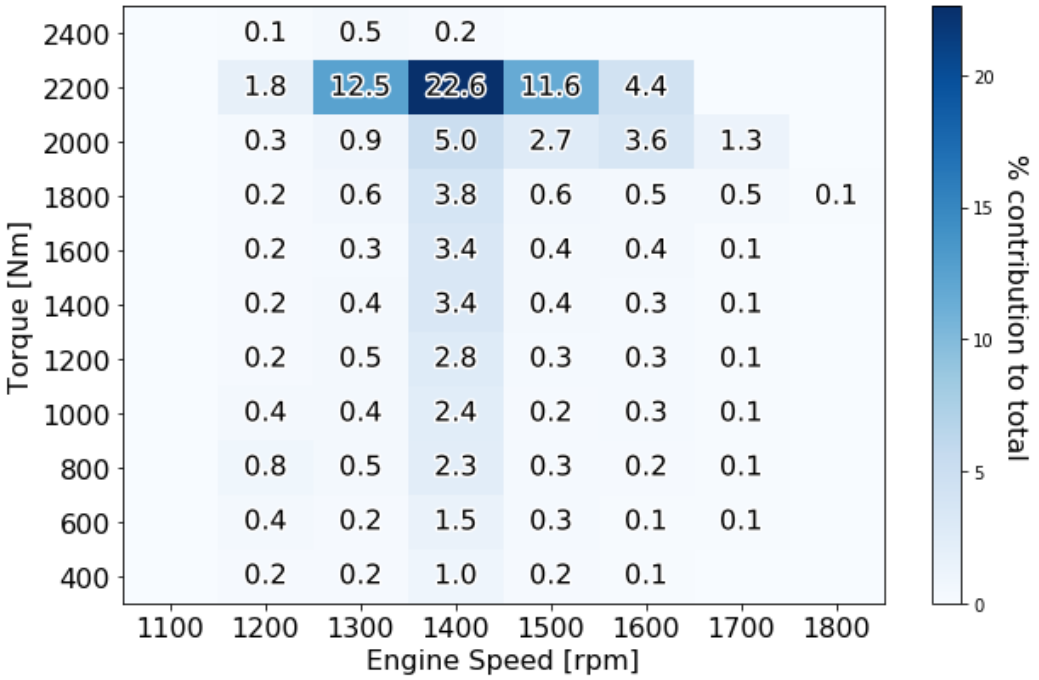

Figure 5-21: NOx % contribution – hydrogen/diesel loaded

5.4.5 PM Maps

Specific PM emissions are presented in **Figure 5-22** and **Figure 5-23**.

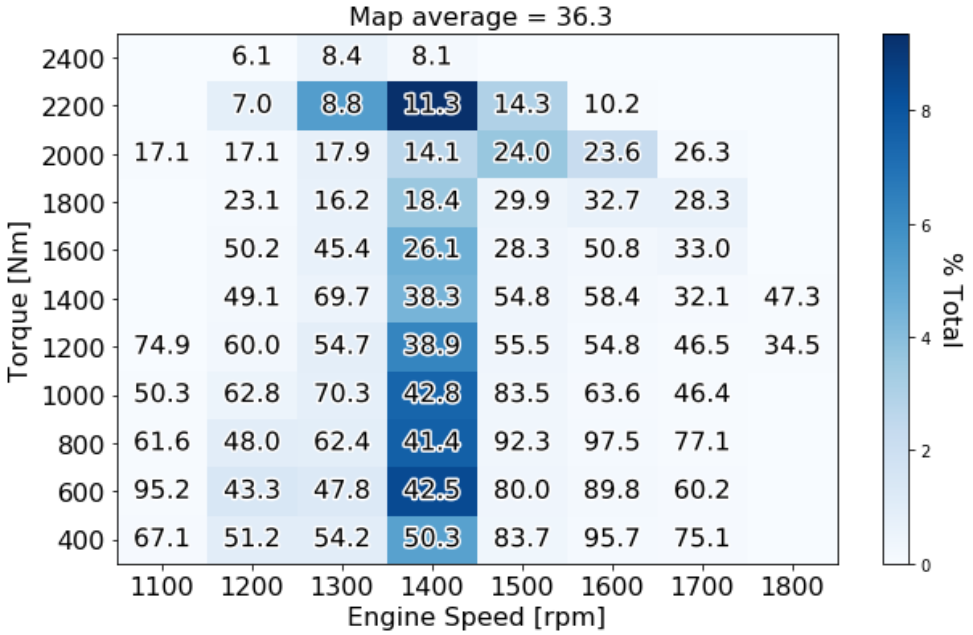

Figure 5-22: PM [mg/kW.h] – diesel baseline

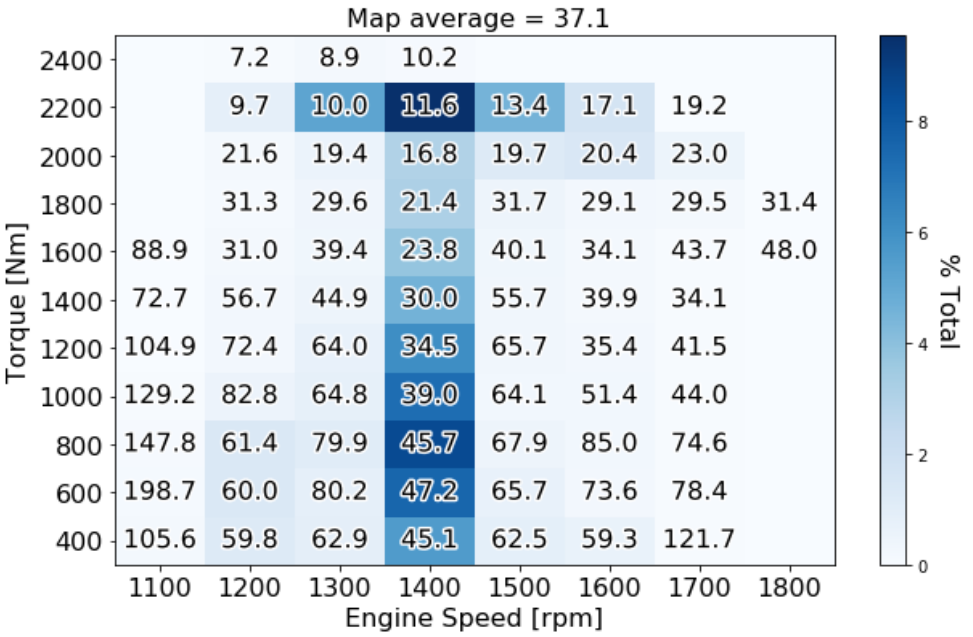

Figure 5-23: PM [mg/kW.h] – hydrogen/diesel

The trend in these PM figures is notably different than the corresponding CO_2 and NOx figures. First, the emissions in the 1400 rpm column, where the engine spends most of its time during

the drive cycle, are similar between the two fueling modes, but slightly higher in hydrogen/diesel co-combustion mode. Second, PM emissions tend to go up both above and below the 1400 rpm speed column. This is true in both fueling modes and the increases can be quite pronounced. A potential explanation is that outside the 1400 rpm speed column, loads points are more likely to correspond to transient engine operation and in these cases mixture control is not as good, hence there is an increase in PM emissions.

The relative contribution of each point in the operating map to the total PM output while the truck unloaded is presented for each fueling mode in **Figure 5-24** and **Figure 5-25**.In the unloaded case the highest amount of PM is generated by the most common operating points. This is true for both fueling modes and follows the same trend seen for CO_2 and NOx emissions.

The percent contribution for PM while loaded in each fueling mode is shown in **Figure 5-26** and **Figure 5-27**. Here the percent contribution maps reveal something interesting. While the largest contributor in each fueling mode is still 2200 N-m at 1400 rpm, the most common operating point, the percent contribution is now much smaller. In terms CO_2 and NOx, this cell contributes 22-23% of the total emission, whereas for PM it is less than half of that.

Overall the percent contribution plots show that, in the case of PM emissions, improvements in engine calibration should be focused in the low torque regions.

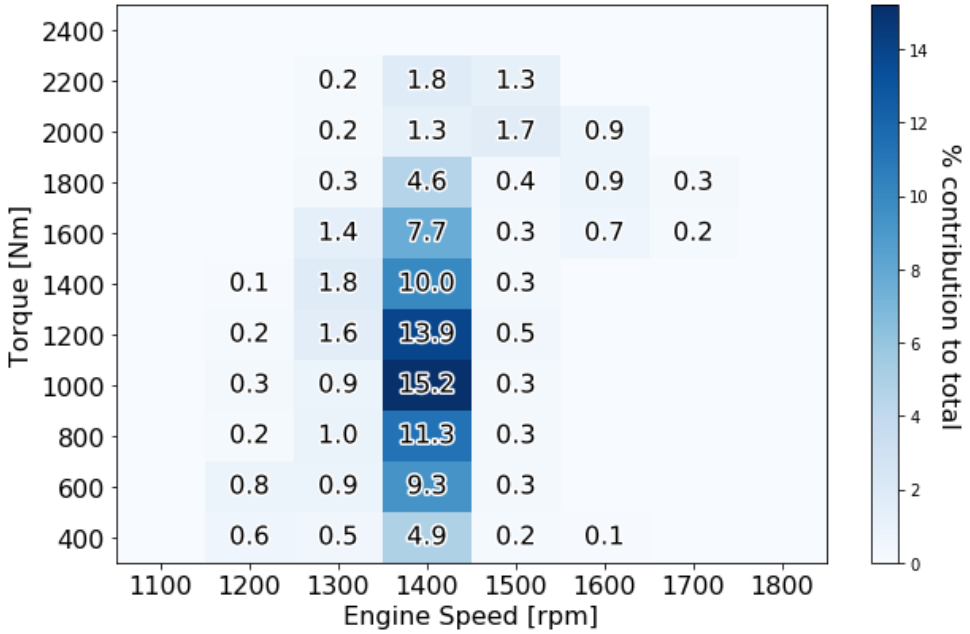

Figure 5-24: PM % contribution – diesel unloaded

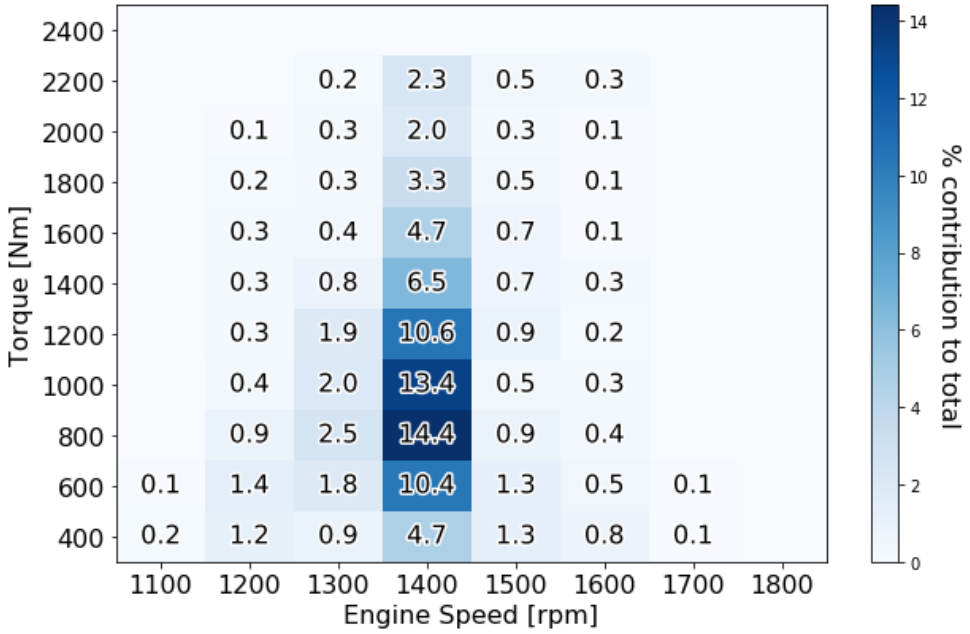

Figure 5-25: PM % contribution – hydrogen/diesel unloaded

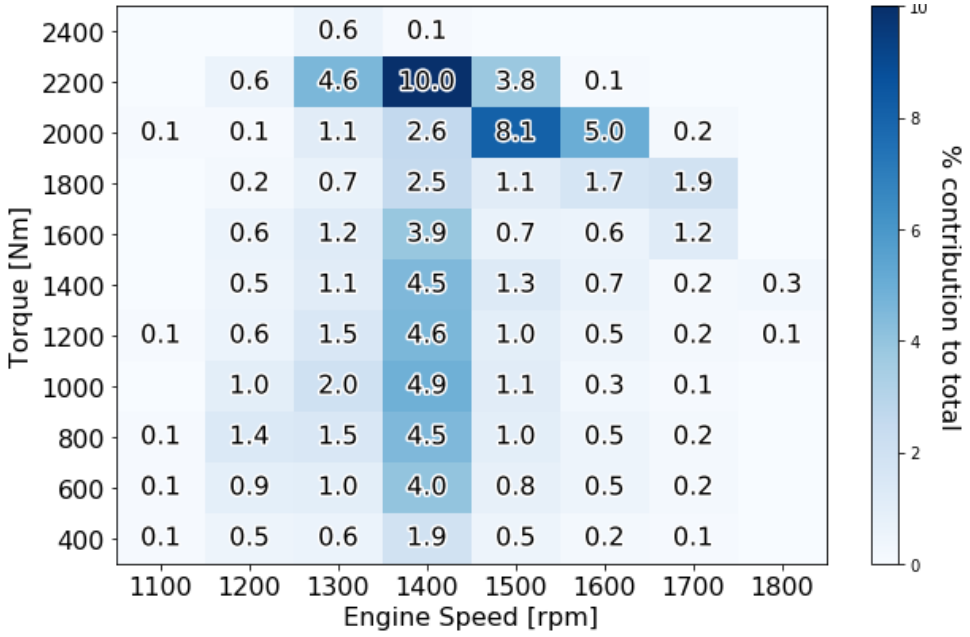

Figure 5-26: PM % contribution – diesel loaded

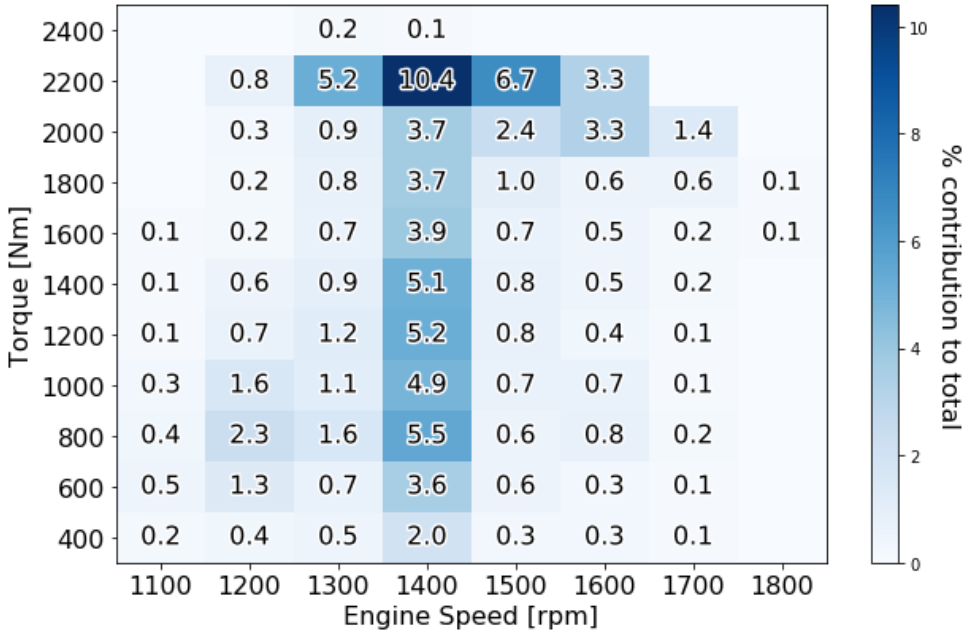

Figure 5-27: PM % contribution – hydrogen/diesel loaded

5.4.6 Exhaust Gas Temperature Maps

Exhaust gas temperature maps are presented in **Figure 5-28** and **Figure 5-29**. Exhaust gas temperatures are noticeably increased across operating range with the addition of hydrogen. The increases of 30-50℃ may be due to hydrogen's hotter adiabatic flame temperature or could be due to other effects, such as ignition delay. This will be discussed further in *Section 5.5.*

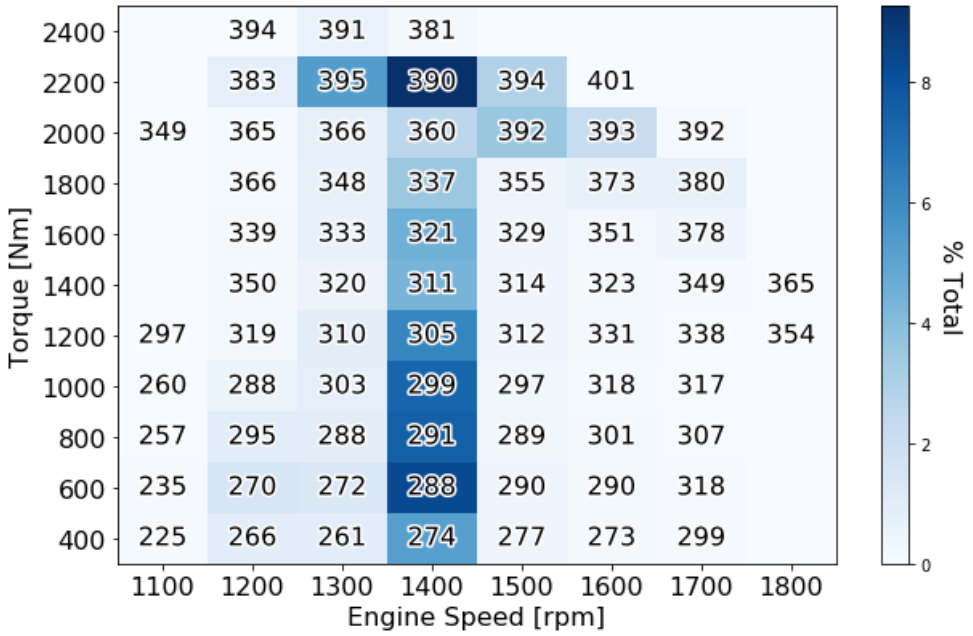

Figure 5-28: Exhaust gas temperature [℃] – diesel baseline

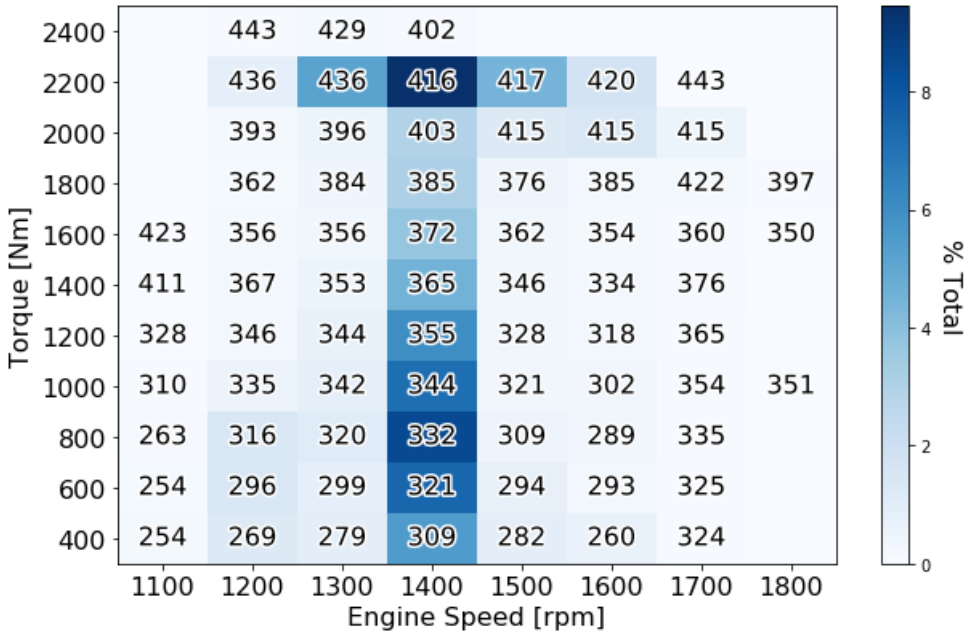

Figure 5-29: Exhaust gas temperature [C] – hydrogen/diesel

5.4.7 Global Equivalence Ratio Maps

The global equivalence ratio is investigated as a potential cause for changes in emission rate. Global equivalence ratio is calculated in **Equation 5-2**:

$$\phi = \frac{A/F_{stoich}}{A/F_{actual}} = \frac{\dot{m}_{hydrogen} A/F_{stoich,hydrogen} + \dot{m}_{diesel} A/F_{stoich,diesel}}{\dot{m}_{air} + \dot{m}_{EGR}(1-\phi)} \quad (5\text{-}2)$$

Where each ṁ is the mass flow rates for each fuel, for air, and for the exhaust gas recirculation (EGR). This last parameter complicates the simple equivalence ratio calculation from **Equation 2-4** but is important because in lean combustion the EGR reintroduces unreacted oxygen from the exhaust stream back to the intake. A/F_{stoich} is the stoichiometric air-fuel ratio for each fuel: 34.3 for hydrogen and 14.6 for diesel. Rearranging **Equation 5-2** reveals a quadratic expression which must be solved for ϕ, as shown in **Equation 5-3**.

$$\phi^2 \dot{m}_{EGR} - \phi(\dot{m}_{air} + \dot{m}_{EGR}) + \dot{m}_{hydrogen} A/F_{stoich,hydrogen} + \dot{m}_{diesel} A/F_{stoich,diesel} = 0 \quad (5\text{-}3)$$

As shown in **Figure 5-30** and **Figure 5-31** the global equivalence ratio is generally richer when operating in hydrogen/diesel mode. The magnitude of the change, however, is small. Measurement of excess oxygen at the inlet to the aftertreatment system, as reported on J1939 message, is included in **Appendix 4**. The same trend is shown, less excess oxygen is present when the truck is operating in hydrogen/diesel fueling mode, but the magnitude of the difference is noticeably higher.

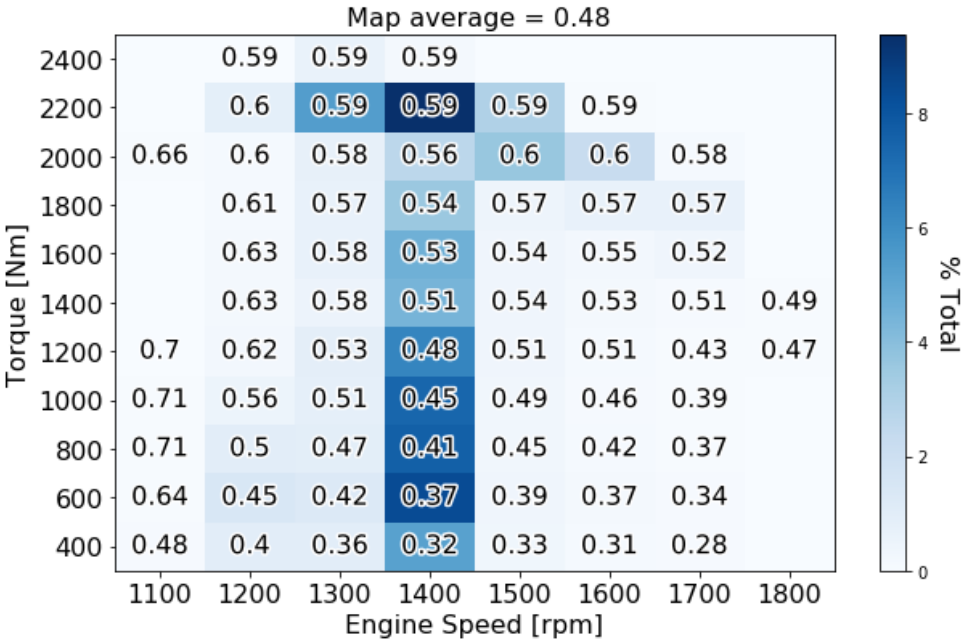

Figure 5-30: Global equivalence ratio – diesel baseline

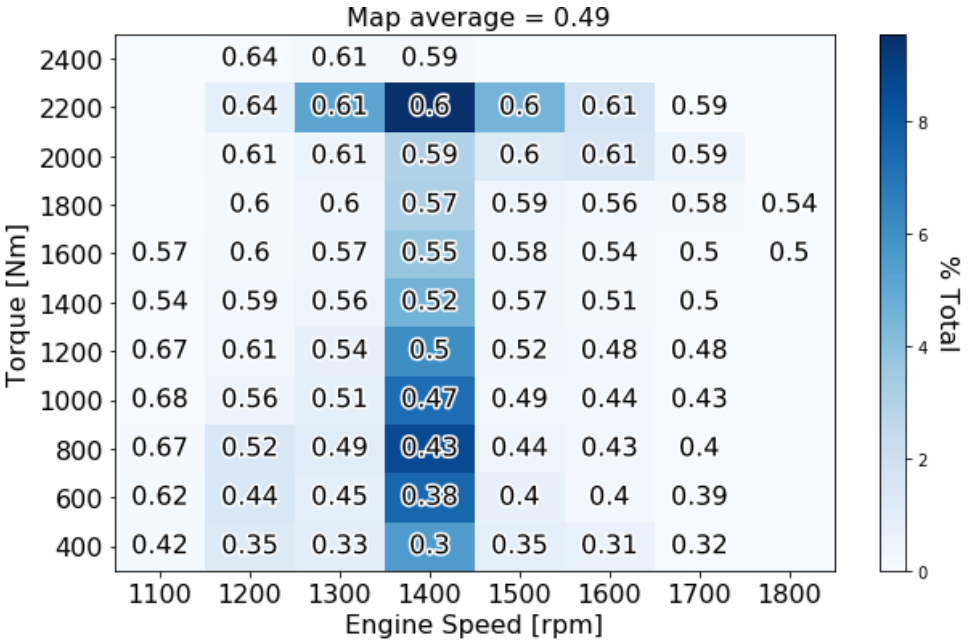

Figure 5-31: Global equivalence ratio – hydrogen/diesel

5.4.8 Exhaust Gas Recirculation Maps

Exhaust gas recirculation (EGR) rate is shown in **Figure 5-32** for the diesel baseline and **Figure 5-33** for hydrogen/diesel co-combustion. There is a noticeable increase in EGR flow rate when operating in hydrogen/diesel mode, especially pronounced at the common 2200 N-m @ 1400 rpm operating point. Increasing EGR rate is a known strategy for in-cylinder NOx control [10] and, while the exact cause of the increased EGR is unknown, it is plausible that the base diesel engine controller is detecting the elevated engine-out NOx levels shown in Section 5.2.4 and responding by increasing the EGR flow rate. EGR as a NOx control strategy comes with a trade-off though, it tends to increase PM production [10] [1]. Therefore, this change in EGR rate could be limiting the increase in NOx levels at the expense of increased PM. It would be interesting to run the two fueling modes with a fixed EGR rate to better isolate the change in fueling but that is probably not feasible with the way the truck is setup. EGR rate is controlled by the base diesel ECU and not accessible.

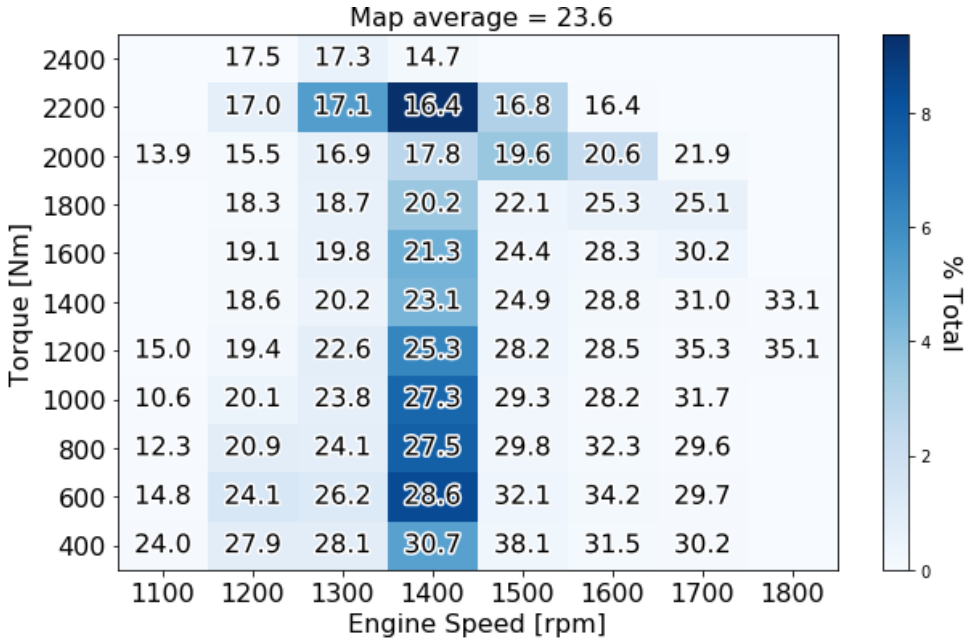

Figure 5-32: EGR rate [%] – diesel baseline

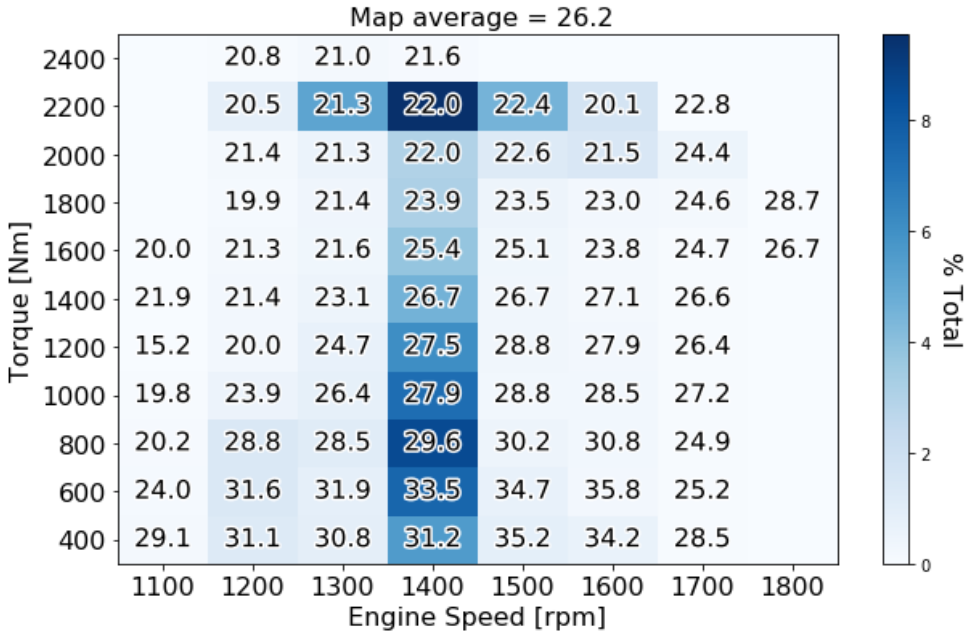

Figure 5-33: EGR rate [%] – hydrogen/diesel

5.4.9 Post-Aftertreatment NOx and Diesel Exhaust Fluid Maps

Compared to the diesel baseline, the post-aftertreatment, NOx decreased noticeably when the truck was operating in hydrogen diesel mode, as shown in **Figure 5-34** and **Figure 5-35**. This is surprising considering that the pre-aftertreatment NOx increased. A potential explanation is that the increased EGTs increase the NOx conversion efficiency in the SCR. Diesel Exhaust Fluid (DEF) consumption rate increased only slightly in hydrogen/diesel mode versus the diesel baseline as shown in **Figure 5-36** and **Figure 5-37**.

Cross-sensitivity to ammonia is a concern with the electrochemical NOx sensor used to read post-aftertreatment NOx. In co-combustion mode the DEF dosing rate increased, and the exhaust temperature also increased and therefore, based on **Equation 3-1**, ammonia slip would, if anything, push post-aftertreatment NOx levels erroneously high in hydrogen/diesel mode. The decrease in post-aftertreatment NOx shows that this is not happening. Another possibility is that ammonia slip is occurring in the baseline diesel fueling mode. This seems unlikely given that the aftertreatment system was designed and calibrated around the baseline diesel configuration. Further testing would be needed to rule this out entirely however.

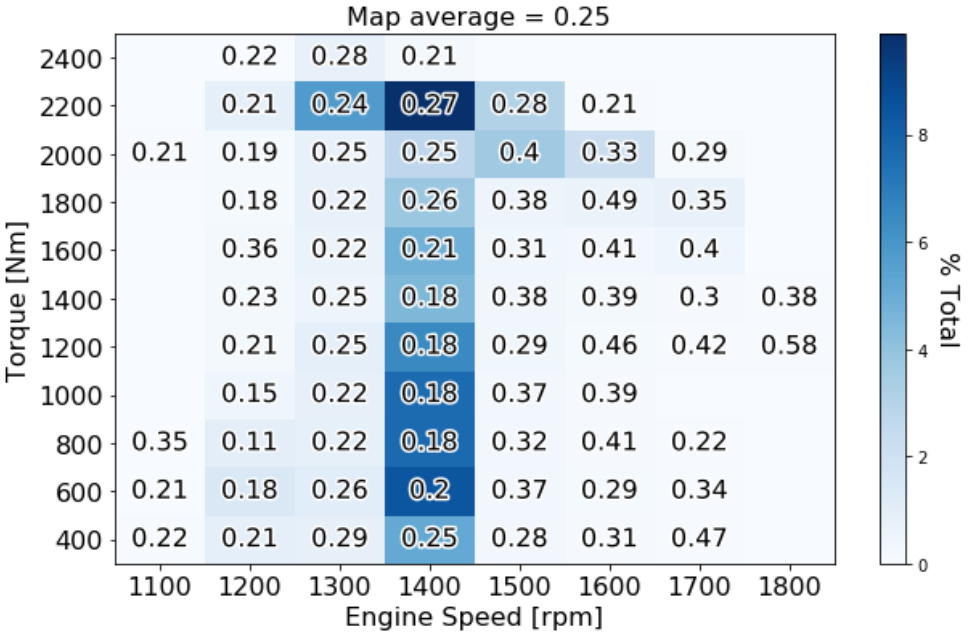

Figure 5-34: Treated NOx [g/kW.h] – diesel baseline

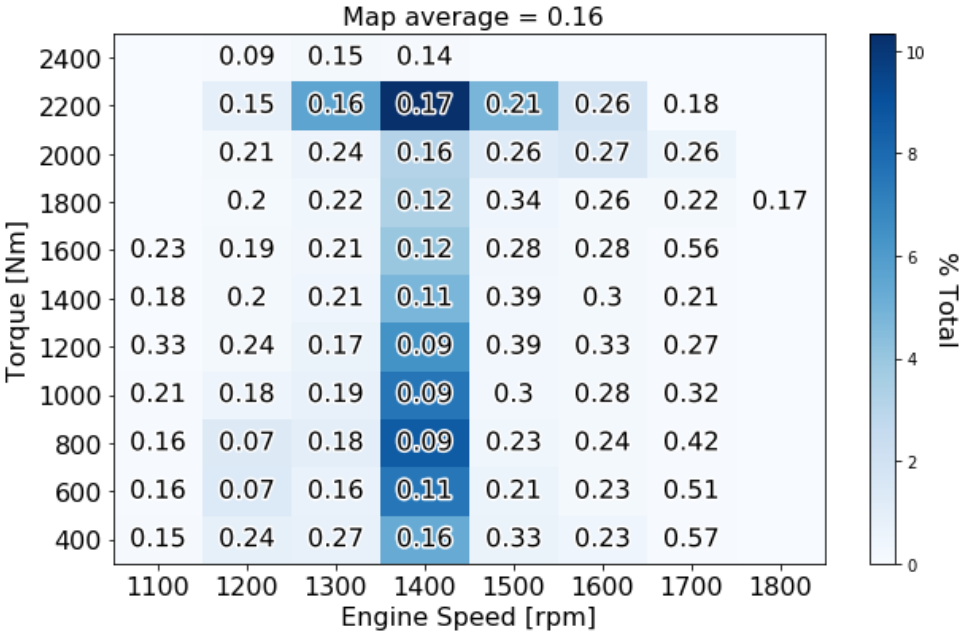

Figure 5-35: Treated NOx [g/kW.h] – hydrogen/diesel

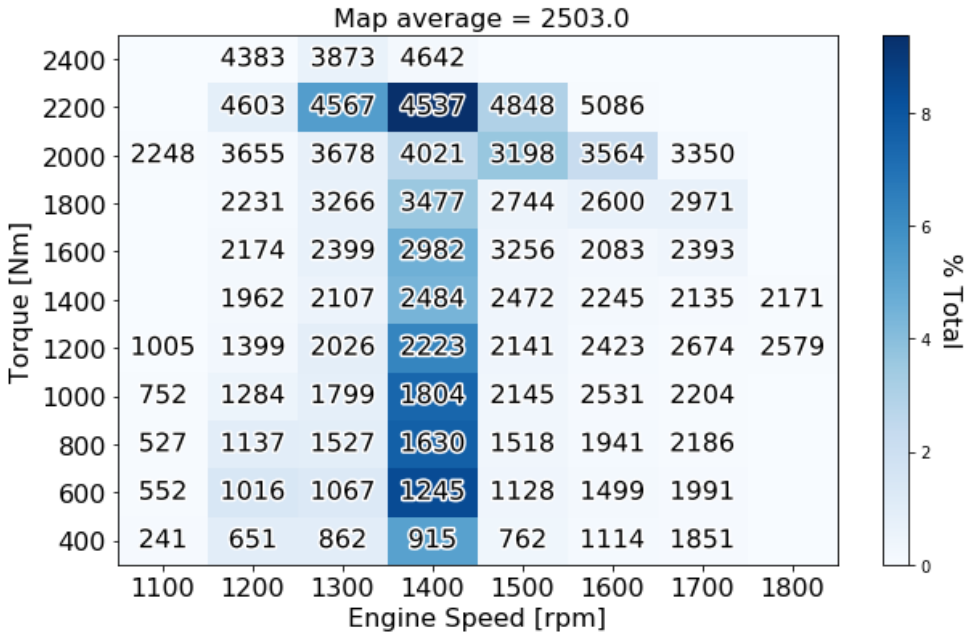

Figure 5-36: DEF dosing rate [g/hr] – diesel baseline

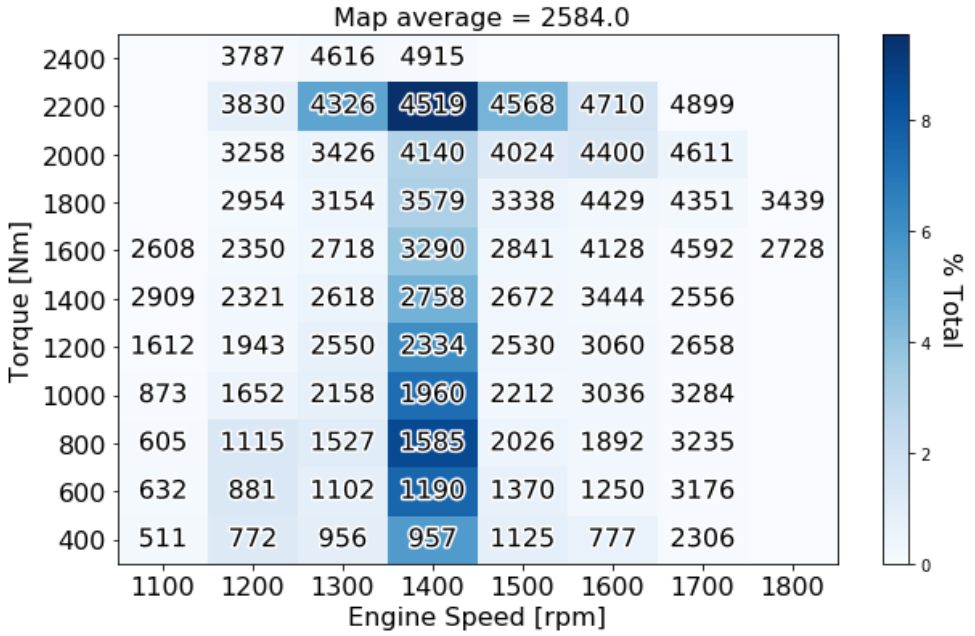

Figure 5-37: DEF dosing rate [g/hr] – hydrogen/diesel

5.5 Mechanisms for EGT Increase

Several factors may contribute to the elevated exhaust gas temperatures seen in hydrogen/ diesel mode: hydrogen's higher adiabatic flame temperature, a slightly richer mixture, and delayed ignition timing. This section investigates these potential mechanisms to find which are significant.

The approach is to calculate an adiabatic flame temperature in the cylinder based on the known parameters and then to apply an adiabatic expansion to the contents to estimate the exhaust gas temperature. The purpose of this simplified approach is to find the trends and relative contributions of the potential mechanisms, rather than a precise final temperature.

Adiabatic flame temperature was calculated based on the enthalpies of formation and the enthalpies as a function of temperature of the reactants and products.

$$\sum_P \left(\bar{h}_f^\circ + \bar{h} - \bar{h}^\circ\right)_p = \sum_r \left(\bar{h}_f^\circ + \bar{h} - \bar{h}^\circ\right)_r \qquad (5\text{-}4)$$

Table 5-4: Enthalpies of formation [48]

Species	$\bar{h}_f^\circ$ [kJ/kmol]
$C_{12}H_{26}$	-291,010
CO_2	-393,520
H_20	-241,820

Reactant temperatures are elevated based on isentropic compression of the incoming air charge as shown in **Equation 5-5**.

$$T_2 = T_1(CR)^{k-1} \qquad (5\text{-}5)$$

The incoming air temperature, T_1, is considered as 300 K. During the 2019 measurement campaign, observed intake air temperatures ranged between 286 K and 340 K. Therefore 300 K is a reasonable, perhaps slightly low, assumption. The ratio of specific heats, *k*, is considered a constant 1.4. The volume ratio CR is considered as the nominal compression ratio of the engine which is 18.5.

Combustion occurs near top dead centre and full fuel conversion was assumed as shown in **Equation 5-6**.

$$C_{12}H_{26} + aH_2 + b(O_2 + 3.76N_2) \rightarrow cCO_2 + dH_2O + (b-1)O_2 + b3.76N_2 \qquad (5\text{-}6)$$

The equilibrium effects which prevent full reaction completion at high temperature is ignored, as is the formation of unwanted by products, such as NO and NO_2. Therefore, this calculation will somewhat overestimate the adiabatic flame temperature. Furthermore, inside the cylinder there will also be heat transfer which will also lower the maximum temperature achieved. The purpose here is not to achieve a high accuracy number, but instead estimate the change between the two fueling modes. Utilizing this approach **Table 5-5** shows the adiabatic flame temperature at a common high torque point and a common low torque point for each operating mode.

Table 5-5: Adiabatic flame temperature - common operating points

Operating Condition	Diesel Baseline	Hydrogen-diesel co-combustion
2200 N-m @ 1400 rpm	φ = 0.63 AFT = 2250 K	%H_2 = 12.7 φ = 0.66 AFT = 2350 K
600 N-m @ 1400 rpm	φ = 0.43 AFT = 1920 K	%H_2 = 35.2 φ = 0.44 AFT = 2000 K

Real in-cylinder maximum temperatures are unknown and therefore comparison to the experimental results requires calculating the expected exhaust gas temperature following expansion. The approach was to consider instantaneous combustion at the same crank angle, followed by an adiabatic expansion of the products with constant ratio of the specific heats, as shown in **Equation 5-7**.

$$T_4 = \frac{T_3}{(ER)^{k-1}} \qquad (5\text{-}7)$$

Where T_3 is the adiabatic flame temperature, T_4 is the exhaust gas temperature, ER is the expansion ratio and k is the ratio of specific heats. The expansion ratios used are listed in **Table 5-6** and come from considering expansion from an instantaneous point of combustion at some point after top dead centre. There was no in-cylinder measurement conducted during the testing and therefor CA50 can't be verified. In lieu of this, values of 5, 10, and 15 degrees after top dead centre have been chosen to cover the likely range of values. These are considered as the

values for CA50 of the diesel baseline and potential ignition delay from the addition of hydrogen was considered on top of this. Testing under relevant conditions has shown that hydrogen may introduce an ignition delay of approximately 0.8 ms [49] which at 1400 rpm corresponds to 7 crank angle degrees. The motivation is to see if an increase in exhaust gas temperatures signals an increase in the peak in-cylinder temperature or if it may instead be caused by ignition delay. The calculated effects on EGT of increased AFT alone and increased AFT plus this ignition delay versus the diesel baseline are presented in **Table 5-6**.

Table 5-6: Exhaust gas temperature calculations [℃]

Operating Condition	CA50 = 5 deg aTDC			CA50 = 10 deg aTDC			CA50 = 15 deg aTDC		
	Diesel Base-line	AFT change only	AFT change + 0.8 ms ignition delay	Diesel Base-line	AFT change only	AFT change + 0.8 ms ignition delay	Diesel Base-line	AFT change only	AFT change + 0.8 ms ignition delay
Expansion Ratio	18.5	18.5	18.3	18.4	18.4	18.2	18.3	18.3	18
2200 N-m @ 1400 rpm	427	458	460	429	460	465	430	462	468
600 N-m @ 1400 rpm	326	349	351	326	351	355	327	352	358

As shown in **Table 5-6** the dominant effect on elevated exhaust gas temperatures is the increase in the adiabatic flame temperature caused by a combination of the presence to the hydrogen plus the slightly richer mixture, this can increase the exhaust gas temperature 23-32℃. The effect of ignition delay was smaller, increasing the exhaust gas temperature 2-6℃.

Table 5-7 compares the preceding calculations to the experimental results shown previous in *Section 5.2.6*.

Table 5-7: Exhaust gas temperature - comparison calculations to experimental results [C]

Operating Condition	Calculations			Experimental Results		
	Diesel Baseline	Hydrogen-diesel co-combustion	Difference	Diesel Baseline	Hydrogen-diesel co-combustion	Difference
2200 N-m @ 1400 rpm	427-430	458-468	21 – 38	390	416	26
600 N-m @ 1400 rpm	326-327	349-358	23 – 31	288	321	33

In all cases the calculations overpredict the measured exhaust gas temperature. This is expected as the calculated values neglect heat transfer losses. Instead the change in temperature between the two fueling modes is key. In both the high torque and low torque cases the calculations predict an increase which is similar to the observed increase. In the low torque case, the predicted increase is less than the measured increase suggesting either that the ignition delay in this case is longer than assumed or perhaps something else is pushing the temperature up. A more in-depth analysis should consider effects of reaction equilibrium and NOx production on predicted EGT.

5.6 Variability in Emissions vs Variability in Drive Cycle

Implicit in on-road testing is the idea that changes in the drive cycle change vehicle emissions. *Section 5.3* showed that, for the week of testing, the cycle was fairly consistent for both unloaded and loaded runs, but there were some differences in speed and power profiles. Therefore, when comparing the two fueling modes, it is important to try to isolate these changes in drive cycle from the changes in specific emissions.

To address this, operating points from a specific run were combined with the aggregate emission maps as follows. First, for a particular run the operating points were binned into speed load points to generate a matrix of operating points [A], with an example shown in **Figure 5-38**.

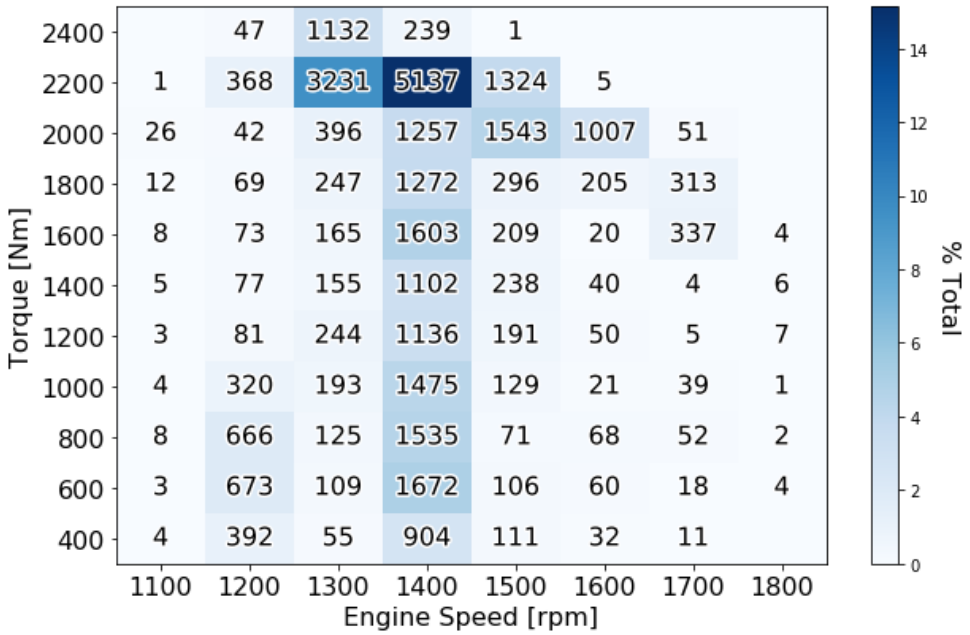

Figure 5-38: Speed/load points example – diesel loaded run

Element-wise matrix multiplication was then performed between this matrix [A] and a matrix of the aggregate emission data [B] to generate a map emission value based on that run's operating points and the aggregate emission map, as shown in **Equation 5-8**. [B] is exactly the CO2, NOx, or PM map presented in *Section 5.4.3, Section 5.4.4 or Section 5.4.5* respectively.

$$\bar{x}_{map} = \frac{\sum_0^J \sum_0^I [[A][B]]_{i,j}}{\sum_0^J \sum_0^I A_{i,j}} \qquad (5\text{-}8)$$

The results are presented alongside the individual run averages for comparison purposes. **Figure 5-39** for CO2, **Figure 5-40** for NOx, and **Figure 5-41** for PM.

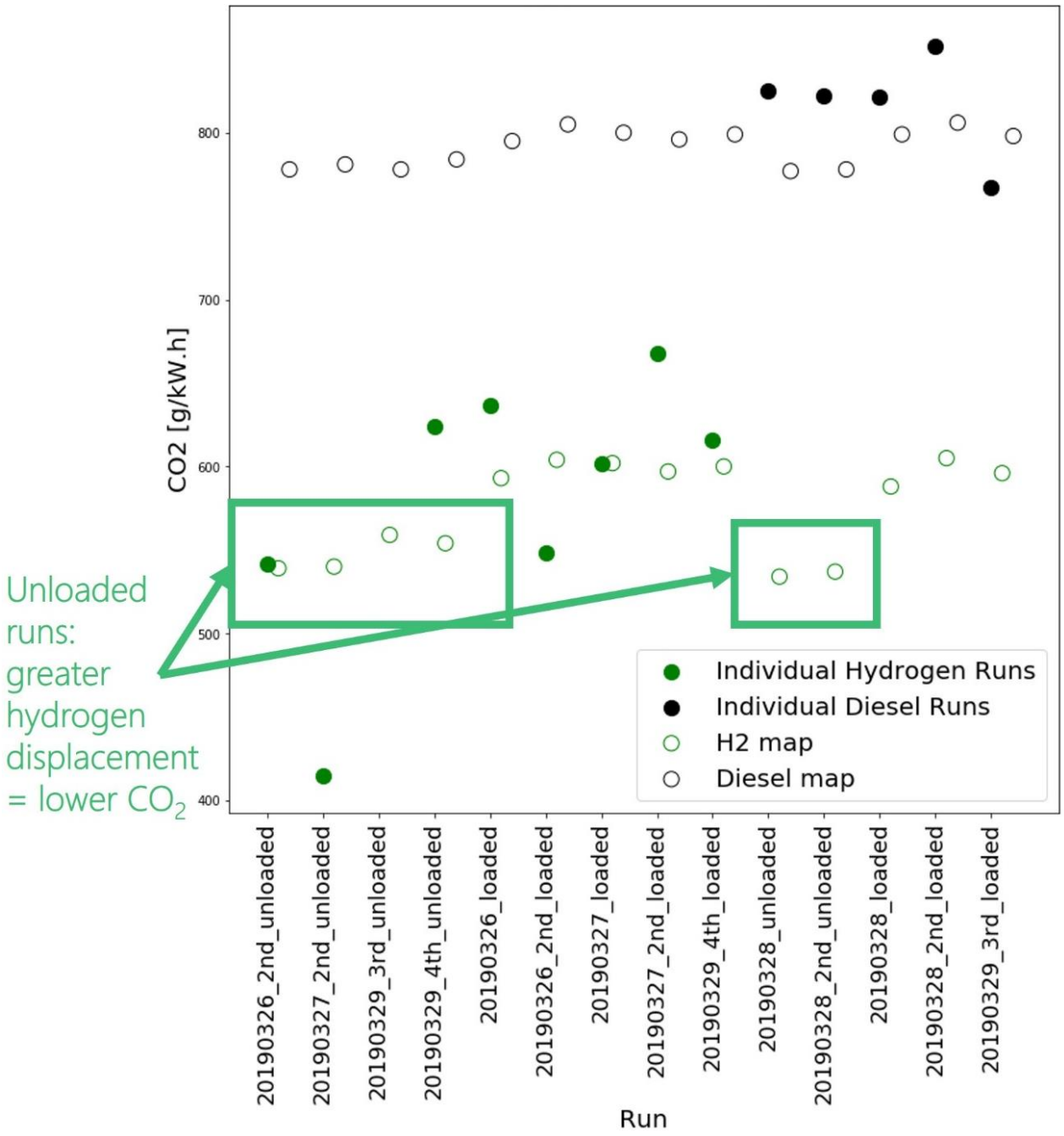

Figure 5-39: CO_2 [g/kW.h] emission vs drive cycle variability

CO_2 emissions are consistently lower with the hydrogen/diesel fueling map than the baseline diesel. Furthermore, the reduction in CO_2 emissions is greater for the unloaded runs, and this is consistent with the greater hydrogen displacement at the lower torque points.

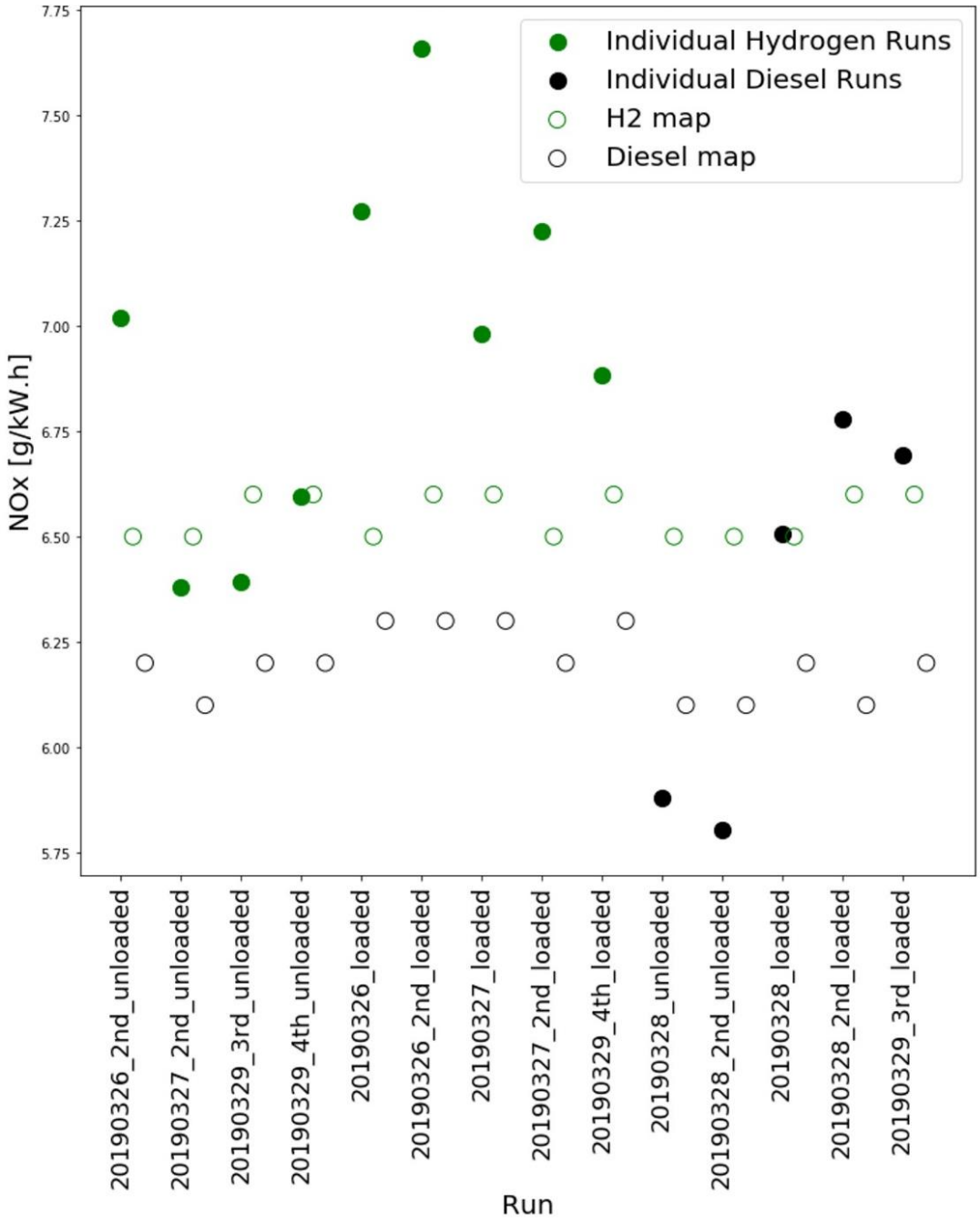

Figure 5-40: NOx [g/kW.h] emission vs drive cycle variability

In the case of NOx emissions, the hydrogen/diesel fueling map produced consistently higher emissions than the diesel map.

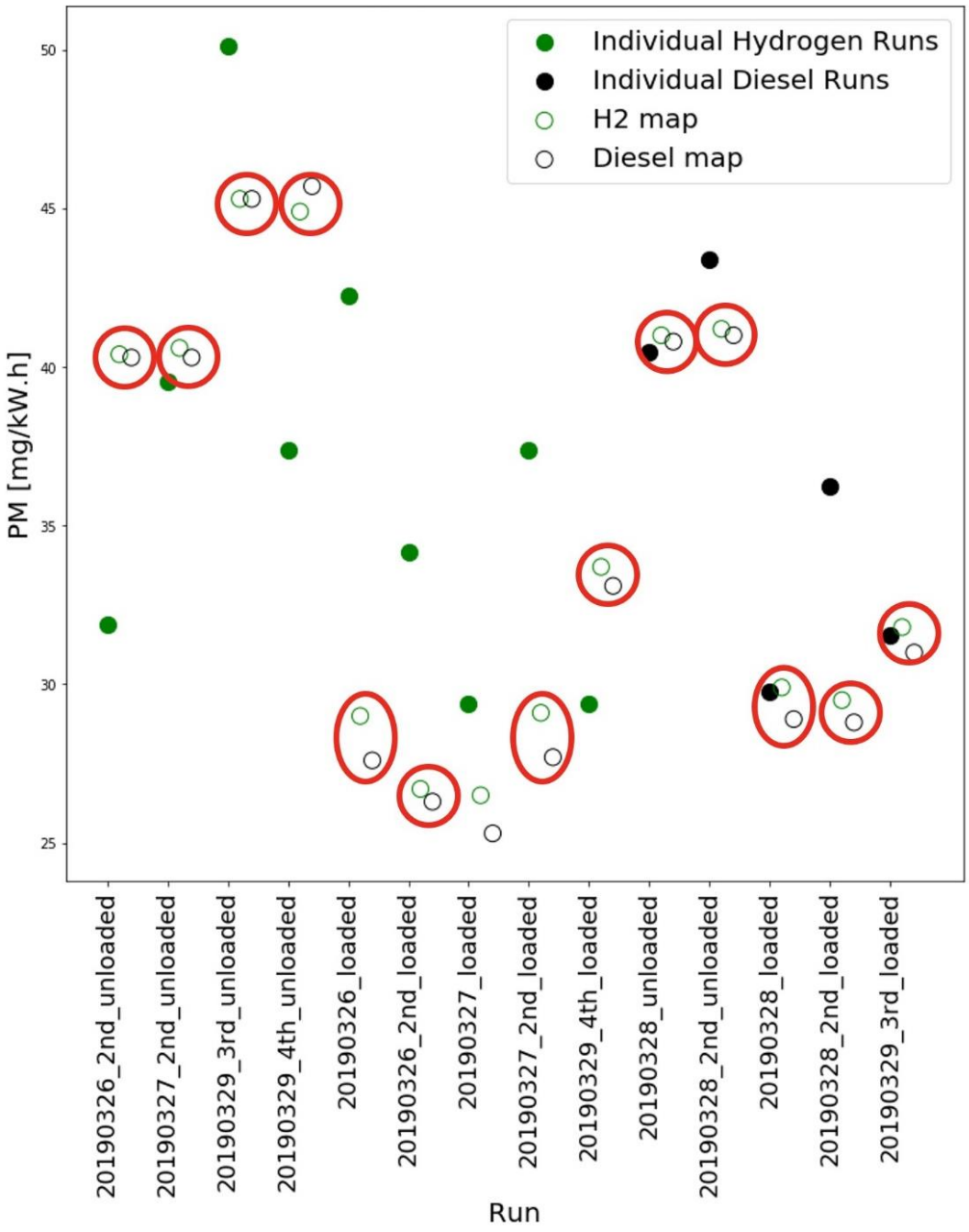

Figure 5-41: PM [mg/kW.h] emission vs drive cycle variability

For PM emissions, note that the emission value changes far more with drive cycle than it does with fueling mode.

In all cases, run to run variation in the drive cycle has an effect on the average emissions for that fueling strategy. For CO_2 and NOx the changes in the map emissions are relatively small run to run. There is also a clear trend in the mapped emissions, CO_2 is always reduced in hydrogen/diesel mode and NOx is always increased. This is not the case for the PM though, as the mapped emissions are nearly as varied as the individual runs. This suggests PM emissions are more sensitive to changes in the drive cycle than either CO_2 or NOx. Based on the emission maps shown in **Figure 5-22** and **Figure 5-23**, it seems that PM emission rates far higher outside the main 1400 rpm column, suggesting a large contribution of less frequent transient points to the overall PM. Furthermore, for PM there is no clear trend for one fueling mode versus the other. In most cases diesel map's PM is virtually the same as hydrogen/diesel map's PM.

A final comparison is to compute the average for each load condition based on the data presented in **Figure 5-39, Figure 5-40, and Figure 5-41**. The results are shown in **Table 5.8**.

Table 5-8: Emission averages – individual runs vs mapped runs

load condition	Mode	CO_2 [g/kW.h]		NOx [g/kW.h]		PM [mg/kW.h]	
		Individual Runs	Map	Individual Runs	Map	Individual Runs	Map
unloaded	H2/Diesel	583	591	6.6	6.6	40.5	40.2
	Diesel	825	824	5.8	5.8	42.3	41.9
	% diff	-29.9	-28.7	+12.9	+13.8	-5.2	-4
loaded	H2/Diesel	618	619	7.2	7.2	35.4	34.8
	Diesel	818	810	6.7	6.7	34.2	32.4
	% diff	-21.1	-23.5	+8.2	+7.5	+6.1	+7.4

5.7 Error Discussion

This section presents two distinct approaches to error calculation. First the propagated error approach is considered and the limitations of that approach for this particular project are discussed. Next a statistical approach is taken the outcome of which is considered more valid and therefore ultimately applied to the results.

5.7.1 Propagated Instrument Error

The first attempt to estimate error in the emissions measurements involved considering error in each measured parameter and propagating it to the final emission value. All sources of error were considered random + independent and combined via root mean square (RMS) method, summarized in **Table 5-9**. Note that this approach may underestimate the effect of bias errors which, if present, should be combined with simple summation to each other and the RMS total. Error introduced by the DAQ, such as analog to digital conversion, is considered negligible by comparison to other sources and ignored.

The error in the J1939 messages is unknown, and the engine rotation speed ω and exhaust mass flow $\dot{m}_{exhaust}$ messages are part of all specific emission calculations. ω is measured with a high-resolution encoder and therefore assumed to be quite accurate at 1%. $\dot{m}_{exhaust}$ is likely less accurate and its error is estimated at 5%. Note that neither of these errors are specified in J1939 documentation, nor was it possible to verify them against a reference instrument. Therefore, they should be considered an educated guess. It is unclear exactly how the truck calculates $\dot{m}_{exhaust}$, but it may be calculated internally based on measured intake air and fuel rates. In that case the truck's ECU will not know about the added mass from the hydrogen injection. To address this mass balance was checked between $(\sum \dot{m}_{fuels} + \dot{m}_{air})$ and $\dot{m}_{exhaust}$ in each fueling mode. The mass added by hydrogen is always small relative to the total mass flow (<1%), nevertheless there was no noticeable offset introduced when operating in hydrogen/diesel mode versus the diesel baseline. NOx [PPM] values as measured by the truck's OEM electrochemical sensor also are reported on the truck's CANbus network as J1939 messages, and the error is unknown but estimated at 10% based the literature review of electrochemical NOx sensors used in other PEMS. Error in many of the other parameters were also an educated guess, including driveshaft properties for the torque calculation, density of the

dilution air, and even the DRXs measurement error. Therefore, the calculated RMS error for each measurement is a rough approximation.

This is not to say there should be no confidence in the measurements. The LI-COR CO_2 sensor was calibrated against reference gases with a near perfect fit (0.999 slope, R^2 =1), the DRX showed good repeatability versus a duplicate DRX in lab testing (R^2 = 0.95), and the dilution ratio was verified in lab. The PEMS also showed good resistance to vibration and electrical interference on the truck, as evident readings at expected background levels while the truck was coasting down hills. However, a lack of reference instruments available to test the PEMS directly against on the truck and the aforementioned lack of information for an error propagation approach motivated a statistical error approach instead. This will be discussed in **Section 5.7.2**.

Table 5-9: Instrument error calculations

Parameter	Error Sources Considered	RMS Error in Parameter
Torque	ID_{shaft}: ± 2% OD_{shaft}: ± 2% E_{shaft}: ± 1% $V_{excitation}$: ± 1% Gxmt: ± 2%	Torque = ± 8%
Dilution Ratio	Pressure Transducer: ± 0.8% FS	DR = ± 0.5 (3% @ DR = 16.5)
CO_2	LI-COR: ± 4% DR: ± 3% $\dot{m}_{exhaust}$: ± 5 % $M_{exhaust}$: ± 2% Torque: ± 8% ω: ± 1%	+/- 10% CO_2 [g/kW.h]
NOx	OEM: ± 10% $\dot{m}_{exhaust}$: ± 5 % $M_{exhaust}$: ± 2% Torque: ± 8% ω: ± 1%	+/- 14% NOx [g/kW.h]

PM	DRX: ±10% DR: ± 3% $\dot{m}_{exhaust}$: ± 5 % ρ_{air}: ± 5% Torque: ± 8% ω: ± 1%	+/- 15% PM [mg/kW.h]

5.7.2 Statistical Error

While overall accuracy is desired, the key goal of this research was to assess the difference in emissions between the two fueling modes. Therefore, the most important thing is the repeatability of the measurement rather than an absolute number. In order to assess repeatability, the standard error was calculated across the engine's operating range for each CO_2, NOx, and PM emissions. Percentage standard error was calculated for each point on the operating map as shown in **Equation 5-9**:

$$\%\ standard\ error = \frac{\sigma}{\sqrt{n}} * \frac{100}{\bar{x}} \qquad (5\text{-}9)$$

Where σ is the standard deviation and $\bar{x}$ is the mean. The key issue, though, is what value to use for n. Initially error maps were generated where, for each cell on the emission map, n was equal to the number of samples in that cell. This seemed intuitive but it gave suspiciously low error values. The problem is that n number of values in the cell may not truly be n independent measurements. For example, if the truck is operating at a steady load point for 3 minutes and the DAQ is logging at 10 Hz, 1800 measurements will be recorded. Those are not truly 1800 independent measurements though. This extreme example shows a potentially huge difference and a difficult problem to solve.

To determine true independent measurements in the data the following approach was taken:

1. For each emission create a vector of all the measurements in the order they were taken
2. Copy this vector but shift the values i places (start with i=1)
3. Find the R^2 between the original vector and the shifted copy
4. Increment i and repeat the process until the calculated R^2 falls below a certain threshold and record the highest value of i.

In the presented error calculations, the R^2 threshold was chosen as 0.3 to represent fairly uncorrelated data and the final value of i when the threshold is reached was called Z. Z represents the number of increments in the emission vector needed before a new independent measurement is encountered, so the true number of independent measurements is simply calculated via **Equation 5-10**. The result can then be substituted into **Equation 5-9** as n.

$$n_{independent} = \frac{n}{Z} \qquad (5\text{-}10)$$

Standard error for CO_2 is presented in **Figure 5-41** and **Figure 5-42**, for NOx in Figure **5-43** and **Figure 5-44**, and for PM in **Figure 5-45** and **Figure 5-46.** Note that for each two averages are presented in the header, the simple weighted average exactly the same as in previous emission maps, but also the RMS error for the map.

Statistical error is similar between fueling modes for each emission. Compared to CO_2 and NOx the PM showed greater statistical error. This serves to confirm what was observed earlier in the effects of data exclusion and drive cycle variability, that PM emission is noticeably more variable than CO_2 or NOx.

Statistical error for Treated NOx is shown in **Figure 5-47** and **Figure 5-48**. It is similar for both fueling modes and interestingly is over double the error for engine-out NOx. This suggests the truck's on-board electrochemical NOx sensors are less accurate when detecting very low NOx concentrations.

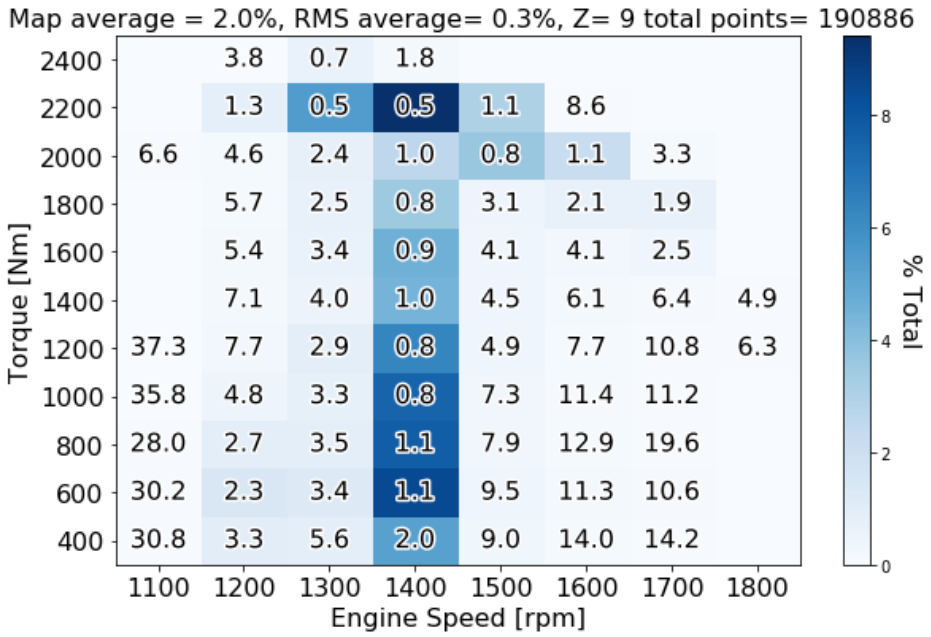

Figure 5-42: CO_2 % standard error – diesel baseline

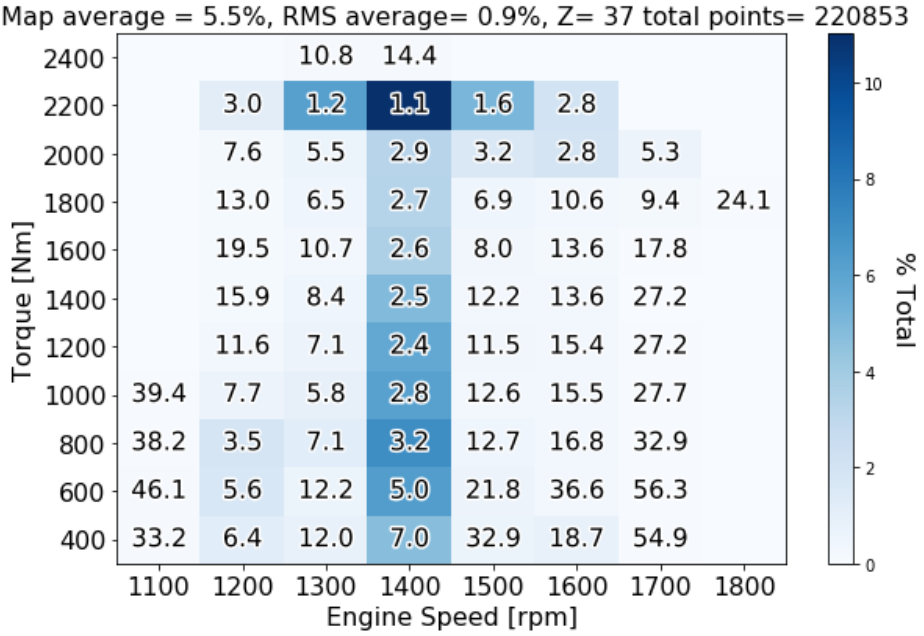

Figure 5-43: CO_2 % standard error – hydrogen/diesel

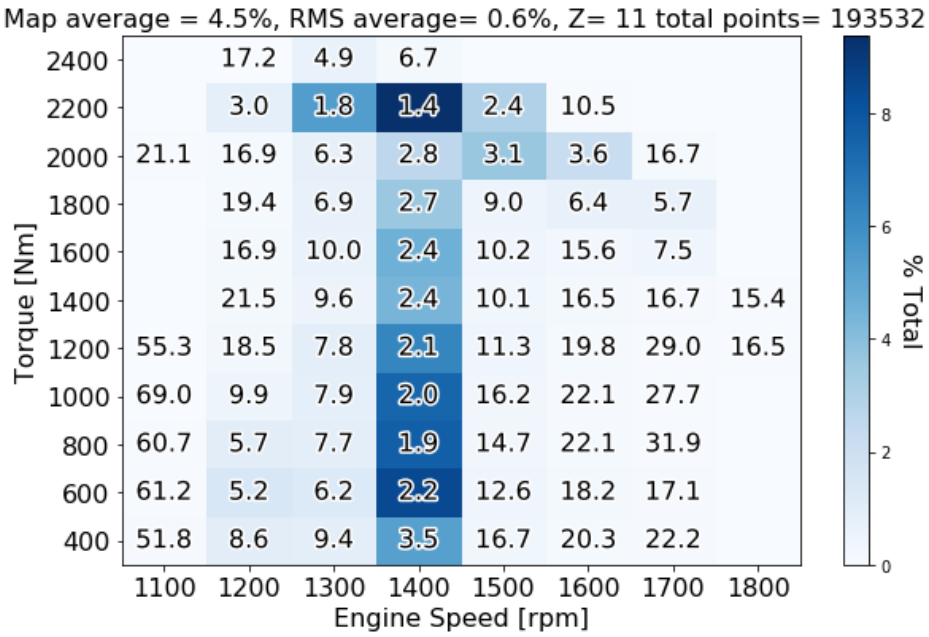

Figure 5-44: NOx % standard error – diesel baseline

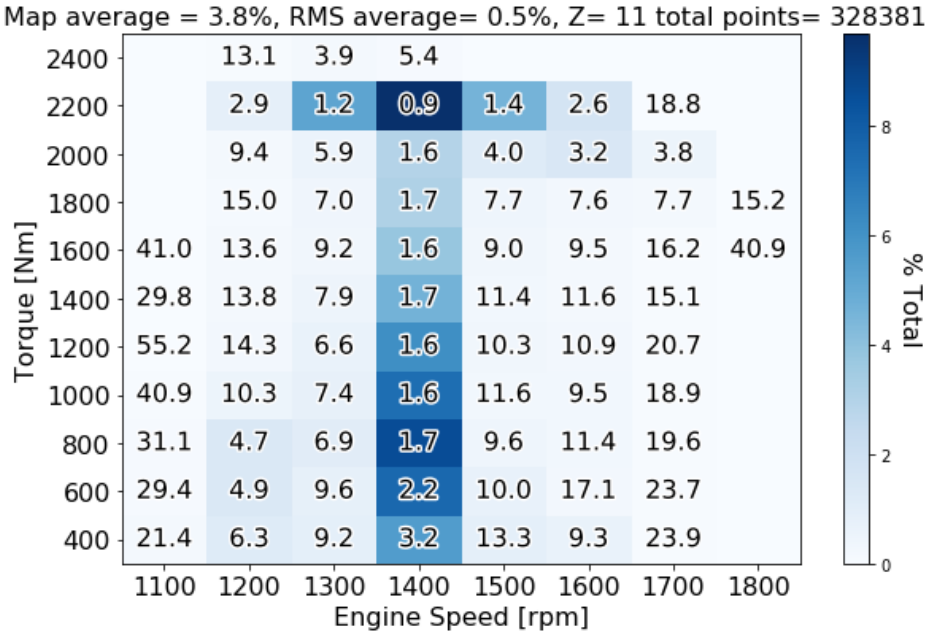

Figure 5-45: NOx % standard error – hydrogen/diesel

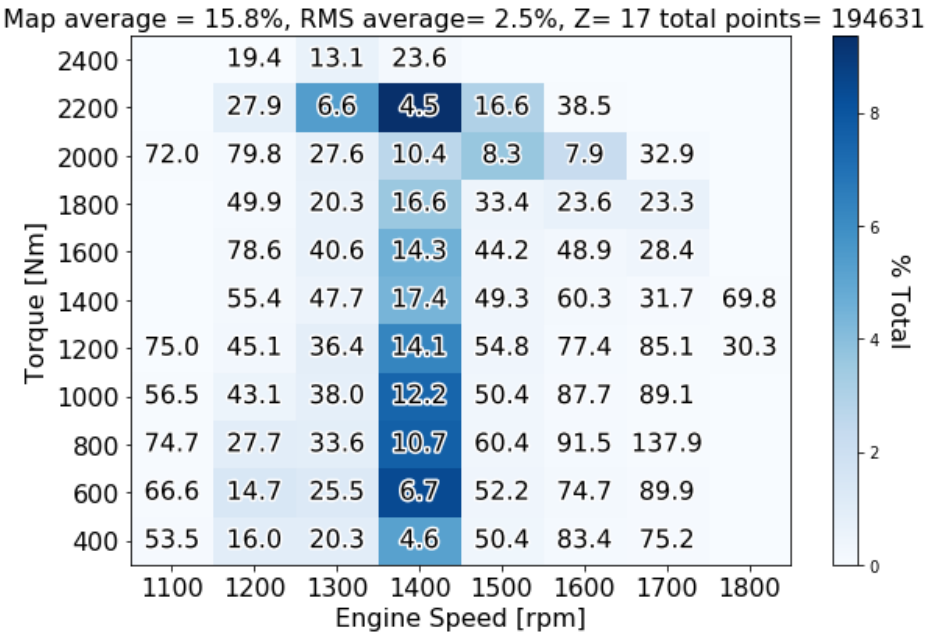

Figure 5-46: PM % standard error – diesel baseline

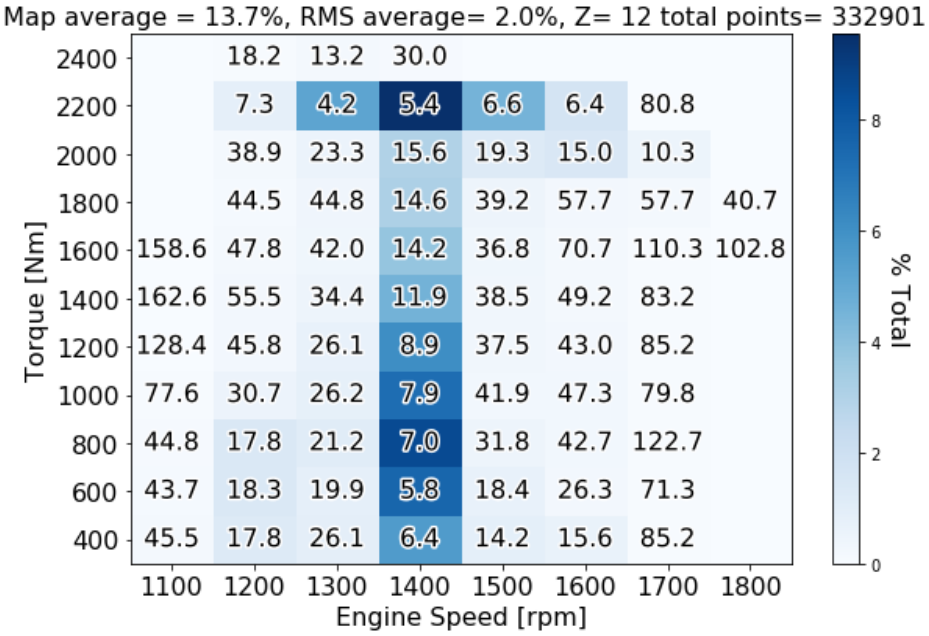

Figure 5-47: PM % standard error – hydrogen/diesel

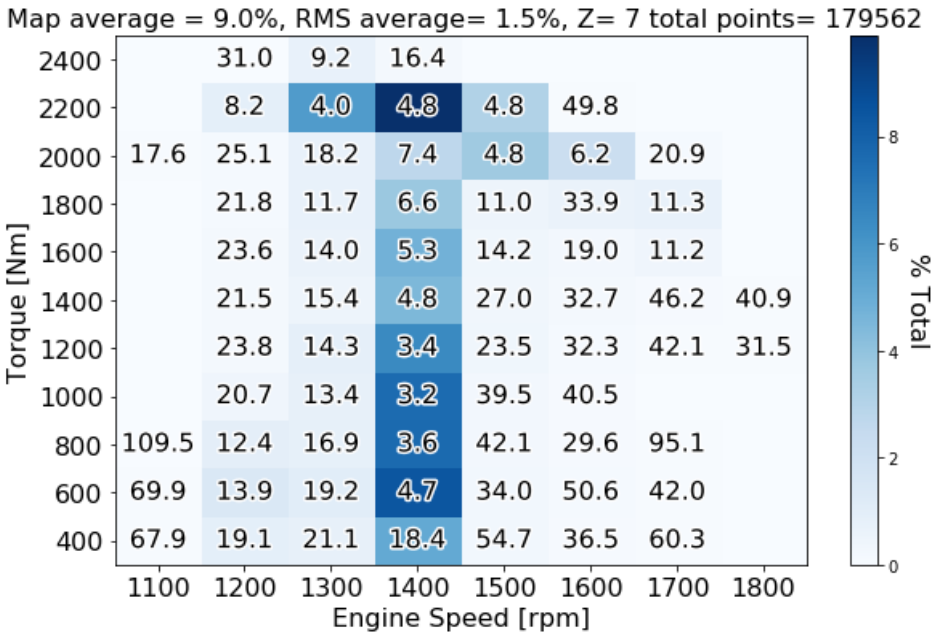

Figure 5-48: Treated NOx standard error – diesel

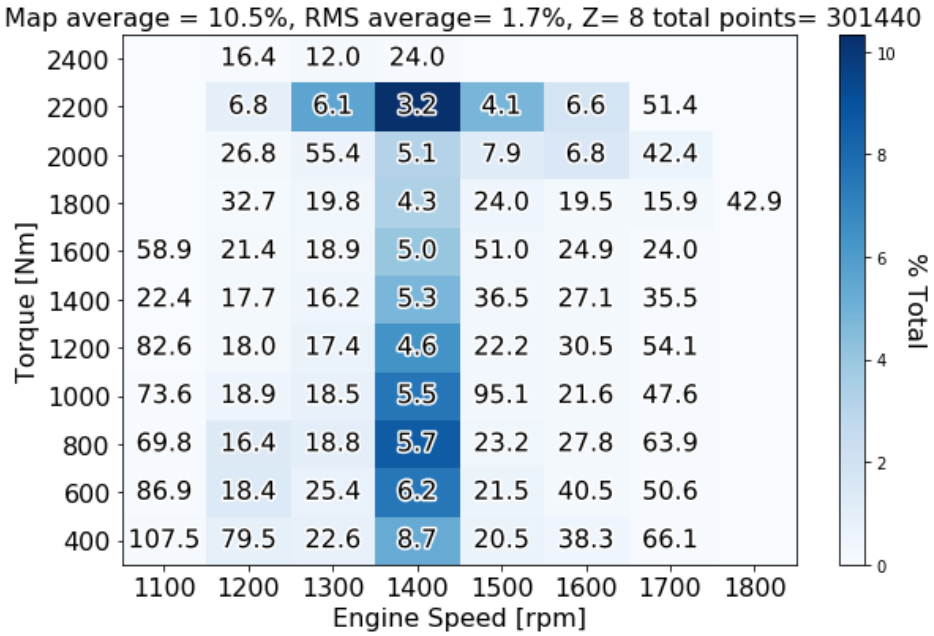

Figure 5-49: Treated NOx standard error – hydrogen/diesel

5.8 Light Scattering vs Gravimetric PM Measurement

Gravimetric PM measurement was conducted as a verification step for the light scattering PM measurement provided by the DustTrak DRX. **Figure 5-49**, compares the PM mass collected on the MTL 37mm Teflon filters to the total integrated value from DRX.

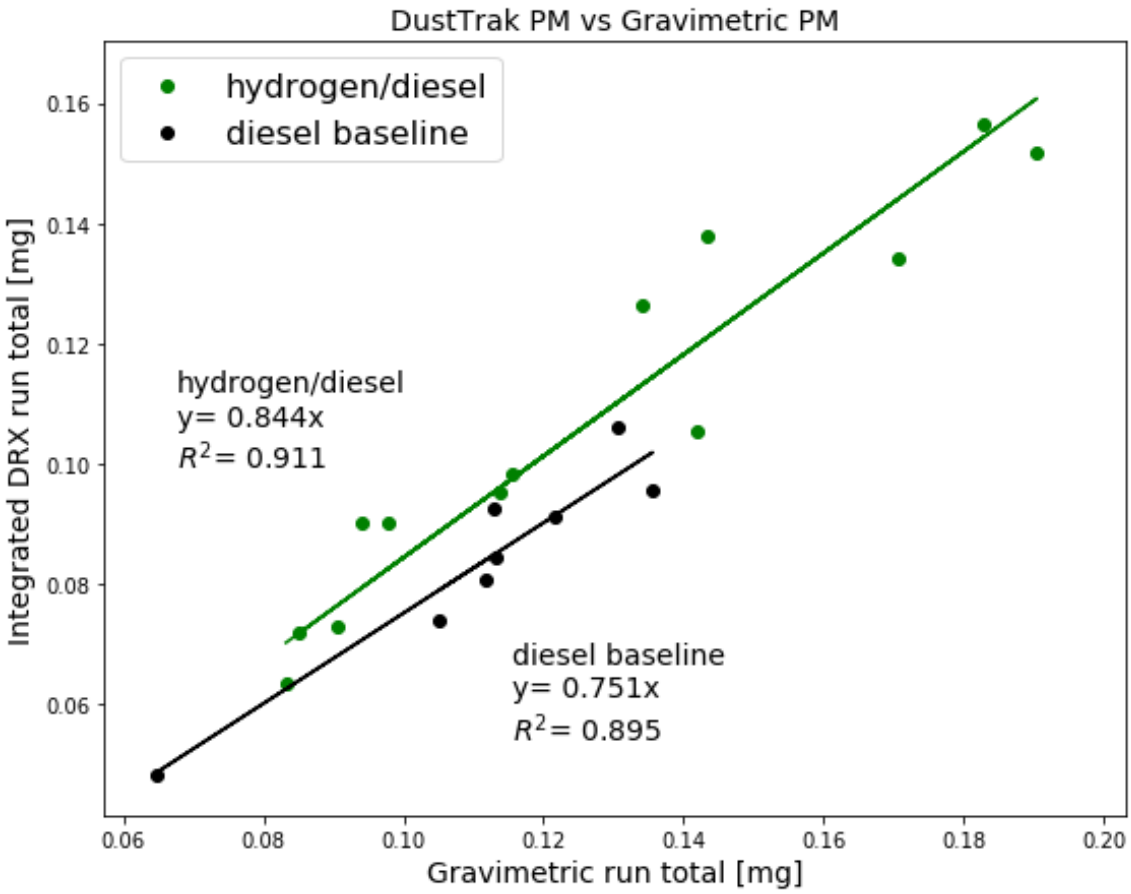

Figure 5-50: PM comparison – light scattering vs gravimetric

Correlation was very good (R^2 = 0.91, and R^2 = 0.90) for both fueling modes but the integrated light scattering value underpredicted the gravimetric value by 16-25%. A potential explanation is that some of the particles are smaller than the DRX's detection range. The underprediction is greater in diesel mode than hydrogen/diesel mode suggesting that particle properties could have changed between the two. Further study is required to say anything conclusive though.

Note that for best accuracy the DustTrak integrated value was taken from the device's internal memory. This is important because the DAQ was not always logging as the DRX was running.

Chapter 6 – Summary, Conclusions and Future Work

6.1 Summary and Conclusions

A custom PEMS system was designed and built to measure the CO_2, NOx, and PM emissions produced by a heavy-duty Class 8 diesel truck equipped with a novel hydrogen/diesel fuel system. Over 2500 kilometers of on-road testing was completed under challenging real-world conditions as the truck operated in fleet service in northern British Columbia. Operating maps were generated to give emissions, and other related parameters as a function of engine speed and torque.

CO_2 and NOx were fairly consistent across the operating range. PM emissions, however, rose rapidly outside the main engine speed range. The emission maps also show where the truck's engine spent most of its time under real operating conditions and where to focus emission reduction efforts. For CO_2 and engine-out NOx it is simply a matter of the load + speed range where the engine spends most of its time. For engine-out PM reduction, however, the lower torque range, is where to focus the attention.

The effect of excluding about half the data based on a stricter set of criteria for torque measurement was shown have to little effect on the CO_2 and NOx emissions but, in some cases, a large effect on the PM emissions. The drive cycle was analyzed for variations that might affect the emissions results. For CO_2 and NOx emissions, changes in the drive cycle had a smaller effect on the average specific emissions, while changes in the drive cycle affected average specific PM emissions much more.

Measured error was investigated with both instrument error propagation and statistical approaches. A lack of information on some instrument errors, lack of reference instruments to compare to, and ultimately the focus on repeatability versus an absolute value for each emission measurement meant that a statistical method of error representation was chosen as most suitable. High frequency measurements of sometimes steady load points meant that the problem of pseudo-replication had to be addressed in calculating this statistical error.

The overall results for each emission in the unloaded, loaded, and combined drive cycles are presented in **Figure 6-1**, **Figure 6-2**, and **Figure 6-3**. These numbers presented come from **Section 5.6**, which combines the aggregate emission data maps for each fueling mode with the operating points for each individual run. Error bars represent the RMS total of the statistical error maps presented in **Section 5.7.2**. Note that these error bars do not include potential biasing factors in the measurements. For that reason, they should give good confidence in the repeatability of the measurement taken and the relative emissions between the two fueling modes, but at the same time care must be taken comparing absolute numbers from this study to numbers attain using different instruments and methods. Although incomplete, the propagated error approach considered in **Section 5.7.1** suggests that absolute error is more likely in the range of 10-15%.

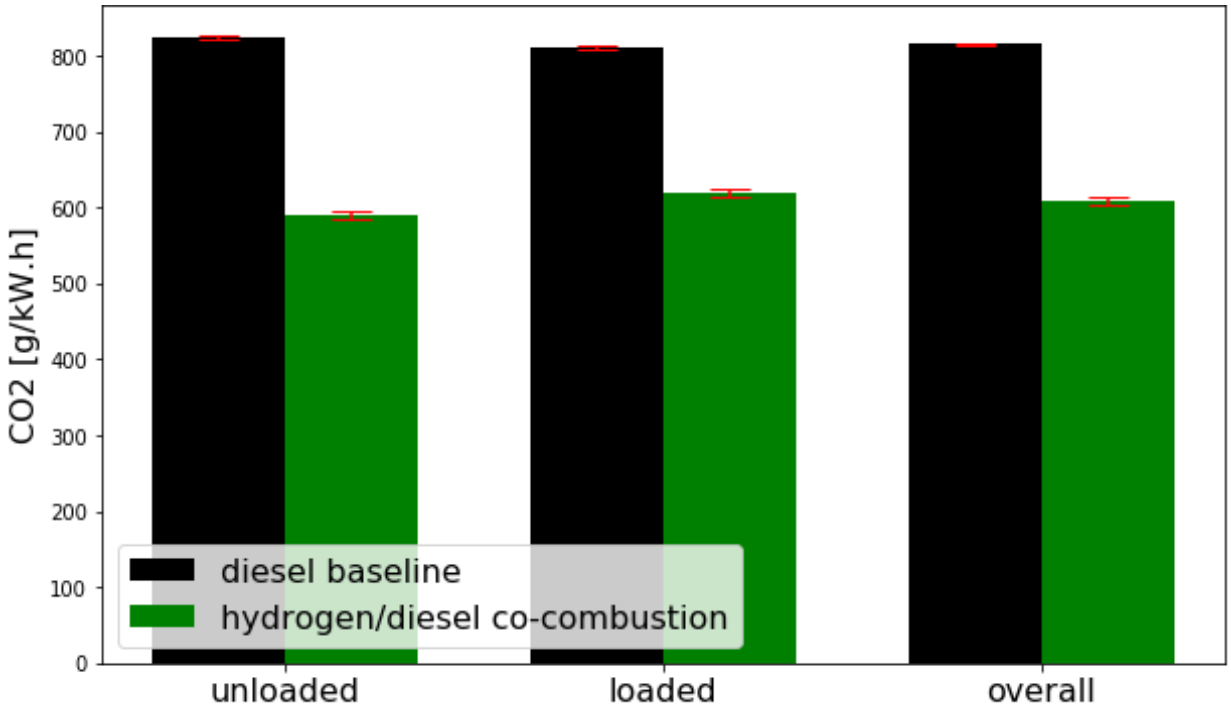

Figure 6-1: Overall CO_2 [g/kW.h]

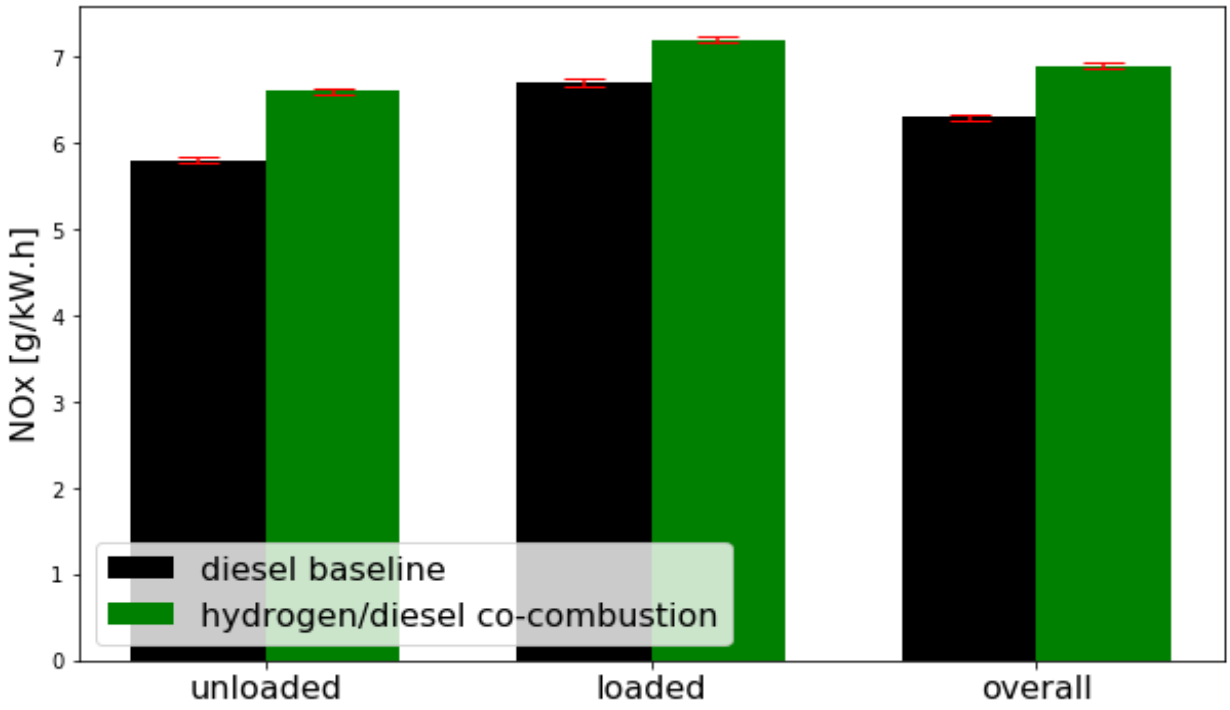

Figure 6-2: Overall raw (pre-aftertreatment) NOx [g/kW.h]

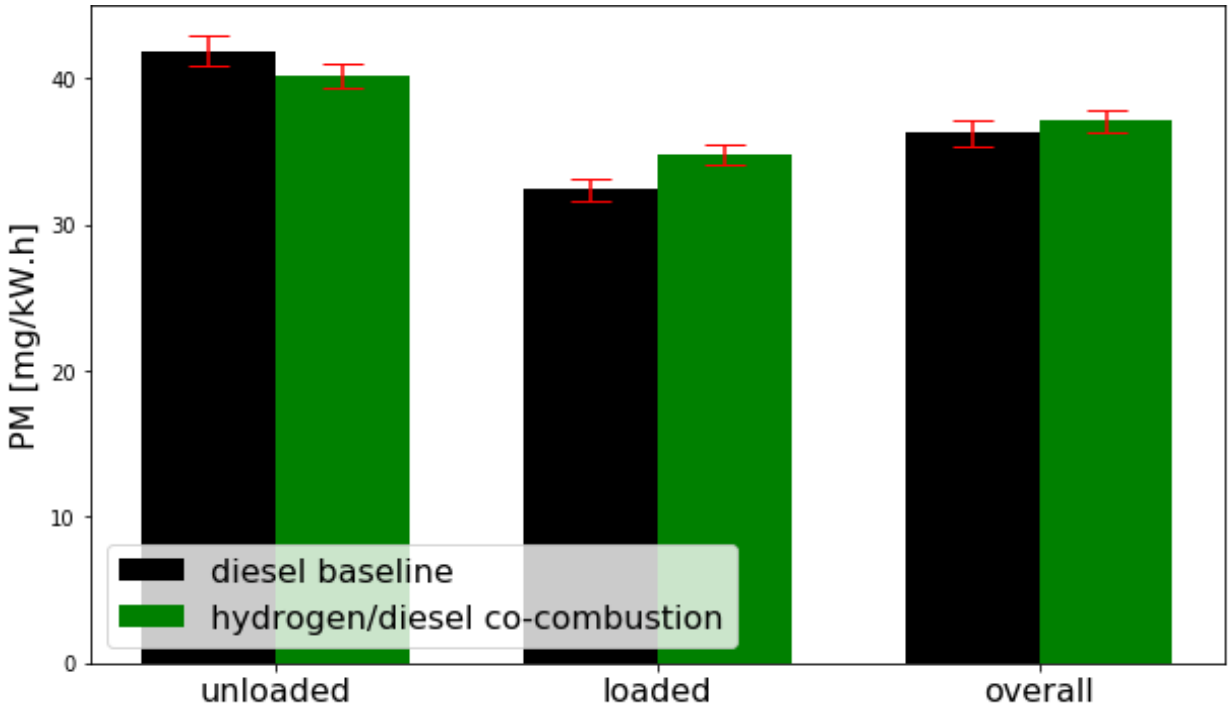

Figure 6-3: Overall raw (pre-DPF) PM [mg/kW.h]

Relative to the diesel baseline, hydrogen/diesel co-combustion caused: a CO_2 reduction of 25 ±1%, an engine-out NOx increase of 10 ±1%, and an engine-out PM increase of 2 ±3 %. From this confidence in the CO_2 decrease is very high while confidence in the NOx increase is moderately high. Based on the statistical analysis, confidence in the PM increase is low, but the increase was also observed in the filter measurements. The small increase in engine-out PM is contrary to most published literature, but of little practical concern given the high effectiveness of modern DPF systems.

Elevated EGT was observed in hydrogen/diesel mode. This increase of 30-50℃ likely came mostly from the hotter adiabatic flame temperature of the hydrogen/diesel mixture. Delayed ignition timing may have also contributed but to a smaller extent. Combustion timing could not be assessed based on the data collected. Increased EGR flow rate was also present in hydrogen/diesel mode. This could have moderated the increased engine-out NOx but at the expense of preventing a decrease in PM.

Overall good correlation was seen between the light scattering and gravimetric methods of PM measurement. The integrated DustTrak DRX values were about 0.8 the total PM value recorded by the gravimetric filters with a correlation coefficient of about 0.9 for both fueling modes. Likely the discrepancy occurs because some of the diesel PM particles are too small to be detected by the DRX.

Preliminary analysis of post-aftertreatment NOx values showed that, despite the higher engine out NOx values, these emissions decreased by 36 ±2% while running in hydrogen/diesel mode. This result is encouraging but should be understood in the context that the measurement method, an OEM electrochemical NOx sensor, may not be the best choice for accurate measurement of very low NOx concentrations. Therefore, it should be verified with another method. Elevated EGTs could play a role on increased NOx conversion efficiency. A small increase in DEF consumption of 3 ±3% was also noted in hydrogen/diesel mode.

6.2 Future Work

While the core objectives of the project were achieved, additional questions remain and there are many potential future projects to address them. First off, NOx values should be verified. In particular, the post-aftertreatment results based on the onboard NOx sensor are promising but do not guarantee compliance with the emission regulations. For engine-out NOx values it would be useful to use a measurement principle that can distinguish NO_2 from NO, as the NO_2/NO ratio can influence how the aftertreatment system works. Specifically, a higher NO_2/NO ratio can improve both passive DPF regeneration and SCR efficiency.

Post aftertreatment PM values should also be measured. At the very low PM concentrations expected post DPF the DustTrak becomes a less reliable measurement instrument [33], so a different measurement technique might be needed. Furthermore, the PM size distribution is expected to shift lower post DPF, potentially putting more of the particles below the DustTrak's detection limit of about 50 nm [35]. A potential solution is to put more focus on run total PM via gravimetric sampling. The specific particulate matter emission [mg/kW.h] results presented in this work are measured by light scattering. The correlation between light scattering measurements and PM mass depends on particle properties and therefore can change as engine operating conditions change [34]. The assumption is that the particle properties did not change significantly between baseline diesel and hydrogen/diesel fueling modes, and the overall good agreement between integrated light scattering results and gravimetric results support this. Future work, however, could include a detailed look at PM size distribution across the operating range and for each fueling mode. This would require the use of a time resolved PM instrument better able to classify small particles. Furthermore, analysis of PM composition and morphology could reveal potential differences in the formation mechanisms and characteristics between fueling modes.

It would be useful to study DPF loading and DPF regeneration frequency. According to the fleet records, the truck investigated in this study, when consistently run in hydrogen/diesel co-combustion mode, saw less active DPF regeneration compared to the same model truck running only on diesel fuel. If engine out PM emissions are unchanged, or even slightly increased this could indicate that the DPF is passively regenerating more effectively while in hydrogen/diesel mode. A potential explanation is the elevated EGTs observed in this study, but

a more detailed look is needed. An increased NO_2/NO ratio could also aid passive DPF regeneration, giving further incentive to measure these independently.

Hydrogen concentration in the exhaust should be measured to determine if any hydrogen is passing through the engine unburned. In particular, the fact that thermal efficiency increased at high loads but decreased at low loads gives some suspicion of hydrogen slip occurring at low load.

The calibration of the supplementary hydrogen injection system could be further optimized. True optimization, however, likely requires modification of the base diesel calibration. For example, advancing base diesel injection to counter the potential ignition delay introduced by hydrogen. A detailed combustion study including cylinder pressure trace history is not feasible during on-road testing but could be accomplished with a duplicate engine on an engine dyno. The results in this thesis show which load points to focus on in such subsequent work. Controlling EGR to achieve the same mass flow rates between the two fueling modes would give further insight into the changes in fueling alone. This would be a very involved task because EGR rate is controlled by the truck's diesel ECU based on a multitude of parameters, not something that can explicitly be set.

References

[1] R. Stone, Introduction to Internal Combustion Engines, 4 ed., Warrendale: SAE International, 2012, p. 70.

[2] S. Verhelst and T. Wallner, "Hydrogen-fueled internal combustion engines," *Progress in Energy and Combustion Science,* no. 35, pp. 490-527, 2009.

[3] H. Li, C. Liew and S. Liu, "Combustion Process of a Heavy-Duty Hydrogen-Diesel Dual Fuel Engine," in *Combustion Institute - Canadian Section*, Toronto, 2018.

[4] T. Sandalcı and Y. Karagöz, "Experimental investigation of the combustion characteristics, emissions and performance of hydrogen port fuel injection in a diesel engine," *International Journal of Hydrogen Energy,* pp. 18480-9, 2014.

[5] J. H. Zhou, C. S. Cheung and C. W. Leung, "Combustion, performance, regulated, and unregulated emissions of a diesel engine with hydrogen addition," *Applied Energy,* no. 126, pp. 1-12, 2014.

[6] H.-W. Wu and Z.-Y. Wu, "Investigation of combustion characteristics and emissions of diesel/hydrogen mixtures by using energy-share method in a diesel engine," *Applied Thermal Engineering,* no. 42, pp. 154-162, 2012.

[7] T. Tsujimura and Y. Suzuki, "The utilization of hydrogen in hydrogen/diesel dual fuel engine," *International Journal of Hydrogen Energy,* pp. 14019-29, 2017.

[8] C. Liew, H. Li, M. C. Besch, B. Ralston, N. Clark and Y. Huang, "Exhaust emissions of a H2-enriched heavy-duty diesel engine equipped with cooled EGR and variable geometry turbocharger," *Fuel,* pp. 155-63, 2012.

[9] M. Talibi, P. Hellier, R. Balachandran and N. Ladommatos, "Effect of hydrogen-diesel fuel co-combustion on exhaust emissions with verification using an in–cylinder gas sampling technique," *International Journal of Hydrogen Energy,* pp. 15088-102, 2014.

[10] J. B. Heywood, Internal Combustion Engine Fundamentals, New York: McGraw-Hill, 2000, p. 572.

[11] Z. Yang, C. Chu, L. Wang and Y. Huan, "Effects of H2 addition on combustion and exhaust emissions in a diesel engine," *Fuel,* pp. 190-197, 2015.

[12] M. Talibi, P. Hellier and N. Ladommatos, "The effect of varying EGR and intake air boost on hydrogen-disel co-combustion in CI engines," *International Journal of Hydrogen Energy,* pp. 6369-6383, 2017.

[13] P. Sharma and A. Dhar, "Effect of hydrogen supplementation on engine performance and emissions," *International Journal of Hydrogen Energy,* pp. 7570-7580, 2018.

[14] A. R. Epling and S. William, "Diesel Oxidation Catalysts," *Catalysis Reviews,* vol. 53, no. 4, pp. 337-423, 2011.

[15] Paccar, Engine Aftertreatment Systems - Operators Manual - 2017 Emissions, Bellevue: PACCAR, 2016.

[16] Cummins Filtration, "Bulletin: Diesel Exhaust Fluid (DEF) Q & A," 2009. [Online]. Available: https://www.cumminsfiltration.com/sites/default/files/MB10033.pdf. [Accessed 23 July 2019].

[17] M. Koebel, M. Elsener and M. Kleeman, "Urea-SCR: a promising technique to reduce NO from automotive diesel engines," *Catalysis Today,* vol. 59, no. 3-4, pp. 335-345, 2000.

[18] B. Shin, Y. Cho, D. Han, S. Song and M. C. Kwang, "Hydrogen effects on NOx emissions and brake thermal efficiency in a diesel engine under low-temperature and heavy-EGR conditions," *International Journal of Hydrogen Energy,* no. 36, pp. 6281-6291, 2011.

[19] "Heavy-Duty FTP Transient Cycle," DieselNet, [Online]. Available: https://www.dieselnet.com/standards/cycles/ftp_trans.php. [Accessed 4 July 2019].

[20] Electronic Code of Federal Regulations e-CFR, "Title 40 Part 1065 - 1065.555c1," [Online]. Available: https://ecfr.io/Title-40/pt40.37.1065#se40.37.1065_1284. [Accessed 18 July 2019].

[21] "Vehicle and Fuel Emissions Testing - Technical Capabilities of the National Vehicle and Fuel Emissions Laboratory (NVFEL)," United States Environmental Protection Agency, [Online]. Available: https://www.epa.gov/vehicle-and-fuel-emissions-testing/technical-capabilities-national-vehicle-and-fuel-emissions. [Accessed 4 July 2019].

[22] H. Wang, Y. Ge, J. Tan, L. Wu, P. Wu, L. Hao, Z. Peng, C. Zhang, X. Wang and Y. Han, "The Real-World Emissions from Urban Freight Trucks in Beijing," *Aerosol and Air Quality Research,* no. 18, pp. 1448-1456, 2018.

[23] P. Dixit, W. J. Miller, D. R. Cocker III, A. Oshinuga, Y. Jiang, T. D. Durbin and K. C. Johnson, "Differences between emissions measured in urban driving and certification testing of heavy-duty diesel engines.," *Atmospheric Environment,* no. 166, pp. 276-285, 2017.

[24] T. Grigoratos, G. Fontaras, B. Giechaskiel and N. Zacharof, "Real world emissions performance of heavy-duty Euro Vi diesel vehicles," *Atmospheric Environment,* no. 201, pp. 348-359, 2019.

[25] T. Cao, R. L. Russell, T. D. Durbin, D. R. Cocker III, A. Burnette, J. Calavita, H. Maldonado and K. C. Johnson, "Characterization of the emissions impacts of hybrid excavators with a portable emissions measurement system (PEMS)-based methodology.," *Science of the Total Environment,* no. 635, pp. 112-119, 2018.

[26] C. V. Oreble, T. E. Cados and R. A. Harley, "In-use Performance and Durability of Particle Filters on Heavy-Duty Diesel Trucks," *Environmental Science and Technology,* no. 52, pp. 11913-11921, 2018.

[27] Dieselnet, "NTE (Not-To-Exceed) Testing," [Online]. Available: https://www.dieselnet.com/standards/cycles/nte.php. [Accessed 4 July 2019].

[28] NTK, "NTK NCEM-8016 Compact Emissions Meter," [Online]. Available: https://www.ntk-ncem.com/en/. [Accessed 15 July 2019].

[29] ECM, "ECM miniPEMS," [Online]. Available: http://www.ecm-co.com/product.asp?mpems. [Accessed 15 July 2019].

[30] K. C. Johnson, T. D. Durbin, D. R. Cocker III, W. J. Miller, D. K. Bishnu, H. Maldonado, N. Moynahan, C. Ensfield and C. A. Laroo, "On-road comparison of a portable emission measurement system with a mobile reference laboratory for a heavy-duty diesel vehicle," *Atmoshperic Environment,* no. 43, pp. 2877-2883, 2009.

[31] J. Yang, T. D. Durbin, Y. Jiang, T. Tange, G. Karavalakis, D. R. Cocker III and K. C. Johnson, "A comparison of a mini-PEMS and a 1065 compliant PEMS for on-road gaseous and particluate emissions from a light duty diesel truck," *Science of the Total Environment,* no. 640-641, pp. 364-376, 2018.

[32] T. D. Durbin, K. Johnson, D. R. C. III, W. J. Miller, H. Maldonado, A. Shah, C. Ensfield, C. Weaver, M. Akard, N. Harvey, J. Symon, T. Lanni, W. D. Bachalo, G. Payne, G. Smallwood and M. Linke, "Evaluation and Comparison of Portable Emissions Measurement Systems and Federal Reference Methods for Emissions from a Back-Up Generator and Diesel Truck Operated on a Chassis Dynamometer," *Environmental Science Technology,* vol. 41, no. 17, pp. 6199-6204, 2007.

[33] Y. M. Khan, K. C. Johnson, T. D. Durbin, H. Jung, D. R. Cocker III, D. Bishnu and R. Giannelli, "Characterization of PM-PEMS for in-use measurements conducted during validation testing for the PM-PEMS measurement allowance program," *Atmoshperic Environment,* no. 55, pp. 311-318, 2012.

[34] S. K. Cheung, S. T. Elder and R. R. Raine, "Diesel Particulate Measurements with a Light Scattering Photometer," 2000.

[35] B. Giechaskiel, M. Maricq, L. Ntziachristos, C. Dardiotis, X. Wang, H. Axmann, A. Bergmann and W. Schindler, "Review of motor vehicle particulate emissions sampling and measurement: From smoke and filter mass to particle number," *Journal of Aerosol Science,* no. 67, pp. 48-86, 2014.

[36] Testing Systems Incorporated, "DRX operating manual," [Online].

[37] A. Mamakos, P. Bonnel, A. Perujo and M. Carriero, "Assessment of portable emission measurement systems (PEMS) for heavy-duty diesel engines with respect to particulate matter," *Journal of Aerosol Science,* no. 57, pp. 54-70, 2013.

[38] Transportation Alberta, "Dimension Limits," 7 March 2017. [Online]. Available: http://www.transportation.alberta.ca/Content/docType281/production/B-train.pdf. [Accessed 8 July 2019].

[39] S. Carstens and W. A. Majewski, "DieselNet Technology Guide>>Sensors for Engine and Emission Control>>NOx Sensors," DieselNet, [Online]. Available: https://www.dieselnet.com/tech/sensors_nox.php. [Accessed 20 July 2019].

[40] R. Moos, "A Brief Overview on Automotive Exhaust gas Sensors Based on Electroceramics," *International Journal of Applied Ceramic Technology,* vol. II, no. 5, pp. 401-413, 2005.

[41] Y.-Y. Wang, H. Zhang and J. Wang, "NOx Sensor Reading Correction in Diesel Engine Selective Catalytic Reduction System Applications," *IEEE/ASME Transactions on Mechatronics,* vol. 21, no. 1, pp. 460-470, 2016.

[42] A. Bonfils, Y. Creff, O. Lepreux and N. Petit, "Closed-loop control of a SCR system using a NOx sensor cross-sensitive to NH3," *Journal of Process Control,* no. 24, pp. 368-378, 2014.

[43] J. C. Chow, J. G. Watson and D. H. Lowenthal, "Loss of PM2.5 Nitrate from Filter Samples in Central California," *Journal of the Air & Waste Management Association,* vol. 55, no. 8, pp. 1158-1168, 2005.

[44] Measurement Technology Laboratories, "Automated Filter Weighing,Automated Filter Weighing and Data Processing SystemsGuaranteed Compliance: EPA 40 CFR 1065; EPA 40 CFR 1066; Euro 4, Euro 5, Euro 6; Japan 10-15 +11 Mode / JC08H/C; China SEPA IV (Euro 4); India Bharat Stage IV; Brazil PROCONVE," MTL, LLC, [Online]. Available: https://mtlcorp.com/filter-weighing/. [Accessed 23 July 2019].

[45] S. Rogak and K. Babaee, "FlareNet Particle Penetration Calculator (FPPC)," UBC, Vancouver, 2018.

[46] "Dieselnet," 9 July 2019. [Online]. Available: https://www.dieselnet.com/tech/dpm_size.php.

[47] LI-COR Biosciences, LI-820 CO2 Gas Analyzer Instruction Manual, Lincoln: LI-COR, 2015.

[48] Y. A. Cengel and M. A. Boles, Thermodynamics - An Engineering Approach 8th Edition, McGraw-Hill, 2014.

[49] O. Nielsen, B. Qvale and S. Sorenson, ""Ignition Delay in the Dual Fuel Engine,"," SAE Technical Paper 870589, 1987.

Appendices

Appendix A - Required Dilution Ratio Calculations

Diesel has been modelled as $C_{12}H_{24}$ and stoichiometric combustion has been considered to set the CO_2 limit.

$$C_{12}H_{24} + 18\,(O_2 + 3.76N_2) \rightarrow 12\,CO_2 + 12\,H_20 + 18(3.76N_2)$$

H_2O limit was determined by considering 40% H_2 substitution, on an energy basis, with the balance being $C_{12}H_{24}$, again considered at stoichiometric conditions. Both of these scenarios are unlikely in a diesel engine as the mixture is always globally lean by design. The intent is to avoid instrument damage or saturation if these “worst case” conditions are encountered during transient operation.

$$C_{12}H_{24} + (0.4/0.6)(LHV_{diesel}/LHV_{hydrogen})(M_{diesel}/M_{hydrogen})H_2 + P(O_2 + 3.76N_2) \rightarrow XCO_2 + Y\,H_20 + Z\,3.76N_2$$

Given:

$$LHV_{diesel} = 43.4\,MJ/kg\,; LHV_{hydrogen} = 119.96\,MJ/kg;\; M_{C_{12}H24} = 168\,g/mole; M_{hydrogen} = 2\,g/mole$$

Then

$$(0.4/0.6)(LHV_{diesel}/LHV_{hydrogen})(M_{diesel}/M_{hydrogen}) = 20.26;\; P = Z = 28.13, X = 12, Y = 32.26$$

Temperature has been approximated based on as a simple mix of two air streams of different temperatures, with any difference in specific heat ignored. This is estimate is nevertheless very conservative, as heat loss in the system is ignored.

Appendix B – Instrument Calibration Records

B.1 – LI-COR Calibration

Two-point calibration was performed on the LI-COR LI-820 CO_2 meter using CO_2 calibration gases. It was then compared to four different CO_2 concentrations and reference zero.

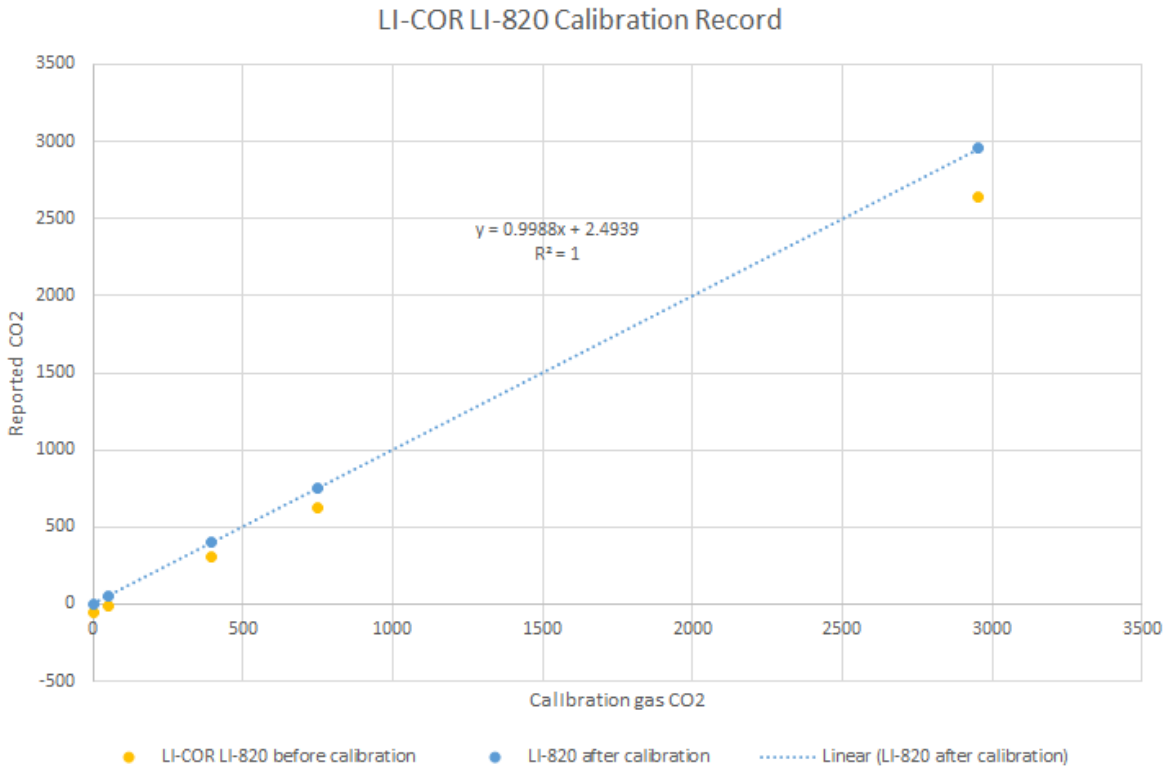

B.2 – DRX vs DRX Comparison

Two DustTrak DRX 8533s were used in parallel to sample PM produced by UBC's Single Cylinder Research Engine (SCRE), a direct injection natural gas engine with diesel pilot ignition. There was consistent repeatability of the two units over a range of test points. Note, however, that one unit gave readings that were consistently 30% lower than the other. The CERC DRX was freshly calibrated from TSI at the time of this test and was the one used for the on-road testing in this project.

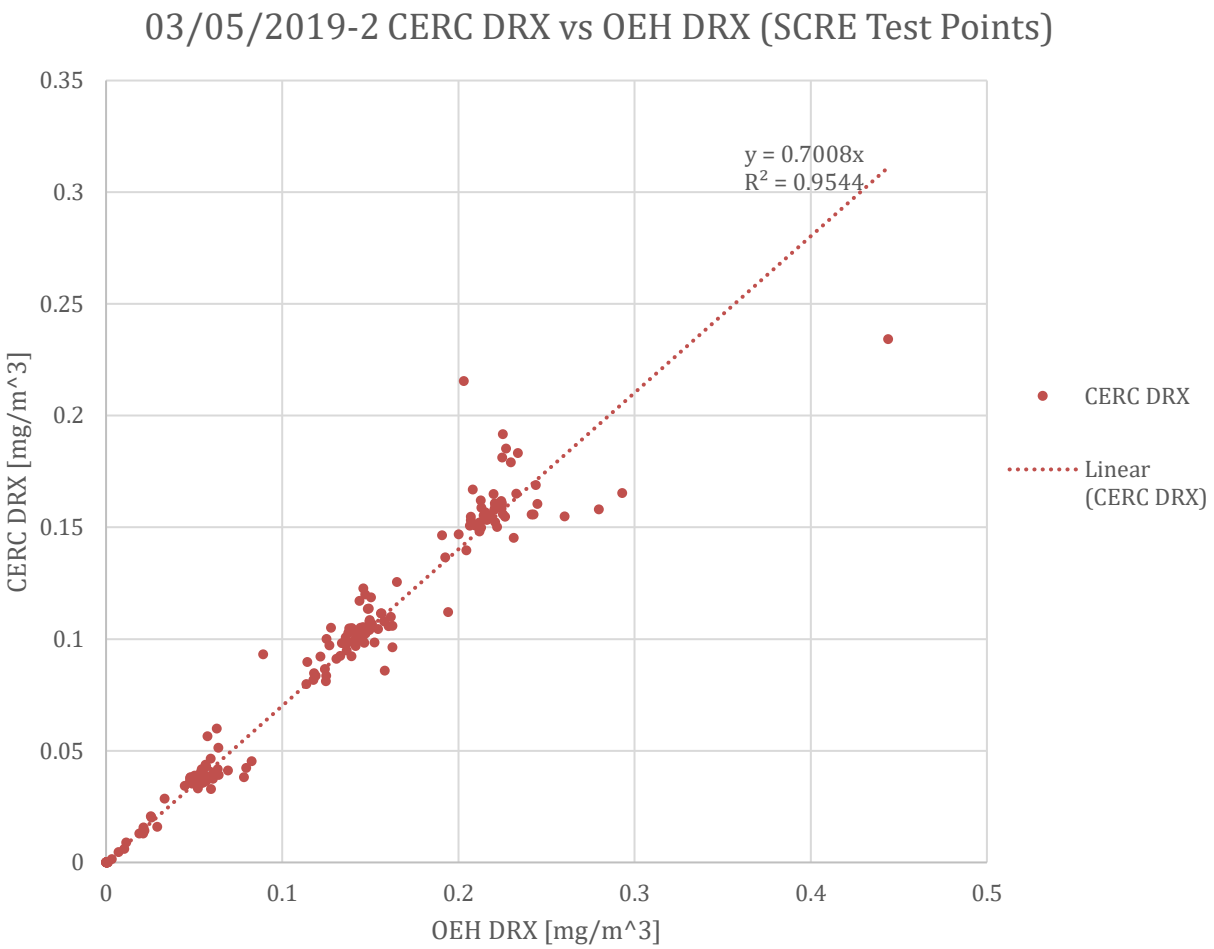

B.3 – Dilution Ratio Lab Check

The dilution ratio provided by the nozzle was check by running the system on UBC's Single Cylinder Research Engine (SCRE) in parallel with the AVL Emission Test Systems CEB2 emissions bench. Dilution ratio was checked over a variety of operating points and exhaust pressures by comparing the CO_2 reported by the LI-COR and the CO_2 reported by the AVL. Background CO_2 was checked before and after the test for a more accurate comparison.

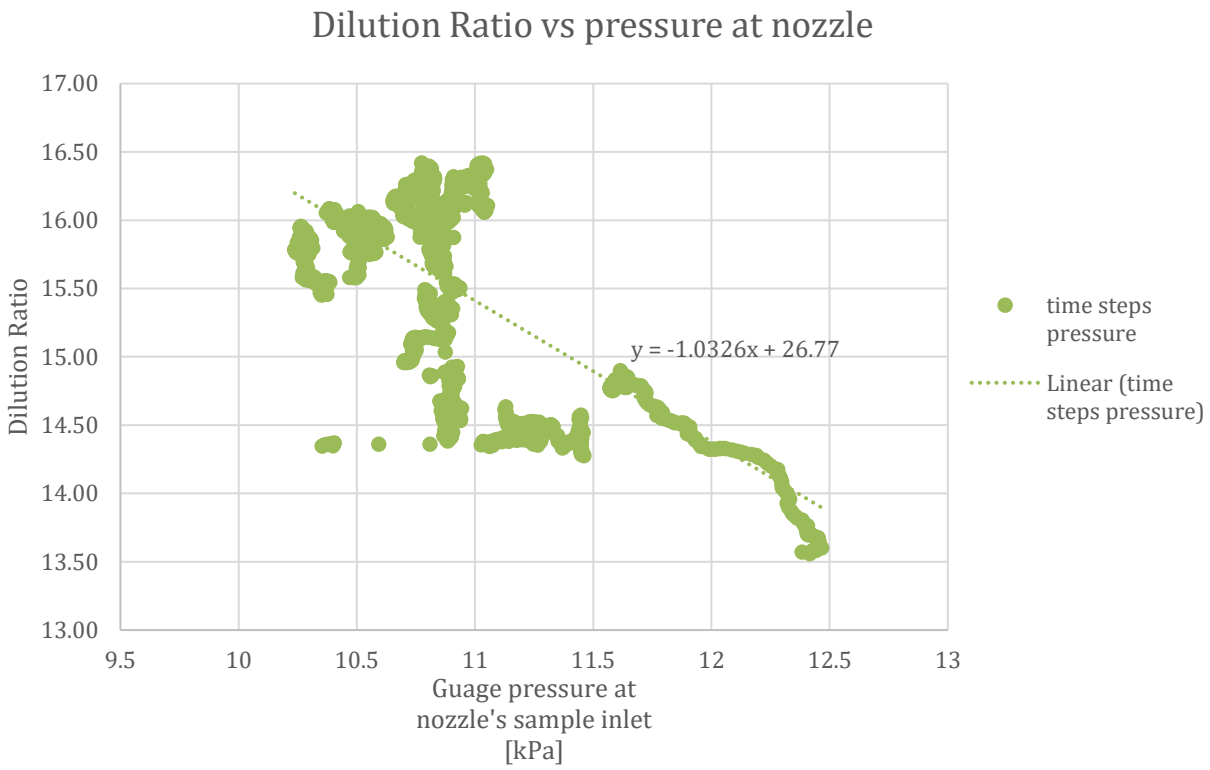

Note that the range of pressures tested was higher than the pressures encountered during on-road testing. This is because it was not possible to get stable operating conditions on the SCRE at lower exhaust back pressure. The effect is that the dilution ratios encountered during testing, typically 16.6-17.3, (as shown in Appendix 4.2) requires some extrapolation beyond these test points. A first order curve fit was chosen as the best compromise based on the available data points and the relatively small pressure range encountered. The response of the dilution ratio to changes in pressure at the sample inlet is not truly linear though. Further characterization of the dilution nozzle could improve the overall accuracy of the CO_2 and PM emission numbers. Nevertheless, because the pressures observed at the sample inlet were very similar between the two fueling modes this curve fit should not introduce a bias error between the two.

Appendix C – Driveline Status Data Exclusion Trade-Off

The section shows the correlation between measured driveshaft torque and broadcast J1939 reference torque while operating in diesel mode before and after applying ('GearPosition' <= 18). For both the unloaded and loaded cases applying the stricter exclusion criteria eliminates more than half the data while the curve fit and correlation values are essentially unchanged.

C.1 – Diesel Unloaded Run

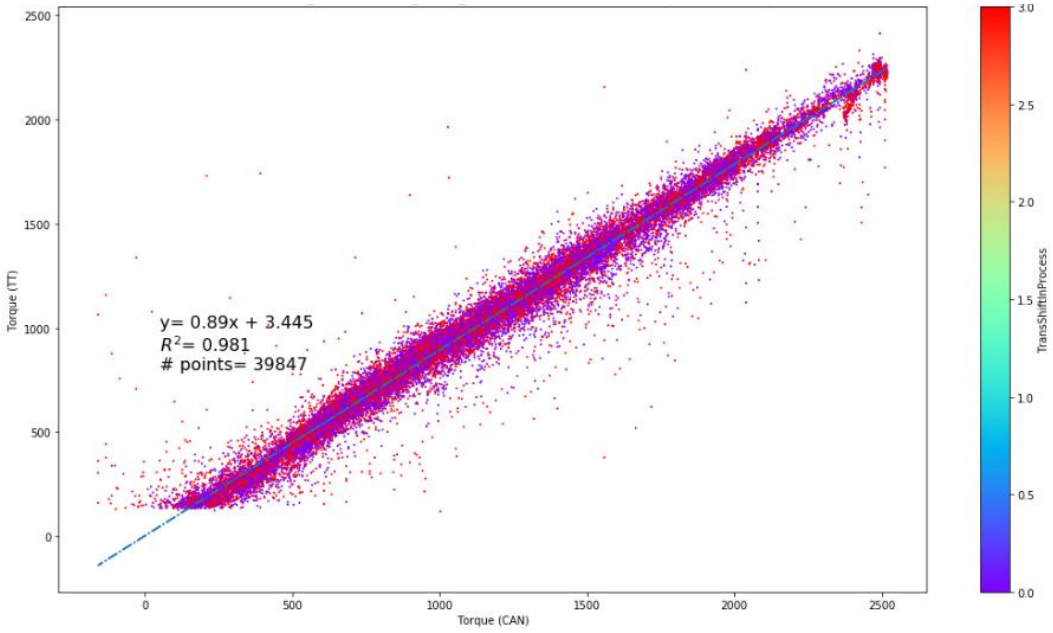

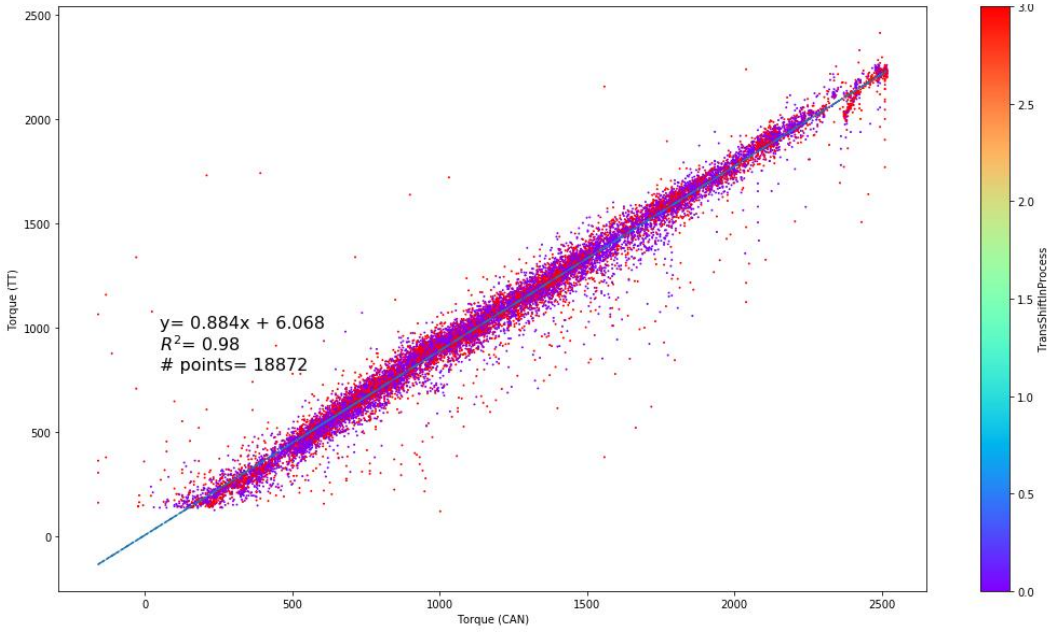

C.2 – Diesel Loaded Run

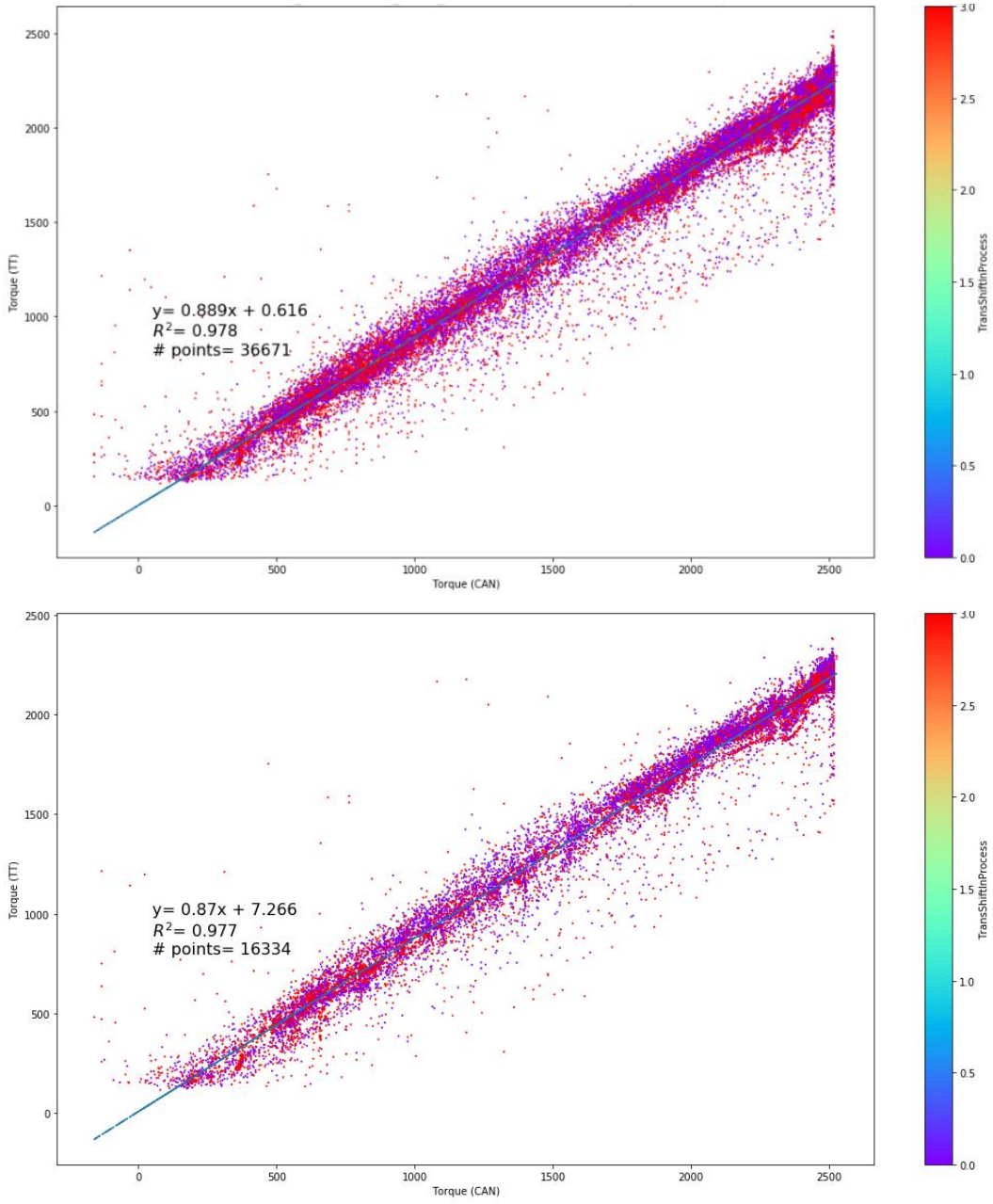

It is also interesting to note the slope in each case. It is always less than one because measured torque is taken after the gearbox while reference torque represents torque at the flywheel. Disregarding error sources this hints that the gearbox efficiency is likely around 89%, an interesting observation but not used in the calculated specific emissions presented in this thesis.

Appendix D – Supplemental Results Maps

D.1 – Example of Unloaded and Loaded Operating Points

Here is presented an example of emission maps separated into the unloaded and loaded cases. The operating range is noticeably different between unloaded and loaded cases while it is quite similar between the two fueling mode in each of those cases. If the engine speed and torque completely characterize the engine state, then maps should be identical for the two load cases. They are not identical, so system state involves more dimensions not captured on the maps.

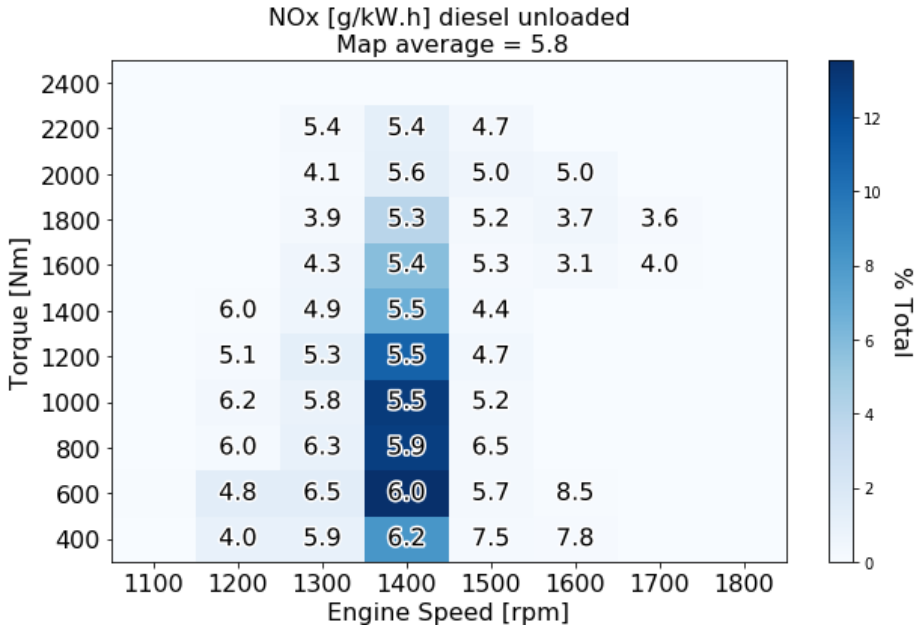

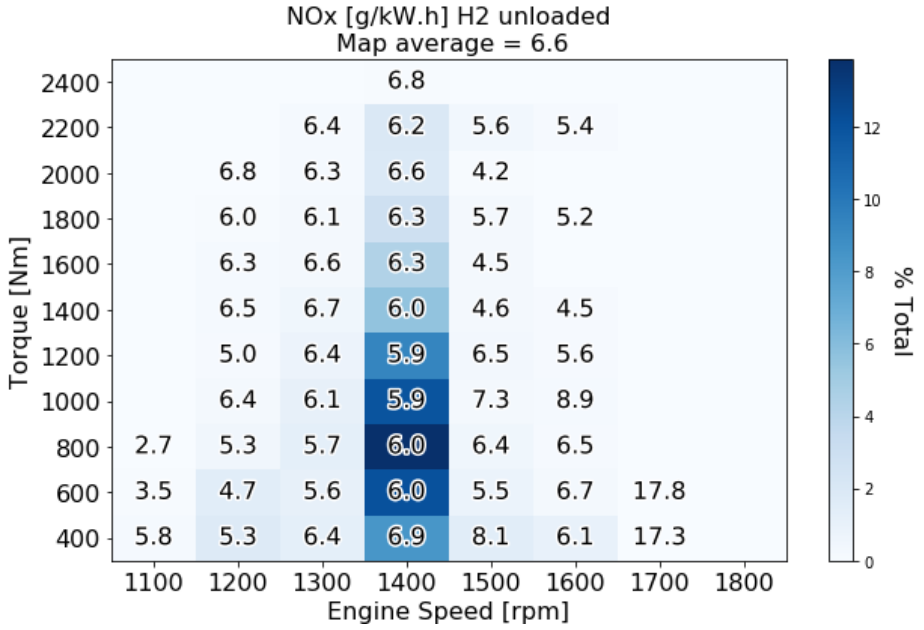

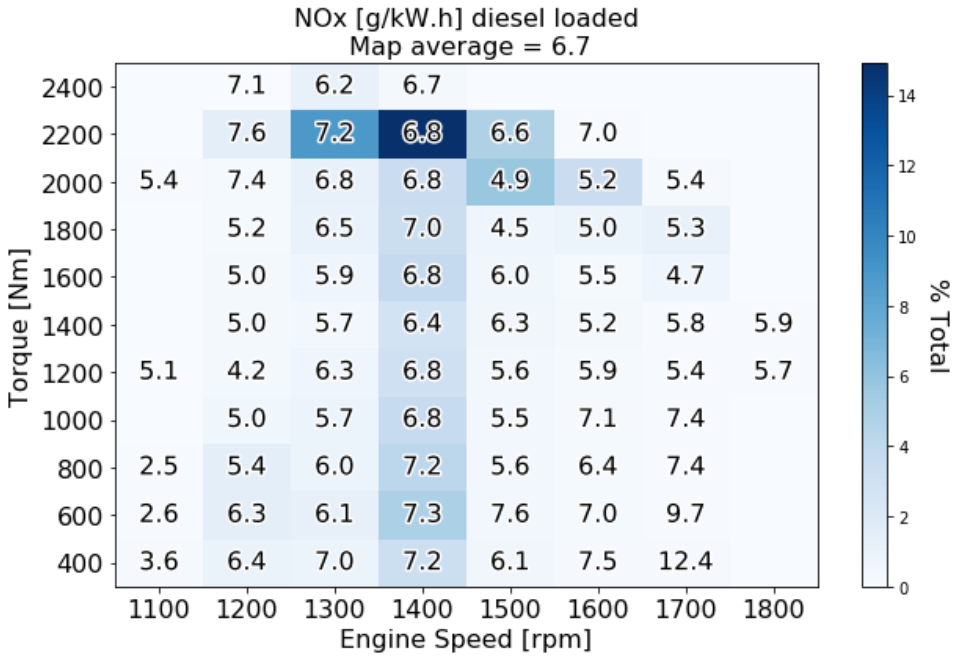
NOx [g/kW.h] diesel loaded
Map average = 6.7
Torque [Nm]
2400 7.1 6.2 6.7
2200 7.6 7.2 6.8 6.6 7.0
2000 5.4 7.4 6.8 6.8 4.9 5.2 5.4
1800 5.2 6.5 7.0 4.5 5.0 5.3
1600 5.0 5.9 6.8 6.0 5.5 4.7
1400 5.0 5.7 6.4 6.3 5.2 5.8 5.9
1200 5.1 4.2 6.3 6.8 5.6 5.9 5.4 5.7
1000 5.0 5.7 6.8 5.5 7.1 7.4
800 2.5 5.4 6.0 7.2 5.6 6.4 7.4
600 2.6 6.3 6.1 7.3 7.6 7.0 9.7
400 3.6 6.4 7.0 7.2 6.1 7.5 12.4
1100 1200 1300 1400 1500 1600 1700 1800
Engine Speed [rpm]
% Total
0 2 4 6 8 10 12 14

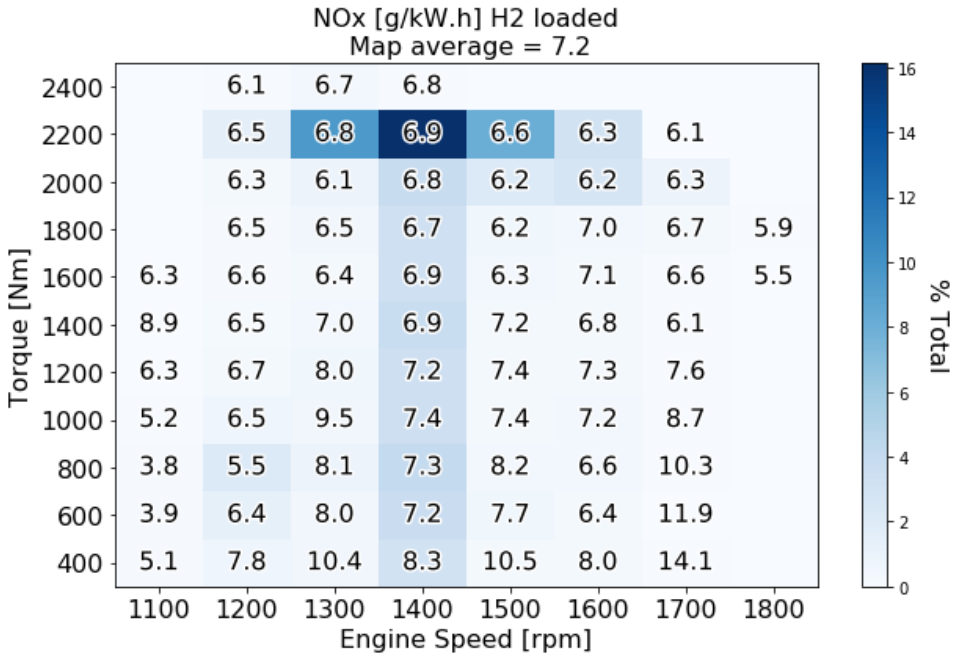
NOx [g/kW.h] H2 loaded
Map average = 7.2
Torque [Nm]
2400 6.1 6.7 6.8
2200 6.5 6.8 6.9 6.6 6.3 6.1
2000 6.3 6.1 6.8 6.2 6.2 6.3
1800 6.5 6.5 6.7 6.2 7.0 6.7 5.9
1600 6.3 6.6 6.4 6.9 6.3 7.1 6.6 5.5
1400 8.9 6.5 7.0 6.9 7.2 6.8 6.1
1200 6.3 6.7 8.0 7.2 7.4 7.3 7.6
1000 5.2 6.5 9.5 7.4 7.4 7.2 8.7
800 3.8 5.5 8.1 7.3 8.2 6.6 10.3
600 3.9 6.4 8.0 7.2 7.7 6.4 11.9
400 5.1 7.8 10.4 8.3 10.5 8.0 14.1
1100 1200 1300 1400 1500 1600 1700 1800
Engine Speed [rpm]
% Total
0 2 4 6 8 10 12 14 16

D.2 – Dilution Ratio Maps

The dilution ratio is lower when the pressure at the nozzle is higher. This occurs when exhaust flow rate is higher which corresponds in the maps to higher engine torque and speed.

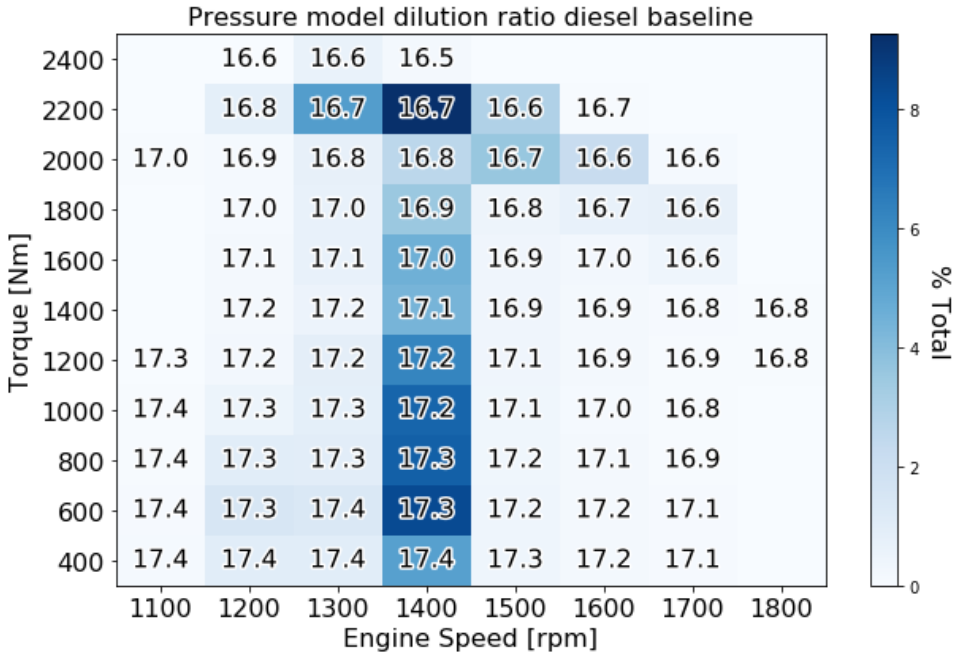

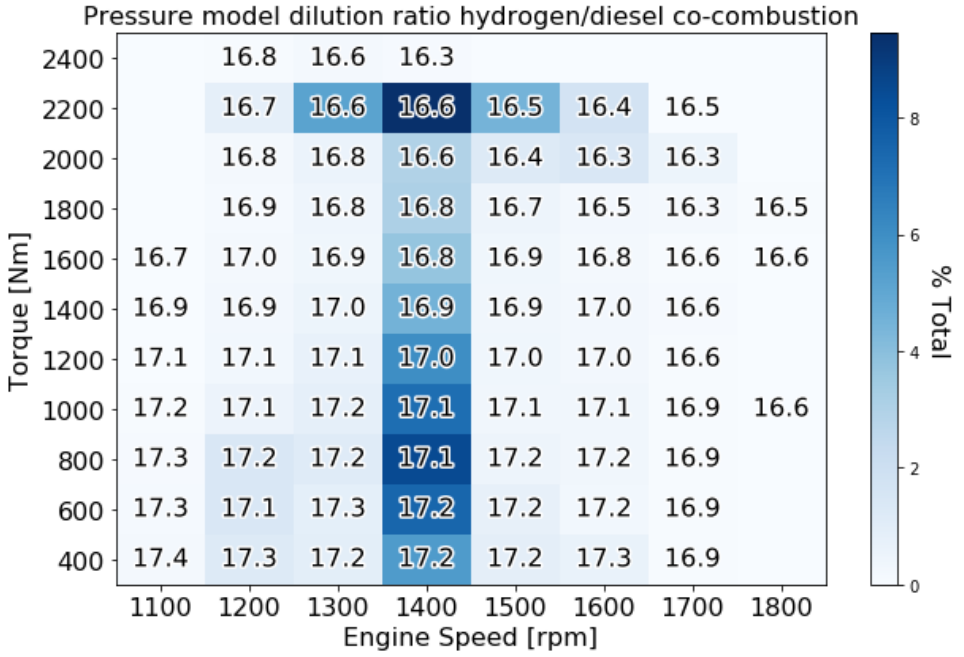

D.3 – Fuel-Specific CO_2 Maps

There is about a 5% difference between the weighted averages of fuel specific CO_2 emissions and also variation within each operating map. There may be a slight change in fuel conversion efficiency across the operating maps and between the two fueling modes, however, most of the difference likely comes from error in the measurements or from assumptions in data processing.

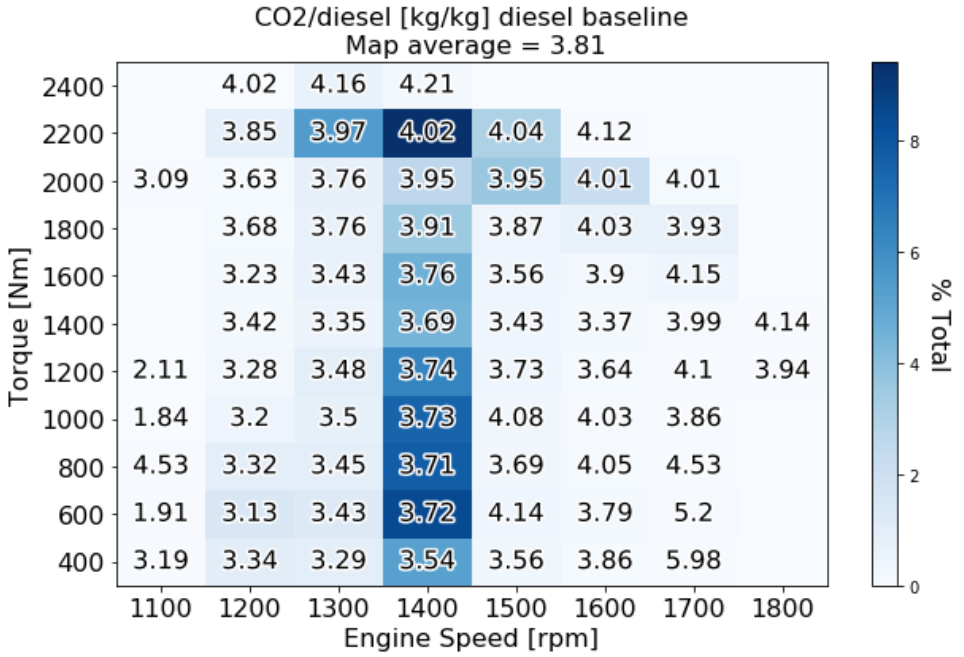

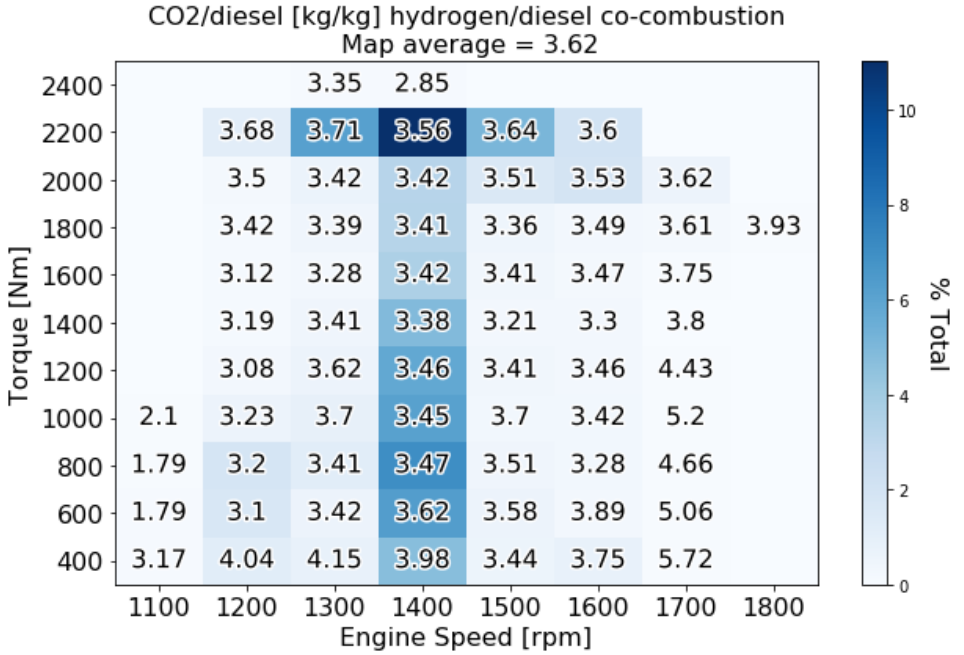

D.4 – Aftertreatment Excess O_2 Maps

The excess oxygen at the inlet to the aftertreatment system as reported by J1939 message.

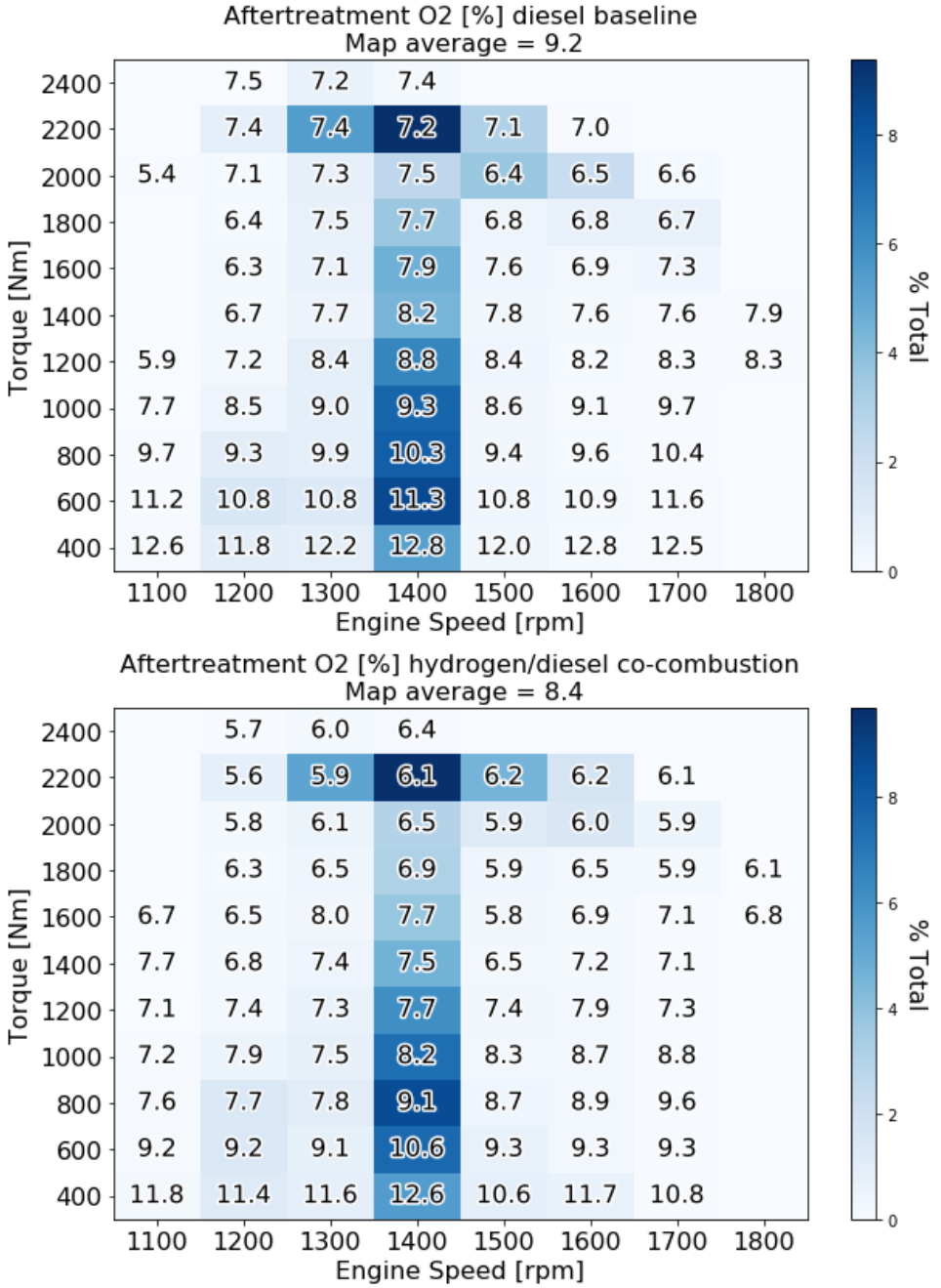

Appendix E – Z Parameter Calculation Script

```
def DOF(parameter):

    r2=1
    i=0
    while (r2 >= 0.3 and i <=limiter):

        dfDOF = pd.DataFrame(parameter,columns = ['parameter'])
        dfDOF['shift'] = dfDOF['parameter'].shift(i)
        dfDOF=dfDOF.dropna()


        r2vec=np.corrcoef(dfDOF['parameter'],dfDOF['shift'])**2
        r2=r2vec[0,1]

        i=i+1
    Z=i
    return Z
```

Appendix F – Overall Processing Script

"""
Created on Thu May 24 11:46:04 2018

The overall processing script for PEMS emission data. This is version is pared down to the essentials for clarity of presentation.

@author: Jeff Meiklejohn
"""

```
##------------import needed packages-----------------
import pandas as pd
import numpy as np
import math
import matplotlib.pyplot as plt
import matplotlib.patches as mpatches
import matplotlib.lines as mlines
from nptdms import TdmsFile
from openpyxl import load_workbook
from scipy import integrate
import scipy.stats as st

##---------------define constants-------------
ref_torque = 2654 #reference torque in N-m
LI_gain = 20000/5 #LI-COR gain in PPM/Volt
ftlbs_Nm = 1.3558 #conversion from ft-lbs to N-m
Dusttrak_gain = 10/5 #convert to mg/m^3 from Volts
TorqueTransducerGain = 813.346#[N-m/Volt]
dieselDensity = 0.848 #kg/l
air_density = 1.18 #kg/m^3
joule_to_BHPHR = 1/(0.372506*(10**6)) #unit conversion
psiToPa = 6894.76
```

```
litreToGallon = 1/3.785
CO2perGallon = 10.16 # kg CO2 per gallon diesel eia.gov
CO2perkg = CO2perGallon * (1/litreToGallon) * (1/dieselDensity)
AtmosphericO2 = 20.95 # atmospheric O2 in [%]
sample_rate = 10 #sample rate in Hz
molarMassDiesel = 0.168 #kg/mol
molarMassCO2 = 44 #g/mol
molarMassAir = 29 #g/mol
molarMassNOx = 46 #g/mol
backGroundCO2 = 405 #PPM
dieselStoich = 14.6 #stoichiometric A/F for diesel
hydStoich = 34.3 #stoichiometric A/F for hydrogen
dieselLHV = 43200 #lower heating value for diesel in kJ/kg
hydrogenLHV = 120000 #lower heating value for hydrogen in kJ/kg
hydrogenDensity = 0.0899 #kg/m^3
licorReferenceTempVoltage = 3.465 #Volts @ 50C
t=1.96 #95% normal distribution

##----------------select cases to process----------------------
##uncomment cases of interest
#cases = ['diesel unloaded']
#cases = ['diesel unloaded','diesel loaded']
#cases = ['H2 unloaded', 'diesel unloaded','H2 loaded', 'diesel loaded']
#cases = ['unloaded', 'loaded']
#cases = ['unloaded']
#cases = ['loaded']
#cases = ['For Patrick']
#cases = ['October 2018 hydrogen','October 2018 diesel']
cases = ['October 2018 hydrogen']
#cases = ['hydrogen/diesel co-combustion','diesel baseline']
#cases = ['diesel baseline']
#cases = ['damaged files']
#cases = ['no torque']
#cases = ['hydrogen/diesel co-combustion']

##----------creat overall storage lists----------
dfSH2 = []
dfSdes = []
dfSH2CO2 = []
dfSdesCO2 = []
dfSH2NOx = []
dfSdesNOx = []
dfSH2PM = []
dfSdesPM = []
avePMkWh = []
PMerr = []
aveNOxkWh = []
NOxerr = []
aveCO2kWh = []
CO2err = []
allResults = []
names =[]
H2comparison=np.zeros((10,2))
Fuelcomparison=np.zeros((3,2))
j=0
```

```
for case in cases:

##----------------------October 2018 campaign---------------------------------------
   if case == 'October 2018 hydrogen':
      files = ['20181019/20181019_PG-Vanderhoof_H2_JM','20181019/20181019_PG-
Vanderhoof2_H2_JM','20181019/20181019_Vanderhoof-PG_H2_JM','20181019/20181019_Vanderhoof-
PG2_H2_JM']
   if case == 'October 2018 diesel':
      files = ['20181019/20181019_PG-Vanderhoof_Diesel_JM','20181019/20181019_PG-
Vanderhoof_Diesel_JM','20181019/20181019_PG-Vanderhoof_Diesel_JM']

##----------------------H2 unloaded files---------------------------------------
   if case == 'For Patrick':
      files = ['20190329/20190329_4thVanderhoof-PG_H2_PS']

##----------------------H2 unloaded files---------------------------------------
   if case == 'H2 unloaded':
      files = ['20190326/20190326_2ndPG-Vanderhoof_H2_JM2','20190327/20190327_2ndPG-
Vanderhoof_H2_JM3','20190329/20190329_3rdPG-Vanderhoof_H2_PS2','20190329/20190329_4thPG-
Vanderhoof_H2_PS']

##---------------------------H2 loaded files---------------------------------
   if case == 'H2 loaded':
      files = ['20190326/20190326_Vanderhoof-PG_H2_JM','20190326/20190326_2ndVanderhoof-
PG_H2_JM','20190327/20190327_Vanderhoof-PG_H2_JM','20190327/20190327_2ndVanderhoof-
PG_H2_JM','20190329/20190329_2ndVanderhoof-PG_H2_JM','20190329/20190329_4thVanderhoof-
PG_H2_PS']

##---------------------------all H2 files---------------------------------
   if case == 'hydrogen/diesel co-combustion':
      files = ['20190326/20190326_2ndPG-Vanderhoof_H2_JM2','20190327/20190327_2ndPG-
Vanderhoof_H2_JM3','20190329/20190329_3rdPG-Vanderhoof_H2_PS2','20190329/20190329_4thPG-
Vanderhoof_H2_PS','20190326/20190326_Vanderhoof-
PG_H2_JM','20190326/20190326_2ndVanderhoof-PG_H2_JM','20190327/20190327_Vanderhoof-
PG_H2_JM','20190327/20190327_2ndVanderhoof-PG_H2_JM','20190329/20190329_4thVanderhoof-
PG_H2_PS']
      #'20190329/20190329_3rdPG-Vanderhoof_H2_PS2'

##--------------------all unloaded files-----------------------------------
   if case == 'unloaded':
      files = ['20190328/20190328 _PG-Vanderhoof_Diesel_JM2','20190328/20190328 _2ndPG-
Vanderhoof_Diesel_JM2','20190326/20190326_2ndPG-
Vanderhoof_H2_JM2','20190327/20190327_2ndPG-Vanderhoof_H2_JM3','20190329/20190329_3rdPG-
Vanderhoof_H2_PS2','20190329/20190329_4thPG-Vanderhoof_H2_PS']
      graphnames =
['20190328_unloaded_diesel','20190328_2_unloaded_diesel','20190326_2_unloaded_hydrogen','201903
27_2_unloaded_hydrogen','20190329_3_unloaded_hydrogen','20190329_4_unloaded_hydrogen']
##--------------------Diesel unloaded files-----------------------------------
   if case == 'diesel unloaded':
      files = ['20190328/20190328 _PG-Vanderhoof_Diesel_JM2','20190328/20190328 _2ndPG-
Vanderhoof_Diesel_JM2']
      graphnames =['20190328_unloaded_diesel','20190328_2_unloaded_diesel']
##--------------------all loaded files-----------------------------------
   if case == 'loaded':
```

```
        files = ['20190328/20190328 _Vanderhoof-PG_Diesel_JM','20190328/20190328 _2ndVanderhoof-
PG_Diesel_JM','20190329/20190329_3rdVanderhoof-PG_Diesel_PS','20190326/20190326_Vanderhoof-
PG_H2_JM','20190326/20190326_2ndVanderhoof-PG_H2_JM','20190327/20190327_Vanderhoof-
PG_H2_JM','20190327/20190327_2ndVanderhoof-PG_H2_JM','20190329/20190329_4thVanderhoof-
PG_H2_PS']
        graphnames
=['20190328_loaded_diesel','20190328_2_loaded_diesel','20190329/20190329_3_loaded_diesel','20190
326_loaded_hydrogen','20190326_2_loaded_hydrogen','20190327_loaded_hydrogen','20190327_2_load
ed_hydrogen','20190329_4_loaded_hydrogen']

##-------------------Diesel loaded files-------------------------------------
    if case == 'diesel loaded':
        files = ['20190328/20190328 _Vanderhoof-PG_Diesel_JM','20190328/20190328 _2ndVanderhoof-
PG_Diesel_JM','20190329/20190329_3rdVanderhoof-PG_Diesel_PS']
        graphnames
=['20190328_loaded_diesel','20190328_2_loaded_diesel','20190329/20190329_3_loaded_diesel']

##-------------------all Diesel files-------------------------------------
    if case == 'diesel baseline':
        files = ['20190328/20190328 _PG-Vanderhoof_Diesel_JM2','20190328/20190328 _2ndPG-
Vanderhoof_Diesel_JM2','20190328/20190328 _Vanderhoof-PG_Diesel_JM','20190328/20190328
_2ndVanderhoof-PG_Diesel_JM','20190329/20190329_3rdVanderhoof-PG_Diesel_PS']

##----------------------damaged files-----------------------------------------
    if case == 'damaged files':
        files = ['20190327/20190327_2ndPG-Vanderhoof_H2_JM3']
    if case == 'diesel unloaded no torque':
        files = ['20190329/20190329_PG-Vanderhoof_Diesel_JM2']
    if case == 'no torque':
        files = ['20190329/20190329_PG-Vanderhoof_Diesel_JM2','20190329/20190329_Vanderhoof-
PG_Diesel_JM','20190329/20190329_2ndPG-
Vanderhoof_H2_JM2','20190329/20190329_2ndVanderhoof-PG_H2_JM']

##-----------storage lists for within each case-----------------
    dfS = []
    dfSCO2 = []
    dfSNOx = []
    dfSTreatedNOx = []
    dfSPM = []
    avePMmgm3 = []
    aveCO2ppm = []
    aveNOxppm = []
    results = np.zeros((len(files),14))
    fileNames = []
    speed = [[] for i in range(len(files))]
    power = [[] for i in range(len(files))]
    i=0
    for x in files:
        file = x
        df=pd.read_excel(file+'.xlsx', 1, header=0, names=None, index_col=None, usecols=None,
squeeze=False, dtype=None, engine=None, converters=None, true_values=None, false_values=None,
skiprows=None, nrows=None, na_values=None, parse_dates=False, date_parser=None,
thousands=None, comment=None, skipfooter=0, convert_float=True)

##-----------special things for Ocotober 2018 log files----------------------
```

```
        if (case == 'October 2018 hydrogen' or case == 'Ocotober 2018 diesel'):
            df['PT1'] = df['PT2'] #PT naming convetion changed
            df['LI-COR1 CO2'] = df['LI-COR1'] #label changed
            df['LI-COR2 Temp'] = 3.4 #temp not logged 2018 campaign

##----------------primary calculations-----------------------
        df['PM (mg/m^3)'] =  df['Dustrak']*Dusttrak_gain
        df['MeasuredTorque'] = df['DriveshaftTorque']*TorqueTransducerGain*(1/df['TransActualGearRatio'])
        df['Fuel']=df['EngFuelRate']*dieselDensity #fuelling in kg/hr
        df['PressureModelDilutionRatio'] = df['PT1']*(-8.89)+26.77 #from most recent SCRE test Feb 2019,
July 2019 analysis
        df['Phi']= df['Fuel']*dieselStoich/df['EngIntakeAirMassFlowRate'] # diesel only
        df['Lambda'] = df['EngIntakeAirMassFlowRate']/(df['Fuel']*dieselStoich +
df['HydrogenConsumption']*hydStoich)#diesel + hydrogen
        df['Phi2'] = 1/df['Lambda']
        df['ExhaustTempNozzle']=df['TC0']
        df['ExpectedO2'] = AtmosphericO2 * (1.0-df['Phi2'])
        df['CombinedMassFlow']=df['Fuel']+df['HydrogenConsumption']+df['EngIntakeAirMassFlowRate']
        df['CO2'] = df['LI-COR1 CO2']*LI_gain #CO2 in PPM
        df['LICORTemp'] = df['LI-COR2 Temp']
        #df['CO2 corrected'] = df['LI-COR1 CO2']*(licorReferenceTempVoltage/df['LI-COR2 Temp'])*LI_gain
#to investigate grounding issue

##-------time offest CO2 and PM signals, calc raw (undiluted) values---
        df['CO2_lag3']= df['CO2'].shift(-30)
        df['CO2_lag28']= df['CO2'].shift(-28)
        df['PM_lag26']= df['PM (mg/m^3)'].shift(-26)
        df['ExpectedO2lag8']= df['ExpectedO2'].shift(8)
        df['CO2raw']=df['CO2_lag3']*df['PressureModelDilutionRatio']
        df['PMraw']=df['PM_lag26']*df['PressureModelDilutionRatio']

##----------------H2 displacement calculations----------------------
        df['EnergyFractionH2'] =
(100*df['HydrogenConsumption']*hydrogenLHV)/(df['HydrogenConsumption']*hydrogenLHV+df['Fuel']*die
selLHV)
        df['%volHydrogen'] =
100/(1+(hydrogenDensity/air_density)*(1/df['Phi2'])*(hydStoich+(hydrogenLHV/dieselLHV)*((100-
df['EnergyH2'])/df['EnergyH2'])*dieselStoich))
        df['EquivFuel'] = df['Fuel'] + df['HydrogenConsumption']*(hydrogenLHV/dieselLHV)

##-------------modelled CO2 output---------------------
        df['CO2PPMv'] =
df['Fuel']*(1/molarMassDiesel)*12*(0.012+0.016*2)*(1/df['Aftrtreatment1ExhaustGasMassFlow'])*1000000
*(molarMassAir/molarMassCO2)
        df['ExpectedCO2'] = df['CO2PPMv']/df['PressureModelDilutionRatio']+backGroundCO2
        #df['eiaCO2'] = df['Fuel']*CO2perkg ##CO2 reality check

##----------------------general run stats stuff--------------------
            speed[i] = df['FrontAxleSpeed'].tolist()
        results[i,3] = df['EngFuelRate'].sum()*(1/36000)
        results[i,4] = df['HydrogenConsumption'].sum()/36000
        df=df.dropna()

##--------------------calculate emission mass flows-----------------------
        df['PM (kg/hr)'] = df['PMraw']*df['Aftrtreatment1ExhaustGasMassFlow']*(1/air_density)*(1/1000000)
```

```
        df['CO2 (kg/hr)'] =
df['CO2raw']*(molarMassCO2/molarMassAir)*df['Aftrtreatment1ExhaustGasMassFlow']*(1/1000000)
        df['CO2/diesel [kg/kg]']= df['CO2 (kg/hr)']/df['Fuel']
        df['UntreatedNOx'] = df['Aftertreatment1IntakeNOx'].shift(8)
        df['TreatedNOx'] = df['Aftertreatment1OutletNOx'].shift(8)
        df['NOx (kg/hr)'] =
df['UntreatedNOx']*(molarMassNOx/molarMassAir)*df['Aftrtreatment1ExhaustGasMassFlow']*(1/1000000)
        df['Treated NOx (kg/hr)'] =
df['TreatedNOx']*(molarMassNOx/molarMassAir)*df['Aftrtreatment1ExhaustGasMassFlow']*(1/1000000)

##----------data exclusions, new datafame for each emission----------
        dfCO2=df[(df.CO2_lag3<= 20000)&(df.CO2_lag3>= 0)&(df.LICORTemp>= 3.3)]
        dfNOx = df[(df.UntreatedNOx != -200)&(df.UntreatedNOx <= 3063.94)]
        dfTreatedNOx = df[(df.TreatedNOx >= 0)&(df.TreatedNOx <= 3063.94)]
        dfPM=df[df.PM_lag26>= 0]

##----------store totals not dependant on driveline status----------
        results[i,5] = dfCO2['CO2 (kg/hr)'].sum()/36000
        results[i,6] = dfNOx['NOx (kg/hr)'].sum()/36000
        results[i,7] = dfPM['PM (kg/hr)'].sum()/36000
        results[i,12] = dfTreatedNOx['Aftrtrtmnt1SCRActlDsngRgntQntity'].sum()/36000

##----------CO2 modelled to measured comparison----------
#       fig6,ax = plt.subplots()
#
dfCO2.plot.scatter(figsize=(18,10),x='ExpectedCO2',y='CO2_lag3',c='PressureModelDilutionRatio',colorm
ap = 'rainbow',s=1,ax=ax)
#       # calc the trendline (it is simply a linear fitting)
#       x = dfCO2['ExpectedCO2']
#       y = dfCO2['CO2_lag3']
#       z = np.polyfit(x, y,1)
#       p = np.poly1d(z)
#       slope,intercept,r_value,p_value,std_err = st.linregress(x,y)
#       r2=pow(r_value,2)
#       plt.plot(x,p(x),"-",0.5)
#       plt.text(200,200,'y= '+str(round(z[0],3))+'x + '+str(round(z[1],3)) + '\n$R^2$=
'+str(round(r2,3)),fontsize=16)
#       plt.title(file+ ' modelled vs measured CO2')

##----------driveline status exclusions----------
        df=df[df.TransDrivelineEngaged !=0] #key J1939 message for torque calculation
        df['kW (CAN)']= df['ActualEngPercentTorque']/100*ref_torque*df['EngSpeed']*(np.pi/30)*(1/1000)
        df['Torque (CAN)']= ((df['ActualEngPercentTorque']+df['ActlEngPrcntTorqueHighResolution']*.125-
df['NominalFrictionPercentTorque'])/100)*ref_torque ##torque from J1939 broadcast messages
        df['kW (TT)']=
df['DriveshaftTorque']*TorqueTransducerGain*(1/df['TransActualGearRatio'])*df['EngSpeed']*(np.pi/30)*(1/
1000)
        df['Torque (TT)']= df['DriveshaftTorque']*TorqueTransducerGain*(1/df['TransActualGearRatio'])
        df['ThermalEfficiency'] = (df['kW
(TT)']/((df['HydrogenConsumption']*hydrogenLHV+df['Fuel']*dieselLHV)/3600))*100
        df['ShaftPower']=df['kW (TT)']
        df = df[df.ShaftPower >=20]
        df = df[df.ShaftPower <=5000]

##----------Torque comparison, only valid in diesel mode----------
```

```
#       fig7,ax = plt.subplots()
#       df.plot.scatter(figsize=(18,10),x='Torque (CAN)',y='Torque (TT)',c='TransShiftInProcess',colormap =
'rainbow',s=1,ax=ax)
#       # calc the trendline (it is simply a linear fitting)
#       x = df['Torque (CAN)']
#       y = df['Torque (TT)']
#       z = np.polyfit(x, y,1)
#       p = np.poly1d(z)
#
#       slope,intercept,r_value,p_value,std_err = st.linregress(x,y)
#       r2=pow(r_value,2)
#       plt.plot(x,p(x),"-.",0.5)
#       plt.text(50,800,'y= '+str(round(z[0],3))+'x + '+str(round(z[1],3)) + '\n$R^2$= '+str(round(r2,3))+'\n#
points= '+str(len(df['Torque (CAN)'])),fontsize=16)
#       plt.title(file+ ' measured vs reference torque')

##--------------record power specific emissions-------------------------
        #power[j][i] = df['ShaftPower'].tolist()
        power[i] = df['ShaftPower'].tolist()
        df['CO2 g/kW.h']= (df['CO2 (kg/hr)']*1000)/df['kW (TT)']
        df['NOx g/kW.h']= (df['NOx (kg/hr)']*1000)/df['kW (TT)']
        df['Treated NOx g/kW.h']= (df['Treated NOx (kg/hr)']*1000)/df['kW (TT)']
        df['PM mg/kW.h']= (df['PM (kg/hr)']*1000*1000)/df['kW (TT)']

        df=df[df.TransShiftInProcess !=1]#driveline exclusion
        #df=df[df.TransCurrentGear<=18] #additional driveline exclusion, ultimately not used

##---------create new df each emission after driveline exclusions-------------
        dfCO2=df[(df.CO2_lag3<= 20000)&(df.CO2_lag3>= 0)&(df.LICORTemp>= 3.3)]
        dfNOx = df[(df.UntreatedNOx != -200)&(df.UntreatedNOx <= 3063.94)]
        dfTreatedNOx = df[(df.TreatedNOx >= 0)&(df.TreatedNOx <= 3063.94)]
        dfPM=df[df.PM_lag26>= 0]

##----------store totals----------------------------
        results[i,9] = dfCO2['CO2raw'].mean()
        results[i,10] = dfNOx['UntreatedNOx'].mean()
        results[i,11] = dfPM['PM (mg/m^3)'].mean()
        results[i,0] = dfCO2['CO2 g/kW.h'].mean()
        results[i,1] = dfNOx['NOx g/kW.h'].mean()
        results[i,2] = dfPM['PM mg/kW.h'].mean()
        results[i,8] = df['kW (TT)'].sum()/36000

        fileNames.append(file)
        dfS.append(df)
        dfSCO2.append(dfCO2)
        dfSNOx.append(dfNOx)
        dfSTreatedNOx.append(dfTreatedNOx)
        dfSPM.append(dfPM)

        if (case == 'hydrogen/diesel co-combustion' or case == 'October 2018 hydrogen'):
            dfSH2 = pd.concat(dfS)
            dfSH2CO2 = pd.concat(dfSCO2)
            dfSH2NOx = pd.concat(dfSNOx)
            dfSH2PM = pd.concat(dfSPM)
```

```
        if (case == 'diesel baseline' or case == 'October 2018 diesel'):
            dfSdes = pd.concat(dfS)
            dfSdesCO2 = pd.concat(dfSCO2)
            dfSdesNOx = pd.concat(dfSNOx)
            dfSdesPM = pd.concat(dfSPM)

        i = i+1

##----------speed + power histogram plotting----------------

#    k=0
#    fig2=plt.figure(figsize=(8,6))
#    ax=plt.subplot()
#    for k in range(len(files)):
#        y,binEdges = np.histogram(power[k],range=(0,400),bins=16,density=True)
#        bincenters = 0.5*(binEdges[1:]+binEdges[:-1])
#        menStd     = np.sqrt(y)
#        width      = 400/(16*len(files))
#        ax.step(bincenters, y, label=graphnames[k])
#        #plt.bar(bincenters, y, width=width, color='r', yerr=menStd)
#    plt.xlabel('% kW', fontsize=14)
#    plt.ylabel('# of samples', fontsize=14)
#    plt.title(case+': measured power', fontsize=12)
#    plt.legend()
#    plt.show()
#
#    k=0
#    fig3=plt.figure(figsize=(8,6))
#    ax=plt.subplot()
#    for k in range(len(files)):
#        y,binEdges = np.histogram(speed[k],range=(0,100),bins=10,density=True)
#        bincenters = 0.5*(binEdges[1:]+binEdges[:-1])
#        menStd     = np.sqrt(y)
#        width      = 100/(10*len(files))
#        #ax.bar(bincenters+width*(k+0.5-0.5*len(files)), y, width=width,label=files[k])
#        ax.step(bincenters, y, label=graphnames[k])
#        #plt.bar(bincenters, y, width=width, color='r', yerr=menStd)
#    plt.xlabel('km/hr', fontsize=14)
#    plt.ylabel('# of samples', fontsize=14)
#    plt.title(case+': vehicle speed', fontsize=12)
#    plt.legend()
#    plt.show()

    allResults.append(results)
    names.append(fileNames)
    dfS = pd.concat(dfS)
    dfSCO2 = pd.concat(dfSCO2)
    dfSNOx = pd.concat(dfSNOx)
    dfSTreatedNOx = pd.concat(dfSTreatedNOx)
    dfSPM = pd.concat(dfSPM)
##------run averages + err,ultimately superceded w/aggregate average + stat err calc--------
    avePMkWh.append(dfS['PM mg/kW.h'].mean())
    PMerr.append(t*(np.std(dfS['PM mg/kW.h'])/np.sqrt(len(dfS['PM mg/kW.h']))))
    aveNOxkWh.append(dfS['NOx g/kW.h'].mean())
```

```
    NOxerr.append(t*(np.std(dfS['NOx g/kW.h'])/np.sqrt(len(dfS['NOx g/kW.h']))))
    aveCO2kWh.append(dfS['CO2 g/kW.h'].mean())
    CO2err.append(t*(np.std(dfS['CO2 g/kW.h'])/np.sqrt(len(dfS['CO2 g/kW.h']))))

##------------------------Emission Map Plotting-----------------

##code the parameters of interest

#    __EffMap__(dfS['PressureModelDilutionRatio'].tolist(),dfS['Torque
(TT)'].tolist(),dfS['EngSpeed'].tolist(),case,str('Pressure model dilution ratio'),2)
    __EffMap__(dfSCO2['CO2 g/kW.h'].tolist(),dfSCO2['Torque
(TT)'].tolist(),dfSCO2['EngSpeed'].tolist(),case,str('CO2 [g/kW.h]'),0)
#    __EffMapDot__(dfS['CO2 g/kW.h'].tolist(),dfS['Torque
(TT)'].tolist(),dfS['EngSpeed'].tolist(),case,str('CO2 [g/kW]'),1)
#    __EffMapDot__(dfSCO2['CO2 (kg/hr)'].tolist(),dfSCO2['Torque
(TT)'].tolist(),dfSCO2['EngSpeed'].tolist(),case,str('CO2 [kg]'),1)
    __EffMapErr__(dfSCO2['CO2 g/kW.h'].tolist(),dfSCO2['Torque
(TT)'].tolist(),dfSCO2['EngSpeed'].tolist(),case,str('CO2 [g/kW.h]: standard error %'),1)
    __EffMap__(dfSNOx['NOx g/kW.h'].tolist(),dfSNOx['Torque
(TT)'].tolist(),dfSNOx['EngSpeed'].tolist(),case,str('NOx [g/kW.h]'),1)
#    __EffMap__(dfSTreatedNOx['Treated NOx g/kW.h'].tolist(),dfSTreatedNOx['Torque
(TT)'].tolist(),dfSTreatedNOx['EngSpeed'].tolist(),case,str('Treated NOx g/kW.h'),2)
#    __EffMap__(dfS['AftrtrtmntSCRActlDsngRgntQntity'].tolist(),dfS['Torque
(TT)'].tolist(),dfS['EngSpeed'].tolist(),case,str('DEF dosing rate [g/hr]'),0)
#    __EffMapDot__(dfS['NOx g/kW.h'].tolist(),dfS['Torque
(TT)'].tolist(),dfS['EngSpeed'].tolist(),case,str('NOx [g/kW]'),1)
#    __EffMapDot__(dfSNOx['NOx (kg/hr)'].tolist(),dfSNOx['Torque
(TT)'].tolist(),dfSNOx['EngSpeed'].tolist(),case,str('NOx [kg]'),1)
    __EffMapErr__(dfSNOx['NOx g/kW.h'].tolist(),dfSNOx['Torque
(TT)'].tolist(),dfSNOx['EngSpeed'].tolist(),case,str('NOx [g/kW.h]: standard error %'),1)
##    __EffMap__(dfS['Treated NOx g/kW.h'].tolist(),dfS['Torque
(TT)'].tolist(),dfS['EngSpeed'].tolist(),case,str('Treated NOx [g/kW.h]'),1)
#    __EffMap__(dfS['EngineTurboBoostPressure'].tolist(),dfS['Torque
(TT)'].tolist(),dfS['EngSpeed'].tolist(),case,str('EngineTurboBoostPressure [kPa]'),0)
##    __EffMapOld__(dfS['NOx g/kW.h'].tolist(),dfS['Torque
(TT)'].tolist(),dfS['EngSpeed'].tolist(),case,str('NOx [g/kW.h]'),1)
    __EffMap__(dfSPM['PM mg/kW.h'].tolist(),dfSPM['Torque
(TT)'].tolist(),dfSPM['EngSpeed'].tolist(),case,str('PM [mg/kW.h]'),1)
#    __EffMap__(dfSPM['PM (mg/m^3)'].tolist(),dfSPM['Torque
(TT)'].tolist(),dfSPM['EngSpeed'].tolist(),case,str('PM [mg/m^3]'),2)
#    __EffMapDot__(dfS['PM mg/kW.h'].tolist(),dfS['Torque
(TT)'].tolist(),dfS['EngSpeed'].tolist(),case,str('PM [mg/kW]'),1)
#    __EffMapDot__(dfSPM['PM (kg/hr)'].tolist(),dfSPM['Torque
(TT)'].tolist(),dfSPM['EngSpeed'].tolist(),case,str('PM [kg]'),1)
    __EffMapErr__(dfSPM['PM mg/kW.h'].tolist(),dfSPM['Torque
(TT)'].tolist(),dfSPM['EngSpeed'].tolist(),case,str('PM [mg/kW.h]: standard error %'),1)
#    __EffMapErr__(dfSPM['PM (mg/m^3)'].tolist(),dfSPM['Torque
(TT)'].tolist(),dfSPM['EngSpeed'].tolist(),case,str('PM [mg/m^3]: standard error %'),1)
###    __EffMap__(dfS['EnergyH2'].tolist(),dfS['Torque (TT)'].tolist(),dfS['EngSpeed'].tolist(),case,str('H2
displacement % (Energy Basis)'),1)
##    __EffMap__(dfS['EnergyFractionH2'].tolist(),dfS['Torque
(TT)'].tolist(),dfS['EngSpeed'].tolist(),case,str('H2 displacement % (Energy Basis)'),1)
```

Appendix G – Test Template and Pre-Trip Inspection List

Date of Test:	
Start Time:	Trip out: Return:
Test Route:	Leg 1: Leg 2: Leg 3: Leg 4:
Ambient Temp:	Start: End:
General Description of Weather:	
Driver:	
Trailer Description	Leg 1: Leg 2: Leg 3: Leg 4:
Total weight tractor + trailer	Leg 1: Leg 2: Leg 3: Leg 4:
Instrument Gain Settings:	LI-COR CO2: _____PPM/5V LI-COR TEMP: _____ C/5V DustTrak: _____mg/m^3
Log File Name(s):	
H_2 mass	Trip Start: _____kg Trip End: _____kg

	H_2 filled at end of trip? Y / N If yes, H_2 filled: _____kg
Diesel density **As reported by Lomak*	_____ kg/m^3
Diesel	Diesel full at trip start? Y / N Diesel filled at end of trip? Y / N If yes, Diesel filled: _____l

Pre trip checklist:

Item #	Item	Criteria	Pass/Fail	Notes
1.a	Start Log file	GPS connected, CANbus signals flashing, analog inputs qualitatively appear on screen		
1.b	Torque Transducer Signal	Signal present + stable ~0V		
1.c	Dusttrak Signal	Signal present + stable ~0V		
1.d	LI-COR Channel 1 Signal - CO2	Signal present + stable~0V		
1.e	Pressure Transducer 1 Signal	Signal present ~1V		
1.f	Pressure Transducer 2 Signal	Signal present ~1V		
1.g	Thermocouple 0 Signal	Roughly match ambient temp		Record Temp:_____C
1.h	Thermocouple 1 Signal	Roughly match ambient temp		Record Temp:_____C

1.i	LI-COR Sample Pump Qualitative Function	Feel air flow from exit port		
1.j	MFC Set Correctly	40 slpm set point on display		
1.k	MFC Qualitative Function	Feel air flow from exit port		
1.l	MFC remote shut off	Shut off via toggle switch in cab		
1.m	MFC restart	Turn on via toggle switch in cab		
1.n	Purge valve function	Turn on via toggle switch in cab, feel air at bypass ***run system purge for at least 30s***		
1.o	Exhaust Valve Open	Open 1.4 turn shut off on sample line		
1.p	Log file generated	Save + Open TDMS file with excel		Ensure correct name and saving location
1.q	Log file parameters present	Check A-CAN, V-CAN messages, GPS, Analog,+ Thermocouple Values		
1.r	Check background CO_2 from purge	Should be around 400-420 PPM		Record CO_2: _____PPM
1.s	Check background PM from purge	Should be close to zero		Record PM: _____mg/m^3